Dissertation zur Erlangung des Doktorgrades der Fakultät für Chemie und Pharmazie der Ludwig-Maximilians-Universität München

Nucleobindin-1 modulates extracellular matrix remodeling by promoting intra-Golgi trafficking of matrix metalloproteinase 2

Natalia María Pacheco Fernández

aus

Bogotá, Kolumbien

2020

Note about publication

At the moment of submission of this thesis (27.02.2020), most of the results here shown were under revision for publication in the *Journal of Cell Biology (JCB)*. By the moment of this thesis defense, the paper *Nucleobindin-1 regulates ECM degradation by promoting intra-Golgi trafficking of MMPs* was published by JCB (Available online on June 1st 2020, **https://doi.org/10.1083/jcb.201907058**).

Table of contents

1. List of figures

2. List of tables

3. Summary

Matrix metalloproteases (MMPs) play a crucial role in tissue homeostasis. Profuse literature has studied their roles in cell migration and tissue invasion during cancer metastasis, as well as in inflammatory processes. Although the literature covering MMPs function is abundant, the intracellular trafficking of these proteins remains poorly understood. The aim of the present work was to identify the molecular mechanism of intracellular trafficking of MMPs, with particular focus on MMP2.

A novel mass spectrometry approach revealed nucleobindin-1 (NUCB1), a major regulator of Ca2+ homeostasis at the Golgi, as a potential candidate for the regulation of MMP transport. Using a synchronized cargo trafficking assay, it was possible to demonstrate that in the absence of NUCB1 the intracellular trafficking of MMP2 is delayed. Moreover, this work reveals that NUCB1-dependent MMP2 trafficking is restricted to the Golgi, exclusively delaying its intra-Golgi trafficking at the *cis* compartment and, as a consequence, decreasing MMP2 mediated cell migration and matrix invasion. Furthermore, my findings show that not only MMP2, but also MT1-MMP intra-Golgi trafficking is impaired, implying that this mechanism could also influence the trafficking of other MMPs.

Interestingly, experiments performed with a NUCB1 Ca2+-binding deficient mutant showed that Ca2+ is required, both for the interaction, as well as for proper MMP2 trafficking, suggesting that a specific impairment of *cis*-Golgi Ca2+ homeostasis, rather than an overall Ca2+ deficiency, is essential for proper MMP2 intra-Golgi trafficking.

Taken together the results of this thesis contributed to enlighten the mechanism of MMP2 intracellular trafficking by identifying NUCB1 as a critical player in MMP transport. Importantly, this work highlights the requirement of Ca2+ for proper trafficking, not just at the TGN, as has been documented, but also at the *cis*-Golgi. Although this is a big step towards the understanding of MMP intracellular trafficking, further investigations are required to gain a better understanding of the retention mechanism of NUCB1 at the *cis*-Golgi lumen and a deeper insight into the regulation of intra-Golgi protein trafficking.

4. Introduction

4.1 Protein trafficking in the secretory pathway

The cell is a highly dynamic unit where multiple parallel processes happen to maintain ionic and nutrient homeostasis. Major players in this dynamic environment are proteins that act as messengers, triggers, anchors, transporters and receptors[1]. Some proteins are constitutively synthesized, meaning that the cell produces them constantly throughout its lifetime; however, there are also many proteins, such as MMPs, that require an external signal that induces their production[2].
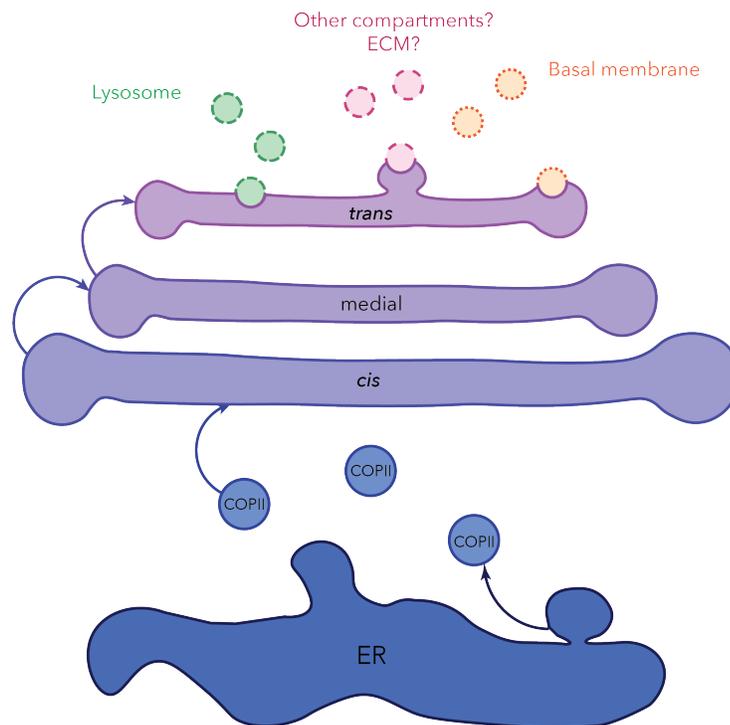
Figure 1. Schematic view of the secretory pathway. Protein cargo is accumulated at ER-exit sites, packed in COPII coated vesicles to reach the *cis*-Golgi and transported thorough the stacks until it reaches the TGN, where proteins are sorted and packed to be delivered to their targeting destination.

After DNA transcription, most of the proteins are synthesized by ribosomes located in the cytosol[3,4]. Although some proteins remain there after their synthesis, many others are directed to different compartments such as mitochondria, lysosomes or the extracellular millieu[3,5]. This compartmentalization creates the need of specific transport mechanism to correctly target newly synthesized proteins to their final destination[6]. In this regard, eukaryotes use 3 major protein mechanisms of active transport: (1) gated, which keeps a bidirectional trafficking of proteins between the nucleus and the cytosol; (2) transmembrane, which deals with the transport of proteins anchored to a membrane; and (3) vesicular, where membrane-enclosed intermediates are in charge of the delivery of proteins from one compartment to another[6]. Vesicular transport is the basis of the trafficking mechanism in which this section is focused: the secretory pathway.

The most common route used for soluble protein trafficking is the secretory pathway, also called the constitutive or canonical pathway[7]. In this pathway, proteins are synthesized, translocated into the endoplasmic reticulum (ER), then transported to the Golgi apparatus, where they traverse its stacks until reaching the *trans*-Golgi network (TGN, Figure 1), the sorting station of the pathway and the place where proteins are packed into vesicles and targeted to their final destination[7–10]. The details of this pathway are described in the following sections.

4.1.1   Protein translocation to the ER

Most secreted proteins, and to some extent also transmembrane proteins, possess a N-terminal sequence, termed signal peptide, that enables their recognition by a signal recognition particle (SRP) and directs their translocation to the endoplasmic reticulum[3,11,12]. Although initially thought as conserved sequence motifs, signal peptides are highly diverse and barely homologous[11]. Nevertheless, they are similar in size (~20-30 amino acids) and possess a similar 3-domain structure: a basic N-terminal domain, a hydrophobic middle region and a slightly polar C-terminal domain[11]. Besides their function in protein relocation, signal sequences are not highly informative and, therefore, easily interchangeable[11].

Protein translocation to the ER starts with signal peptide recognition by SRP[5,11–13]. SRPs were first identified in 1971 and later identified as the 11S ribonucleoprotein (RNP) particle in mammalian cells[5,12,14]. SRP is a protein complex unit containing 2 main domains: the S-domain,

which binds to the signal sequence and promotes translocation, and the Alu domain, which arrests protein elongation (Figure 2)[12,15].

The S-domain is formed by the assembly of half of the 7S RNA SRP, and the subunits SRP19, the heterodimer SRP68/72 and SRP 54[3,12]. The latter recognizes the signal sequence and interacts with the SRP receptor in a GTPase-dependent manner[12]. On the other hand, the Alu domain is composed of the 5' and 3' ends of 7S RNA SRP and the SRP9-14 heterodimer, important for Alu domain activity[3,12].
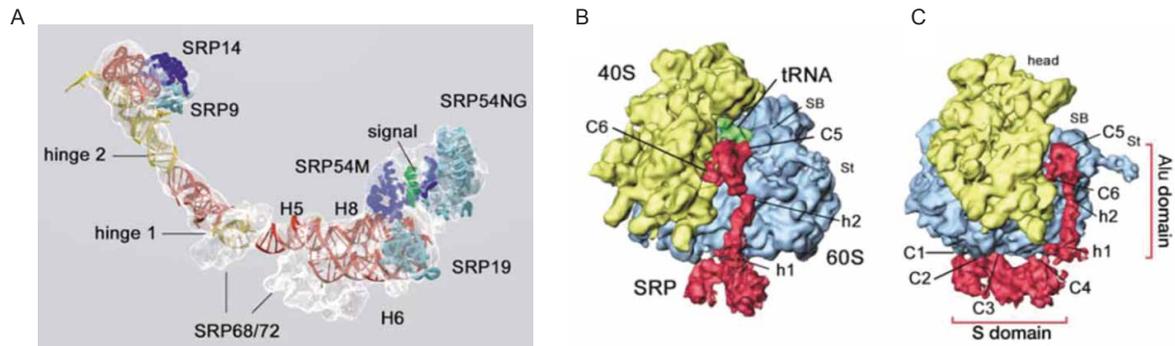
Figure 2.   Mammalian SRP structure. (A) Molecular model of the S-domain and Alu-domain of SRP in mammals. The recognized signal sequence is represented in green. H: RNA helices. (B) Cryo-EM map of the complexed formed between SRP and the ribosome. Ribosome subunit 40S is depicted in yellow, 60S subunit in blue, signal sequence in green and SRP in red. (C) 70° rotation of the image depicted in (B) illustrating both S- and Alu domain of SRP. Figures modified from Halic et al. (2004)[12].

As mentioned above, protein elongation arrest is fundamental to promote translocation of nascent proteins to the ER, so how can SRP at the same time recognize the signal peptide, bind to the ribosome and prevent peptide elongation? Given that SRP and ribosomes do not have an equimolar distribution in the cytoplasm, a previous signal sequence scan is required for SRP to find a functional signal peptide[16]. To initiate such a scanning process, the SRP S-domain interacts initially with the 60S ribosomal subunit, which induces a conformational change that allows the S-domain to initiate a signal peptide scanning[12]. Once it recognizes a functional signal sequence, SRP binds to it and changes to an open conformation, enabling the high affinity binding between SRP and the ribosome[12].

Structural studies of the Alu domain revealed that its contact sites with the ribosome are the same used by the eukaryotic elongation factor 2 (eEF2), which is in charge of promoting protein elongation[3,12]. Given the higher affinity of the Alu domain for ribosomes, the interaction with eEF2 is lost and peptide elongation ceases[3,12].

The formation of a complex between SRP and the ribosome-nascent chain (SRP-RNC) enables its recognition by an SRP receptor (SR) that is formed by 2 subunits: α, which identifies the SRP54 unit and binds to SRP-RNC, and β, which is bound to the ER membrane[12]. The binding is mediated by GTPase activity and promotes the transfer of RNC to a translocon channel that finally delivers the protein into the ER lumen (Figure 3)[3,4,16].
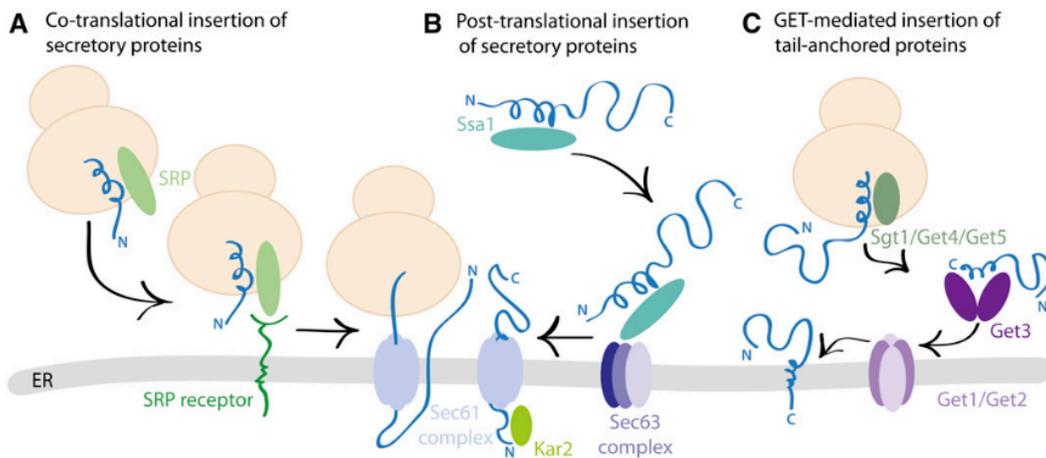
Figure 3. Mechanisms for secretory cargo translocation to the ER. (A) Co-translational insertion of proteins is mediated by SRP recognition of signal peptide (see text above). Proteins can also be translocated into the ER via at least 2 alternative pathways: (B) Post-translational insertion of proteins requires cytosolic chaperones that keep protein cargo in an unfolded state prior to translocation. Hsp70 ATPases (e.g. like Ssa1 in yeast) play this role until the delivery of the protein to Sec63 complex, or (C) Protein insertion via the Get-transmembrane domain recognition complex (TRC) system. Here, tail-anchored proteins are inserted into the ER membrane aided by Get3 (in mammals TRC40), which targets them to Get1/Get2. Get: proteins encoded by the Golgi to ER trafficking deficiency genes in yeast. Figure taken from Barlowe & Miller (2013)[4].

4.1.2 The Endoplasmic Reticulum (ER)

The ER is the protein quality control checkpoint of the secretory pathway[10]. Here proteins arrive in an unfolded state and are continuously challenged by ER resident proteins until finding an optimal thermodynamic state that enables their transport to the next compartment[10].

The ER is also the largest intracellular compartment, with a single continuous membrane and a reticular distribution that extends throughout the cell, occupying up to 30% of its entire volume (Figure 4)[7,10]. It comprises the nuclear envelope and the peripheral ER, which membranes are categorized in two types: the rough (RER) and the smooth (SER)[7,17]. RER is characterized by a tubular shape that is in contact with translating ribosomes, whereas the SER is organized in a cisternal shape and is where lipid biogenesis and calcium regulation take place[7].
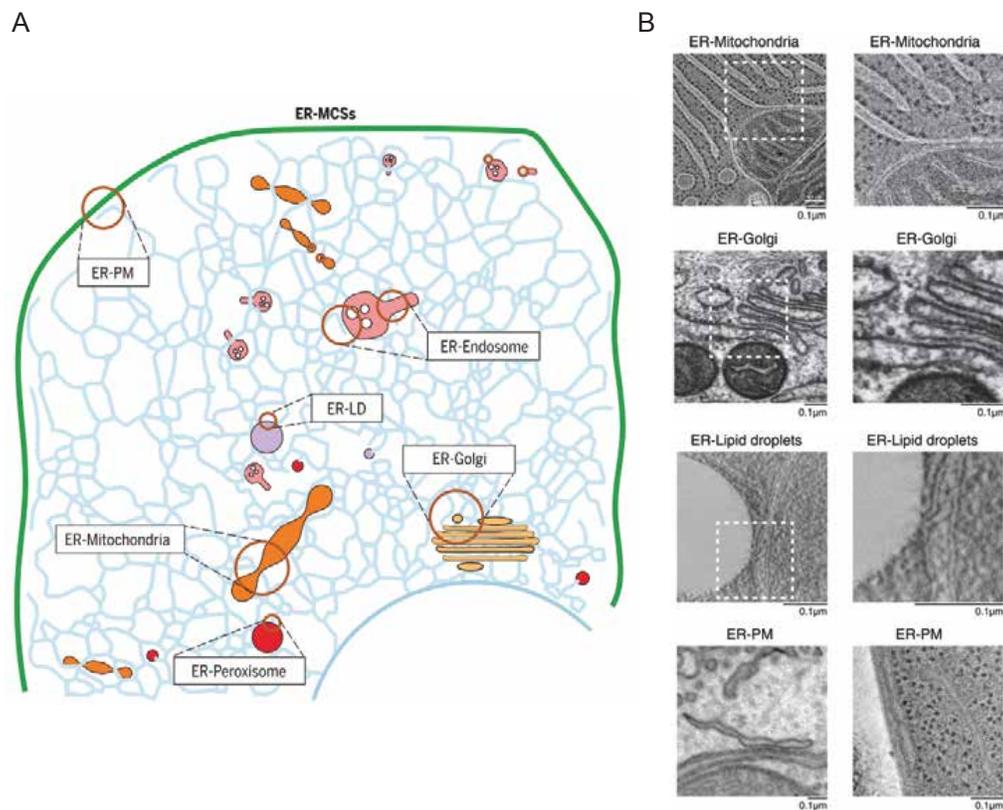
Figure 4. Representation of the ER and its multiple membrane contact sites (MCS). (A) ER and MCSs formed with organelles and the plasma membrane. Brown circles depict contact sites. (B) Electron micrographs of MCSs between ER-organelles (mitochondria and Golgi from rat epithelial

cells), ER-lipid droplets (from yeast cells) and ER-plasma membrane (from mouse neurons). Right column depicts the zoomed area delineated on the left column. Figure modified from Wu et al. (2018)[18].

The ER tubules have also ribosome-free regions that mediate membrane contact with other organelles and the plasma membrane[18,19]. Although for years each organelle was considered as an independent entity, now is clear that organelles "get in touch" with each other and communicate via membrane contact sites (MCSs, Figure 4)[18,19]. Given the broad distribution of the ER throughout the cell, the diversity of ER MCSs is extensive[19]. Interestingly, these contact sites are maintained even during trafficking, fusion and fission of the contacted organelle, illustrating its importance in multiple cellular processes[18].

Soluble resident proteins within the ER are required for the proper chaperoning and transport of secreted proteins[10,20]. They all possess a C-terminal sequence motif, i.e. H/KDEL, that permits their retrieval from the Golgi and retention in the ER and many display Ca2+-dependent activity, making of the ER the largest Ca2+ reservoir inside the cell[7,21–24]. Its role as Ca2+ storage compartment will be discussed further in this section.

Once proteins are properly folded, they accumulate in specialized and highly organized subdomains denominated ER-exit sites (ERES)[7,10,17,25]. ERES are numerously distributed in the ER and constitute the exit point for secretory cargo that needs to be transported to the ER-to-Golgi intermediate compartment (ERGIC)[7,10,13,25]. At ERES proteins that are incorrectly folded are also actively removed and only properly folded ones are allowed to accumulate and be packed into COPII vesicles to be delivered to the ERGIC (Figure 5)[7,10].

The recruitment of protein cargo to ERES is mediated by cargo receptors[10]. These are proteins that recognize properly folded proteins and can recycle back to the ER once their cargo is delivered into the next compartment[10,26,27]. Twenty-four cargo receptors have been identified in mammalian cells, although only few of them bind soluble cargo proteins[10]. ERGIC53, a transmembrane protein that recognizes quality checked pro-cathepsin, α1-antitrypsin and coagulation factors VI/VIII is one of those few identified receptors[27,28].
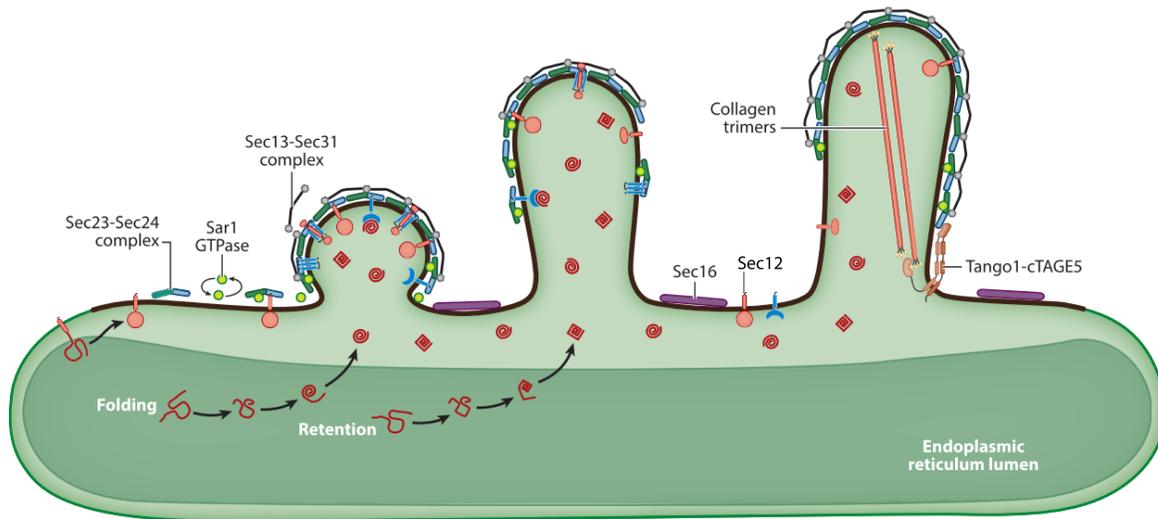
Figure 5. Schematic representation of COPII vesicle formation. COPII assembly begins with the recruitment of Sar1 and its binding to GTP, which allows to recruit the Sec23/Sec24 complex to the ERES membranes. The latter then binds then properly folded cargo, anchoring it to the membrane, while Sec13/31 is recruited. The recruitment of the last complex induces a morphological change in the curvature of the ERES that generates vesicle structures, which later bud and bring cargo to the next compartment in an anterograde manner. Sec16 is a scaffold protein located in the cytosolic face of ERES. Sec16 is thought to stabilize the COPII coat by interaction with the other components, although is not a component of the COPII coat. In addition, TANGO1-cTAGE5 can associate with Sec23A, inhibiting the interaction with Sec13-Sec31 and delaying the vesicle fission. Such a delay has been associated with an increase of size in the carrier that would allow the transport of larger cargo such as procollagen[29]. Figure modified from Barlowe & Helenius (2016)[10].

After cargo binding, the assembly of COPII initiates with the recruitment of Sec12, an integral membrane protein, that mediates the exchange of GDP to GTP (Figure 5)[7,10,30]. Then, Sar1 binds to GTP and recruits Sec23-Sec24 complex, which in turn induces the recruitment of Sec13-Sec31 complexes[10]. These surround the Sec23-Sec24 complex and deform the membrane in a "cage-like" structure that subsequently buds as an anterograde transport vesicle[10,13,29,30].

Although this mechanism is used in general for most of the cargo transported via the secretory pathway, other variables influence protein export and require the use of different transporters[24,29,31,32]. Therefore, in addition to COPII vesicles, Sec16 and TANGO1/cTage5 complexes also coordinate the formation of different transport carriers[24,29]. Nowadays there is

14

no consensus in a single trafficking mechanism, and it is rather alleged that the cell uses in parallel more than one[29]. How does the cell then know which mechanism to choose? The answer relies on characteristics of the cargo such as size and the time frame between fission and fusion of vesicles[29]. This topic will be reviewed with greater detail in a following section.

4.1.3　The ERGIC

Initially ERGIC was not considered a separate compartment but rather the accumulation of a vesicular fraction from the ER[33] or the *cis*-Golgi[34,35] in transit to the next compartment. Nevertheless, currently it is widely accepted that it constitutes a separate and highly dynamic pre-Golgi compartment[24,35]. However, a consensus model that could explain its characteristics and dynamics is still under debate[10,24,35].

Recently, Saraste & Marie (2018) summarized the current 3 models to explain the nature of ERGIC (Figure 6): the first one is based on the concept of transient transport carriers and claims that ERGIC is formed from the fusion of COPII elements that assemble at ERES and move via microtubules coordinated by dyneins in a "stop-and-go" manner (Figure 6a)[35]. In this model, ERGIC is permanently made *de novo* at ERES and fused with *cis*-Golgi, so no difference between transport from ER-to-ERGIC and ERGIC-to-Golgi is made[35].
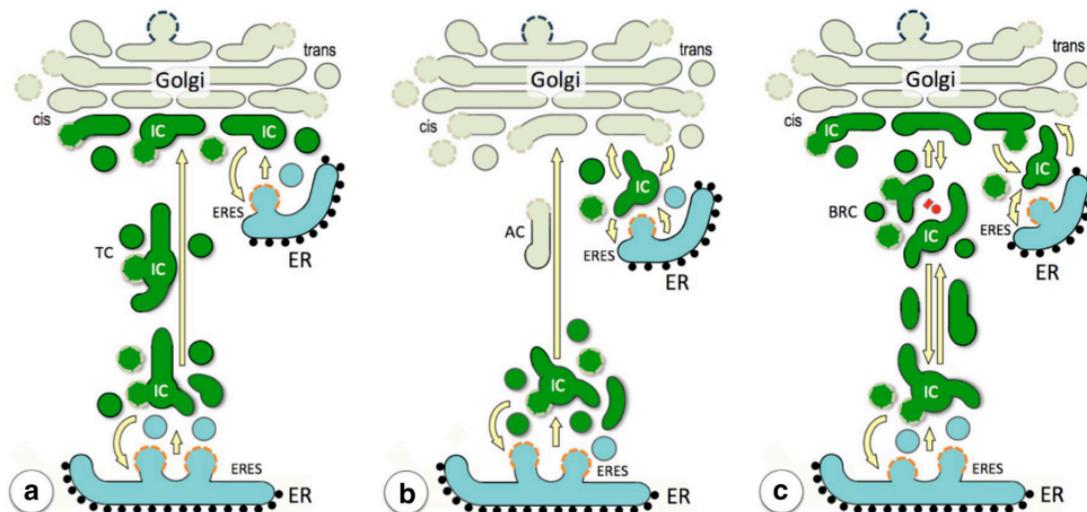
Figure 6.　Models of ERGIC biogenesis. (a) Transient transport carriers' model. In this model, the ERGIC (here named IC: intermediate compartment) is formed by the fusion of ERES-derived COPII vesicles (orange coat) that form tubulovesicular carriers (TC) and mobilize towards the *cis*-Golgi in a "stop-and-go" manner. COPI vesicles can bud from these TCs, and delivery to the Golgi could proceed in a stationary (though vesicles) or maturing fashion (by fusion of several

TCs). Importantly, transport carriers are the same from ER-to-ERGIC and from ERGIC-to-Golgi. (b) Stationary ERES-associated membrane clusters model. Here ERGIC is a defined intermediate compartment with tubulovesiclular clusters residing close to ERES. Cargo transport is accomplished by COPII vesicles from ER-to-ERGIC and by a different anterograde carrier (AC) from ERGIC to *cis*-Golgi. (c) Permanent network of dynamic vacuoles and tubules model. This is the most recently proposed model and combines elements of the two previously described ones. Here ERGIC is mobile but permanent and connects to ERES and Golgi through an interconnected network. Saraste & Marie (2018) define it as a Biosynthetic Recycling Compartment (BRC), where cargo dynamically moves both in an anterograde and retrograde manner. Figure taken from Saraste & Marie (2018).

In the second model (Figure 6b), ERGIC is an independent organelle that communicates with ERES via "tubulovesicular clusters (VTCs)" and has different transport carriers to receive and deliver cargo: from the ER, COPII vesicles arrive, are then fused to ERGIC and newly packed in an anterograde carrier that will deliver cargo to the *cis*-Golgi[35]. This model is supported by the experiments performed with cells previously treated with brefeldin-A (BFA, a compound that disrupts Golgi membranes)[36]. In these experiments, Ward et al. (2001) observed that ERGIC53 was not fused with the ER, but rather remained associated to ERGIC membranes[36]. Also, Ben-Tenkaya et al. (2010) showed that ERGIC does not localize to the Golgi, and Farhan et al. (2008) demonstrated that in neurons, an additional signal is required for GABA-transporters to leave the ERGIC[37,38].

Finally, the third model describes a combination of both previous models (Figure 6c)[35]. Here, ERGIC is considered a permanent, though mobile organelle that is connecting ERES and Golgi via a network that constantly fuses and fissions anterograde, but also retrograde, vesicles[35]. These vesicles and tubules are transported via microtubules in a "stop-and-go" manner[35]. Such a model is supported by recent findings from Park et al. (2015) who showed that COPI vesicles, largely considered exclusive for retrograde transport, could participate in anterograde trafficking to the Golgi and also generate tubules that connect Golgi stacks[39].

ERGIC is not only an important station for anterograde, but also for retrograde trafficking[10]. Currently, 2 mechanisms for the retrieval of ER proteins and membranes have been described: COPI trafficking and Rab6-mediated tubular elements[10]. COPI vesicles are directed to the ER either from the ERGIC or the *cis*-Golgi and mediate retrograde trafficking by recognition of a retrieval signal on the cytosolic side of ER proteins[10,40]. Meanwhile, Rab6-mediated retrograde

transport requires the formation of tubules from the *cis*-Golgi (Rab6 will be described with more detail in a further section)[40].

Although the precise mechanism for Rab6-tubulation is not known, Heffernan & Simpson (2014) proposed that the antagonist activity of cytosolic phospholipase 2 α (cPLA2α) and lysophospholipid acyltransferases could induce tubulation of ER accumulated cargo at the *cis*-Golgi and recruit Rab6 for the subsequent retrograde translocation[40]. Whether this hypothesis holds true requires further investigation.

4.1.4   The Golgi complex

The Golgi apparatus was described for the first time in 1898 by Camilo Golgi as an "internal reticular apparatus"[41]. Later on, with the development of electron microscopy (EM), Palade and Fahrquar developed cytochemical stainings that allowed to identify the *cis*-to-*trans* polarity in the Golgi[42].
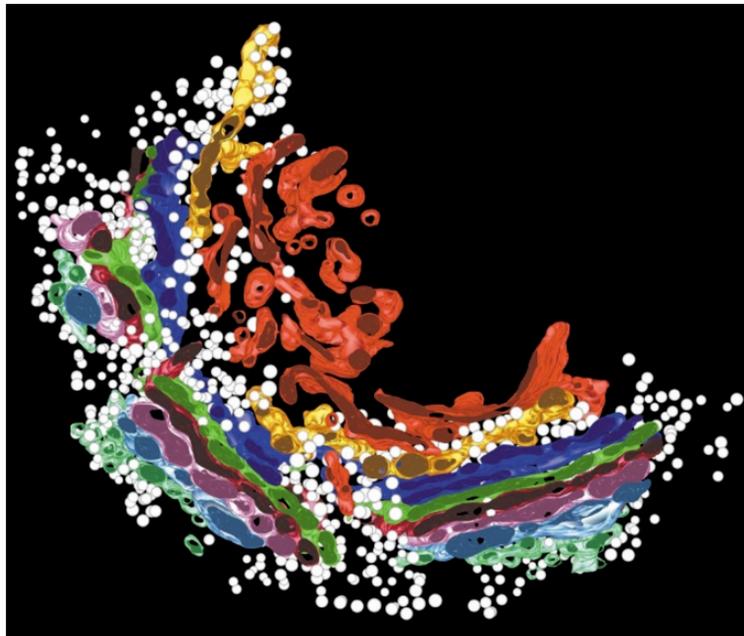
Figure 7.   The Golgi complex. Model of part of the Golgi ribbon from a 3D reconstruction. For this example, the Golgi has seven cisternae, colored from *cis* (in light blue) to the TGN (in red). The white spheres represent both clathrin coated and non-clathrin coated vesicles, illustrating its central role in vesicles trafficking. Figure taken from Marsh & Kowell (2002).

Nowadays, the improvement of CryoEM and 3D-EM techniques, plus the development of fluorescence light microscopy techniques, has allowed to visualize ultra-thin sections of down to 3 µm and to a better understanding of the trafficking dynamics at the Golgi (Figure 7)[43,44].

The Golgi is also the master of the secretory pathway[45]. Here, proteins are glycosylated, segregated and properly sorted into vesicles targeted to the plasma membranes or another specific compartments[44]. Furthermore, lipids and carbohydrates are also constantly participating in these processes[44]. The next sections will focus on how Golgi successfully accomplishes cargo trafficking, sorting and delivery in the secretory pathway.

4.1.4.1 Structure

In order to achieve its multi-tasking role, the mammalian Golgi is segregated into 4 main compartments or cisternae, namely: *cis*, medial, *trans* and *trans*-Golgi network (TGN, Figure 8)[46]. Each of these compartments is organized in such a way that cargo can be modified post-translationally and mature upon its arrival to the TGN[8,47,48]. To do so, specific proteins are associated with each cisterna and a gradient of both Ca2+ and pH is maintained by the constant influx and efflux of ions and membranes[44,49–52].
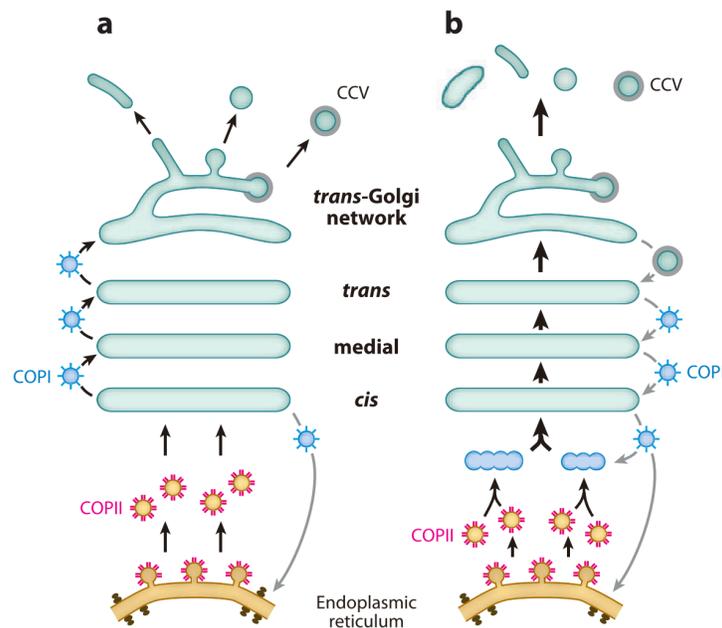
Figure 8. Membrane trafficking models in the Golgi. (a) The stable compartment model claims that each compartment is static or fixed and defined by a specific set of resident Golgi proteins. Cargo is therefore transported in vesicles to the next compartment. (b) The cisternal maturation model states that each compartment is formed *de novo* and progress by permanent vesicle

trafficking until reaching maturation (TGN). In this model, cargo never leaves the compartment. Figure taken from Glick & Nakano (2009)[47].

The mechanism by which this compartmentalization is maintained is still under debate; however, two main models of membrane trafficking are considered more likely: the fixed compartment model and the cisternal maturation/progression model (Figure 8)[47,48,50,53–56]. In the fixed compartment model, the Golgi is seen as a closed membrane that actively transports cargo across stacks by constant vesicle fission and fusion (Figure 8a)[29,56–58].

On the other hand, the cisternal maturation model claims that the process is more dynamic and cargo never leaves the Golgi (Figure 8b)[46,47,59]. Instead, the cisterna matures until becoming TGN and distributes to vesicles that are either recycled to the ER or exported to the target compartment or the plasma membrane[46]. Although the secretory pathway is highly conserved, the cisternal maturation model is mainly supported by data from yeast, whereas the compartment model better explains protein trafficking in mammalian cells[57].

The controversy between those mechanisms remains because up to date there is evidence supporting both[56,60–62]. However, a consensus towards a combination of both mechanisms is lately taking place. In this regard, Kurokawa et al. (2019) showed how in yeast, transmembrane secretory cargo is restricted to an area in the maturing cisterna and then localizes towards a mature zone inside it. Although the data would support the cisternal maturation model, their observations show that the cisternae are not static, and therefore another kind of continuities between Golgi compartments, such as the ones described by Beznoussenko et al. (2014) would be required for cargo transport[48,61].

Golgi compartments are determined by the stack: an accumulation of cisternal membranes one on top of another that are laterally interconnected with tubules (the non-compact zone) and localizes, mainly, in the perinuclear area[44,63]. The accumulation of these structures is known as the Golgi ribbon, and is what gives it its particular shape[63]. Given the continuity in structure, but also the compartmentalization of each stack, how can the Golgi maintain at the same time continuity and separation?

4.1.4.2   Golgi organization

Golgi ribbons are characterized by a flat morphology in the middle (10-20 nm) that expands towards the rims (~100 nm)[44]. Importantly, the Golgi rims display tubular structures

denominated fenestrae, which promote cargo trafficking by increasing "the surface-to-volume ratio of the cisternae and (…) the fraction of the membrane that is highly curved"[47], which stimulates the accumulation of cargo at the rims and the synthesis of vesicles to transport cargo to the next compartment (Figure 9)[43,44,47,56,64].
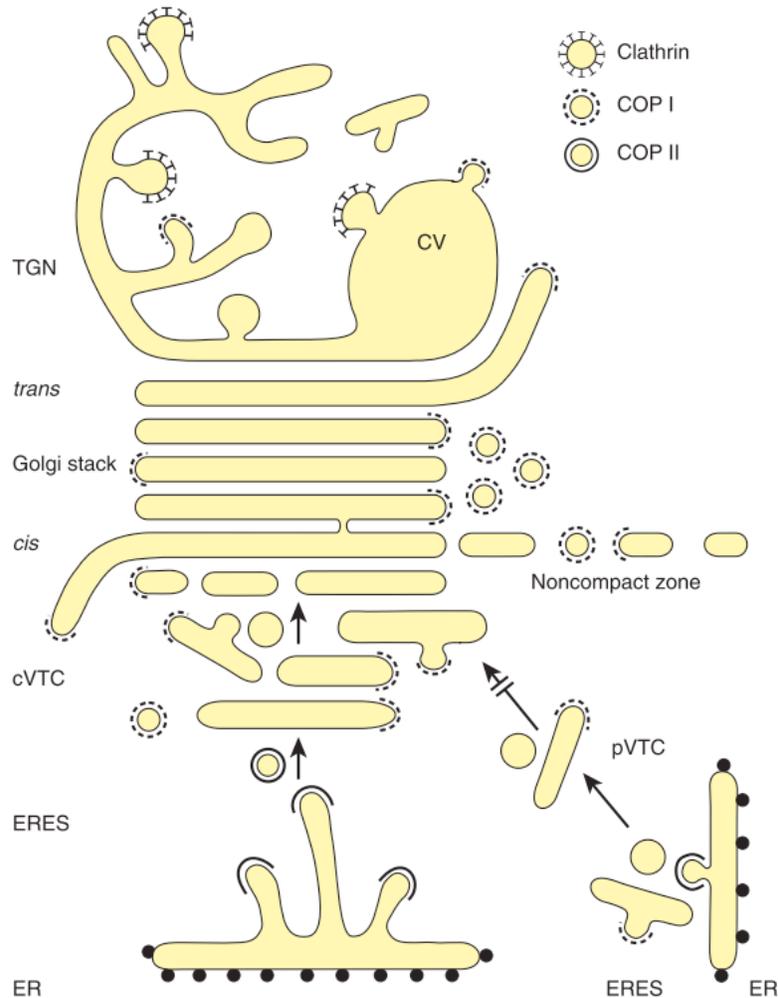
Figure 9. Golgi schematic view with associated membrane network. pVTC: peripheral tubulovesicular carriers; cVTC: central tubulovesicular carriers; CV: condensing vacuole. Figure taken from Klumpermann (2011)[44].

In general, Golgi morphology is maintained by Golgi ReAssemble Stacking Proteins (GRASPs) and Golgins, structural proteins that keep the stacks together and shape the Golgi[44,65–67]. In particular, GRASPs are synthesized in the cytoplasm and subsequently recruited to the cytoplasmic face of the Golgi via N-glycinemyristoylation and binding to Golgins[66,68].

They are characterized by a conformation that enables either *cis* or *trans* interaction with other GRASPs and, depending on the orientation, this promotes GRASPs accumulation or tethering with an opposing membrane (Figure 10)[63,65–67,69,70].

Two GRASPs have been identified as components of the Golgi structure: GRASP55 at the medial-*trans*-Golgi interphase and GRASP65, located at the *cis*-Golgi compartment[66,67,69,71]. Previous reports have demonstrated that in the absence of GRASPs, the Golgi can cope with keeping the stack integrity, but the trafficking of protein cargo is impaired[66,67]. Interestingly, in this scenario, protein trafficking is faster, and cargo is not properly glycosylated, suggesting a role in timing control of trafficking to allow proper protein glycosylation[67].

(A) Tethering/traffic

(B) Tethering/ribbon formation

(C) Tethering/stacking

Legend
golgins
) SNAREs
stacking proteins (e.g. GRASPs)
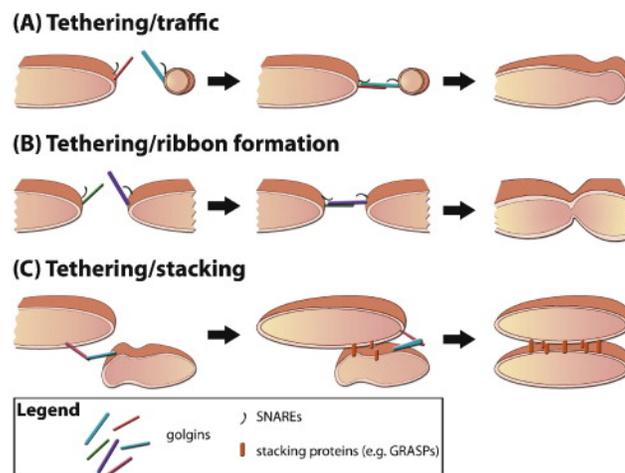
Figure 10. GRASPs and Golgins are responsible for Golgi membrane tethering during membrane trafficking (A), ribbon formation (B) and stacking (C). Figure taken from Barinaga-Remeneria Ramirez & Lowe (2009).

Together with GRASPs, Golgins also participate in trafficking, ribbon formation and stacking[65,72]. Golgins are coiled-coil proteins mainly involved in vesicle "catching" and tethering[63,65,73]. They bind via the C-terminal domain and associate in a direct (via transmembrane domains) or indirect manner (via protein-protein interactions) with the cytosolic face of Golgi membranes[73]. Their distribution is varied both across the membrane compartments, as well as within a stack, with some Golgins having preference for the flat center of the ribbons (like GM130 at the *cis*-Golgi) and others for the rims (i.e. giantin and golgin-84)[65,73].

Most Golgins bind Rab GTPases (Rabs), mediating their membrane recruitment in this way [74]. Rabs belong to the Ras family of small GTPases, which were initially identified in yeast[75]. More than 70 different Ras-like proteins have been identified in mammals and, among these, around 20 are associated with the Golgi, with Rab6 being the most abundant one[75]. Rabs function as a molecular switch, activated by binding to GTP[76]. This activation is mediated by Guanine Exchange nucleotide Factors (GEFs), whereas their inactivation is induced by GTPase activating proteins, which induce GTP hydrolysis to GDP[76].
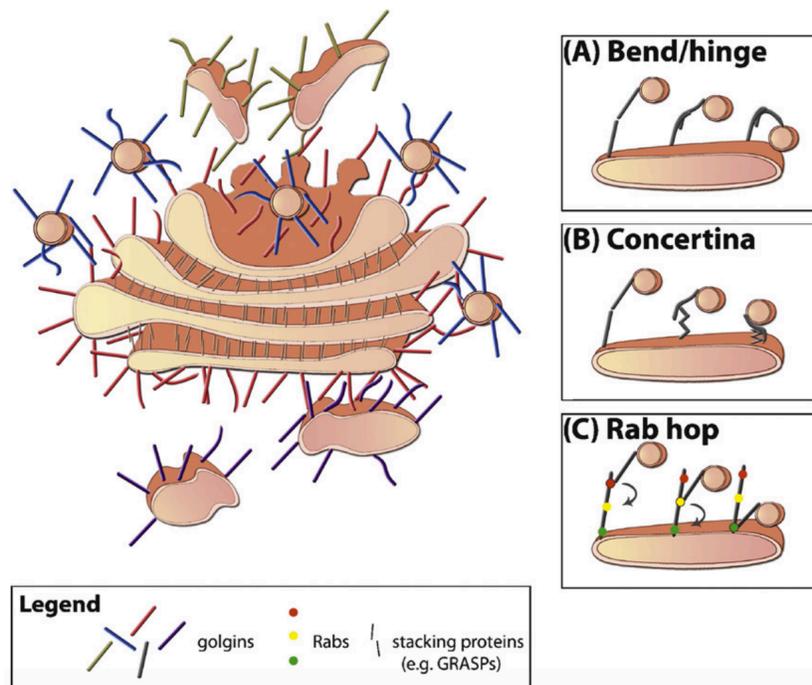
Figure 11. Model depicting the role of Golgins as "tentacles" projecting from the Golgi surface. Golgin tethering can occur via bend (flexible joint that brings membranes together), concertina (bringing membranes together in a "spring-like" manner) and Rab hop (moving the income carrier through differential Rab binding towards the final fusion site). Figure taken from Barinaga-Remeneria Ramirez & Lowe (2009).

These activation/inactivation cycles regulate Rab recruitment of downstream effectors, such as motor proteins and tethering factors, modulating specificity and adequate vesicle targeting to their respective cytoskeletal motor protein or membrane receptor[75]. Recently, it has been shown that Rabs can define the polarity of the secretory pathway by the establishment of Rab cascades, namely the organized sequential recruitment of Rabs due to the differential presence

of effectors along the pathway[75]. However, the discovery and linking of all GEFs and GAPs distributed along the pathway is still required to establish how cells define and "maintain secretory and endocytic pathways"[75].

The interaction between the described elements constitutes the basis for trafficking regulation. In this regard, it is known that the complex formed between GRASP65 and GM130 acts as Rab1 effector that regulates the fusion of COPII vesicles at the *cis*-Golgi[71]. Furthermore, GRIP-domain Golgins –i.e. Golgins with an Arl1 Rab GTPase binding site– are widely localized at the TGN and mediate the retrieval of endosomal cargo back to the Golgi (e.g. TGN46)[77,78]. Besides their tethering and fusion mediating role, some Golgins have been involved in the formation of transport carriers; this is the case for Golgin-160, which mediates Golgi sorting of the GLUT4 glucose transporter in adipocytes[65].

Such diversity in interactions is reflected by the tentacle model proposed by the Munro group, where Golgins are attached to the Golgi surface like tentacles that capture different vesicles, tubules and other Golgi elements via different Rab binding sites[72,79]. In this way, Golgins can promote vesicle or tubular transport along the membranes towards their target destination, resulting in fusion or anchoring to their target membranes (Figure 11)[72,79]. So now, how do vesicles fuse to the *cis*-Golgi and initiate their maturation process?

4.1.4.3   Membrane dynamics

Intracellular vesicle fusion is mainly mediated by Soluble *N*-ethylmaleimide-sensitive factor Attachment protein Receptors (SNAREs)[73,80]. These membrane-associated proteins have 2 characteristic motifs, the vesicle-root SNARE (or vSNARE) and the target membrane-associated one (tSNARE)[73,80,81].

Structurally, SNAREs assemble in a bundle composed by three Q-SNARE chains (belonging to tSNARE) and one R-SNARE chain (from vSNARE), according to their positions in the tethering area (Figure 12A)[80,81]. The described chains can bind from N- to C-termini in a zipper-like manner, bringing two membranes close enough to promote fusion (Figure 12B)[80,81].
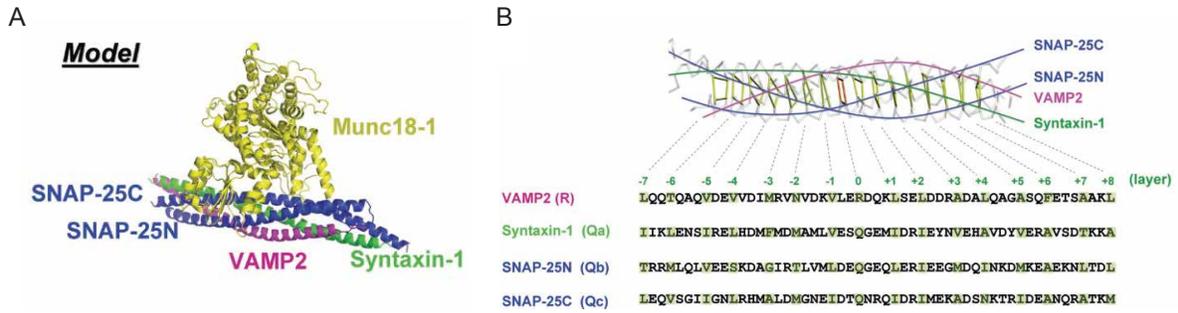
Figure 12. SNAREs as membrane tethers. (A) Model of the complex SNARE-Munc18 (a chaperone protein). The SNARE bundle is formed by VAMP2 (R-SNARE) and the Q-SNARES Syntaxin-1, SNAP-25C and SNAP-25N. (B) Detail of the zipper binding between R-SNARE and the three Q-SNARE helices. Figure modified from Rathore et al. (2011).

A critical aspect of SNARE-mediated fusion is the requirement of Ca2+[81–83]. One of the best described mechanisms for vesicles fusion was first documented in neuronal cells, where it is known that synaptic vesicles fuse only after an increase in the surrounding Ca2+ concentration of around 10-100 fold[83,84]. In synaptic neurons, for example, synaptotagmin-1 is anchored to the membrane and binds Ca2+ in order to enable Q-SNAREs (such as Syntaxin and SNAP-25) to make the bundle with the R-SNARE synaptobrevin[81,82]. This minimal fusion machinery highlights the importance of Ca2+ in membrane trafficking.

4.1.5 Importance of calcium in the secretory pathway

In the secretory pathway, Ca2+ has been shown to be essential for signaling[38,83,85,86], polarity maintenance[49,87,88], trafficking regulation[83,89,90], vesicle fusion[91,92] and sorting[52,93–96]. Two kind of proteins regulate intracellular Ca2+ levels: (1) luminal or cytosolic Ca2+ binding proteins that act as buffers regulating Ca2+ without changing the total amount inside the cell, and (2) transmembrane proteins that regulate Ca2+ concentration in intracellular compartments by active or passive Ca2+ transport across membranes[85,86].

The ER is considered the biggest Ca2+ reservoir in the cell, with luminal concentration ranging from 300-700 μM[52,92]. Ca2+ influx at the ER is regulated by the SarcoEndoplasmic Reticulum Ca2+ transport ATPase (SERCA), whereas Ca2+ efflux takes place via inositol 1,4,5-phosphate receptors (IP₃Rs) and ryanodine receptors (RyRs, Figure 13)[97,98]. Importantly, the maintenance of Ca2+ pools is essential for the formation of Ca2+ gradients for protein trafficking[51,83,85]. It has been shown that Ca2+ leakage is necessary for vesicle fusion with the Golgi, as Ca2+ chelators block intra-Golgi transport[83,99]. Moreover, Porat & Eleazar (2000)

showed that it is actually the Ca2+ gradient what regulates fusion events in the secretory pathway[99].

In order to keep a Ca2+ gradient, several pumps and channels are also expressed in a gradient manner along the Golgi compartments[51,52,98,100–102]. In this regard, the *cis*-Golgi requires SERCA pumps for Ca2+ influx and IP3 channels for Ca2+ release, whereas, at the *trans*-Golgi compartment, Ca2+ transport is mainly regulated by the Secretory Pathway Ca2+ ATPase type 1 (SPCA1, Ca2+ influx) and RyRs (Ca2+ efflux, Figure 13)[49,51,52,89,90,98]. Although still not thoroughly studied, it has been suggested that the medial-Golgi would then harbor a mixture of IP3Rs and SERCA on its *cis* face and RyRs and SPCA1 on the *trans* side[51,52].
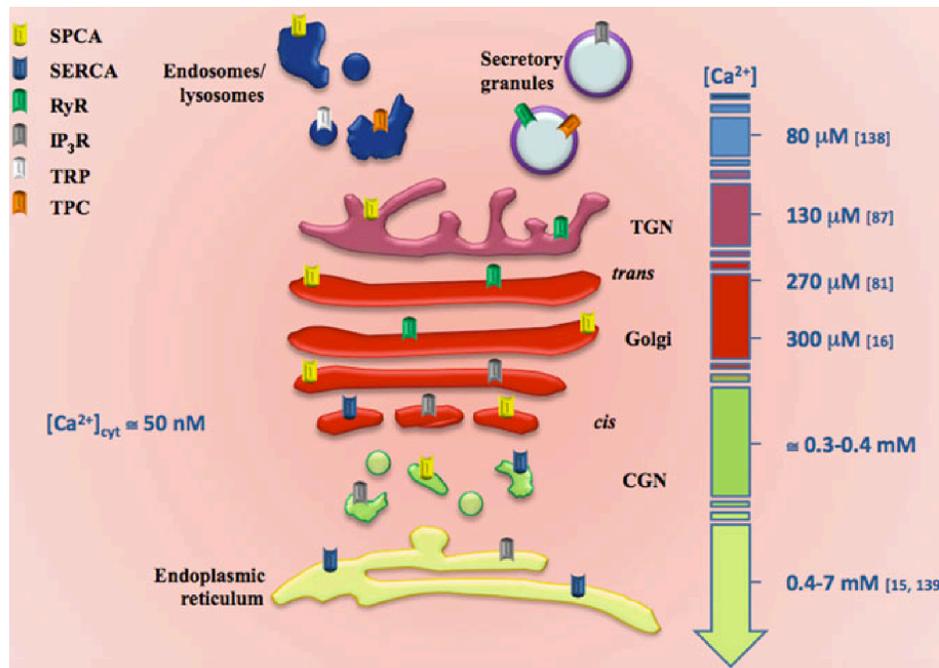
Figure 13. Ca2+ gradient along the secretory pathway. Ca2+ concentration reduces from ER to Golgi owing to the presence of different Ca2+ pumps and ionic channels along the secretory pathway. SPCA: Secretory Pathway Ca2+ ATPases; SERCA: SarcoEndoplasmic Reticulum Ca2+ transport ATPase; RyR: ryanodine receptors; IP3R: inositol 1,4,5-phosphate receptors; TRP: Transient Receptor Potential channel; TPC: Two Pore Channel. Concentration shown on the right side indicate Ca2+ concentrations in each compartment. [Ca2+]cyt: Ca2+ concentration in the cytosol. Figure taken from Micaroni (2012)[85].

Micaroni et al. (2010) documented changes in cytosolic Ca2+ upon arrival of cargo at the *cis*-Golgi and found that Ca2+ concentration increases in the cytosol during cargo passage through the Golgi[83]. They evidenced that the cytosolic Ca2+ gradually changes as long as cargo traffics towards the TGN and therefore suggest that such behavior could be explained by changes in pH caused by the disruption of membrane connections [83,99].

The Ca2+ concentration at the Golgi diminishes from *cis* to *trans* (300 – 150 μM), reaching the lowest concentration at the TGN (50 – 100 μM)[52]. Noticeably, there is a marked separation between the *trans*-Golgi and the TGN, which are segregated by membrane diffusion with no Ca2+ flow between them[52].

In addition to membrane channels and receptors, luminal Ca2+ binding proteins also localize in a gradient manner within the Golgi lumen[103–106]. Here, three proteins are considered the major Ca2+ regulators: nucleobindin-1 (NUCB1) in the *cis*-Golgi[104,106], DNA-binding EF-hand Acidic amino acid-rich non-glycosylated Ca2+-binding protein (NEFA/p54) in the medial[87] and Cab45 in the *trans*-Golgi and TGN[95,96,103,107]. Given the presence of specialized Ca2+ buffers in each cisterna, it is speculated that impairment in cargo trafficking would strongly affect Ca2+ concentrations within the Golgi[85].
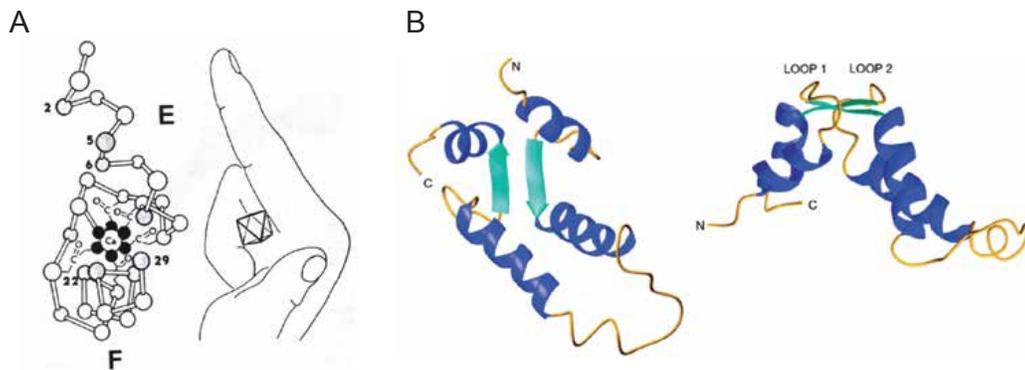
Figure 14.   Structure of the EF-hand domain (A) and ribbon diagram of tertiary fold of human NUCB1's EF-hand domains. Figures adapted from (A) Carafoli & Krebs (2016)[86] and (B) de Alba & Tjandra (2004)[108].

The three mentioned luminal proteins belong all to the Ca2+ binding EF-hand family, a protein group that shares a homologous region called the EF-hand domain (Figure 14)[86,109,110]. This domain consists in a helix-loop-helix motif that binds Ca2+ with high affinity[86,95,109]. The

denomination of EF-hand arose from the orientation of the 5th (E) and 6th (F) α helices at enclosing the Ca2+ binding loop, which resemble a hand shape (Figure 14A)[86,110].

Among the 3 proteins described, Cab45 has been the best characterized. It belongs to the CREC family of proteins (CREC: Cab45, Reticulocalbin, ER55 and Calumenin), a group of EF-hand proteins localized in the secretory pathway[22,111]. Its role in this pathway is still under study, however, research from the von Blume Lab has advanced our knowledge of its role in protein sorting.

The group first showed that Ca2+ is required to retain Cab45 at the TGN[107]. Then, Crevenna et al. (2016) characterized the six EF hand motifs of Cab45 and demonstrated its oligomerization upon SPCA-induced Ca2+ influx[95]. Further on, Deng et al. (2018) demonstrated that Cab45 EF-hand domains are organized in 3 different pairs, and that EF pairs 1 and 3 are essential for Ca2+ binding and proper Cab45 localization in the Golgi; moreover, they propose that oligomerized Cab45 binds to cargo and regulate its sorting into sphingomyelin-rich vesicles (Figure 15)[96].
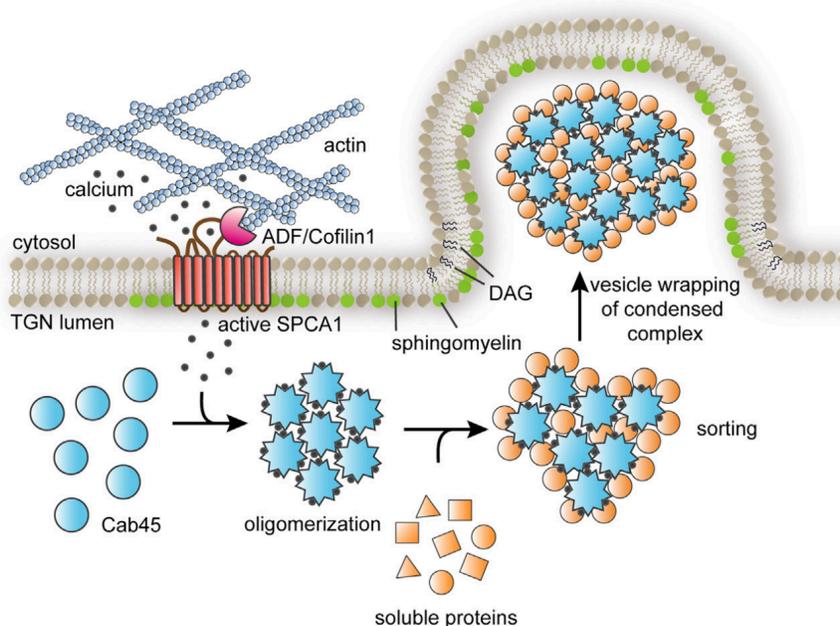
Figure 15. Cab45-mediated protein sorting model. Deng et al. (2018) propose in this model that Cab45 oligomerizes upon Ca2+ influx to the TGN. This influx is provided by SPCA1, which is activated by the interaction with ADF/Cofilin. Once oligomerized, Cab45 binds cargo in an

unknown manner, and promotes its sorting into sphingomyelin-rich vesicles[96]. Figure taken from Deng et al. (2018).

In contrast, the role of NUCB1 in protein trafficking, is poorly characterized. Although Lin et al. (1999) showed that it is a major regulator of Ca2+ homeostasis in the *cis*-Golgi, and that its activity is influenced by SERCA, no role in trafficking has been defined so far[112]. NUCB1, also known as CALNUC in humans or Nuc in rats, displays 2 isoforms, one of which localizes to the Golgi and a cytoplasmic version (sNUCB1), lacking the first 26 amino acids of its signal sequence[106,113]. The latter has been studied more thoroughly and is known to regulate Gai3 activation[114–117], to inhibit amyloid precursor protein (APP) aggregation[118,119] and to participate in LRP9 receptor recycling[120,121]. NUCB1, unlike Cab45, possesses only two EF-hand motifs, though both have been shown to be essential for interaction with G-proteins and the maintenance of Ca2+ homeostasis[108,112].

Finally, NEFA, or p54/NEFA, is the least characterized of these three proteins. It was initially found in a human leukemia cell line and besides its two EF-hand domains (Figure 14B), which show high homology with the ones of NUCB1, it has a DNA-binding domain and a leucin-sipper domain[122,123]. Morel-Huaux et al. (2002) identified it as a medial-Golgi resident protein by co-localization analysis with mannosidase II[87]. Further investigation is required to determine the function of p54/NEFA and its role in protein trafficking.

As mentioned before, Ca2+ entry at the Golgi is tightly regulated by SERCA and SPCA1, but how does this Ca2+ regulation actually influence protein trafficking? One of the first studies that evaluated the role of Ca2+ in cargo trafficking evidenced that a low cytosolic Ca2+ concentration is required for cargo trafficking, since increases above ~100 nM inhibit protein transport at the Golgi[99]. Moreover, Porat & Elazar (2000) demonstrated that Ca2+ efflux was required for protein trafficking at the Golgi, an observation that was later confirmed by experiments from Vanoevelen et al. (2005), who showed that inhibition of SERCA and SPCA1 reduced Ca2+ release to the cytosol.[101] Furthermore, experiments using histamine-induced Ca2+ signaling showed that Golgi integrity is necessary for intracellular Ca2+ signaling[101].

Later on, Lissandron et al. (2010) showed that inhibiting SERCA stimulated faster Ca2+ refilling at the TGN probably due to an increase in cytosolic Ca2+, whereas SPCA1 silencing provoked a delay of cargo trafficking, although not a complete block[49]. Moreover, Aulestia et al. (2015) demonstrated a higher Ca2+ affinity at *trans*-Golgi, than at the *cis*-Golgi or ER,

consistent with the higher affinity of SPCA1 for Ca2+ compared to SERCA[52]. They suggest that the differences in affinities could be explained by the need of keeping stable Ca2+ concentrations at the *trans*-Golgi and TGN to avoid impairments in protein trafficking[52].

In addition to the described Golgi-resident Ca2+ channels, pumps and buffers, another group of proteins, that do not permanently localize to the Golgi, can be recruited upon changes in the cytosolic Ca2+ concentration[85]. This group encompasses kRas, Ras-GRP, Ca2+-sensor proteins (such as hippocalcin) and cPLA2, which will be discussed in more detail below[68,85].

cPLA2 has been shown to be a key element in the regulation of Golgi and ER membrane tubulation[38,48,59,85,124]. cPLA2 is a protein that shuttles between the plasma membrane and the Golgi upon changes of Ca2+ concentrations in the cytosol, with increasing Ca2+ favoring its re-location to the Golgi[38,59].
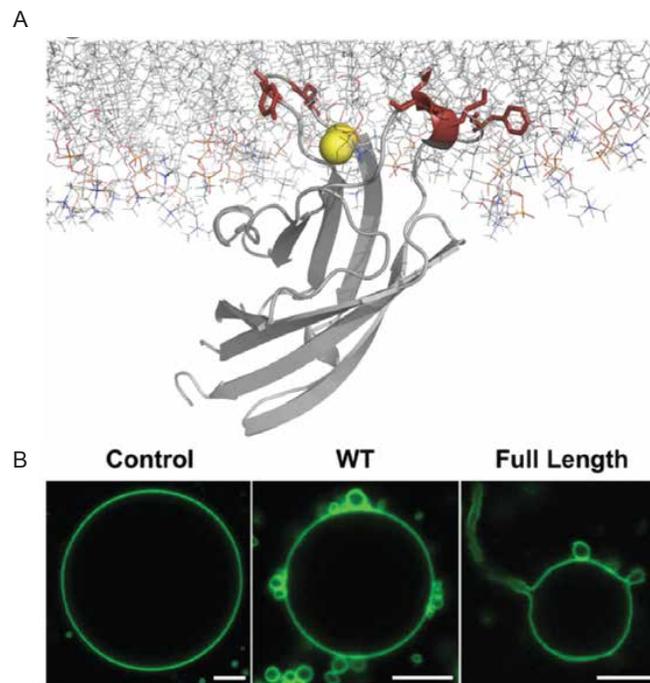
Figure 16. cPLA2α penetrates the membrane upon Ca2+ binding and induces changes in membrane curvature. (A) Structure of the C2 domain of cPLA2α membrane association. Upon Ca2+ binding, the C2 domain interacts with 1-palmitoyl-2-oleoyl-sn-glycero-3-phosphocholine (POPC) membranes via its two Ca2+ binding domains. Image obtained using electron paramagnetic resonance (EPR). (B) WT C2 domain of cPLA2α induced membrane curvature changes in the presence of 500 nM CaCl$_2$ to POPC containing GUVs, but not tubulations. These

were only observed when the full-length protein was evaluated. Figure modified from Ward et al. (2012)[124].

Although cPLA2 activity initiates the arachidonic acid cascade, an α isoform of the protein (cPLA2α) "hydrolyzes the fatty acids (FA) at the middle ester bond of cylindrical phospholipids to form wedge-shaped lysophospholipids"[85]. This reaction is of particular importance since it is known that the accumulation of wedge-like lysophospholipids promotes a spontaneous curvature of the membrane, and this in turn can transform flat membrane cisternae into cylindrical tubular shapes –membrane tubules–, and therefore connect Golgi stacks[59,85,125,126].

Moreover, Ward et al. (2012) demonstrated that the N-terminal C2 domain of cPLA2α penetrates the membrane in a Ca2+-dependent manner, whereas its catalytic C-terminal domain was required for activity. Therefore, the insertion of the full-length protein is required for Golgi tubulation (or vesiculation) as the insertion of the C2 domain only induces curvature albeit not tubulation (Figure 16)[124].

Altogether this evidence highlights the importance of Ca2+ in signaling, protein translocation, Golgi architecture, and protein trafficking. However, the components participating in Ca2+-dependent protein trafficking remain poorly understood. Therefore, a better understanding on the mechanisms behind the regulation of intracellular trafficking would shed light into the dynamics of cell-to-cell or cell-to-matrix communication. Given that a big percentage of the secreted proteins are crucial for the transformation of the extracellular matrix, the components and dynamics of cell-to-matrix communication will be detailed in the next section.

4.2   The Extracellular Matrix

The extracellular matrix (ECM) is the ensemble of proteins, glycans and other molecules that provide structural support for the cells to develop into tissues[127,128]. Besides its scaffold role, it serves as a platform for cell signaling, migration, proliferation and regeneration[129]. The ECM is a 3D network that undergoes permanent remodeling in order to keep tissue homeostasis, which is reflected by the multiple diseases developed upon mutations in genes encoding ECM components, such as cancer, osteoarthritis, Ehlers-Danlos syndrome, Marfan syndrome, congenital muscular dystrophies, among others[127,128].

The ECM can be classified in two kinds: the basal or basement membrane, which is located basolaterally to the epithelium and endothelium, is more compact and provides the support for epithelial cells, and the interstitial connective tissue, which is more flexible and serves as a scaffold for the building of tissue (Figure 17)[127,128]. ECM is remarkably important for the immune system as it provides an insoluble organized structure where leukocytes can migrate and communicate by integrating different signals[130]. In this regard, the ECM provides the platform for leukocytes to trans migrate from blood vessels to the injured tissue and initiate healing processes[130].

More than 300 proteins constitute the ECM in mammals, among them 43 collagen subunits, 36 proteoglycans and more than 200 complex glycoproteins[127]. The interaction of these components with cell receptors and signal molecules enables the complex and dynamic remodeling of the ECM[127].
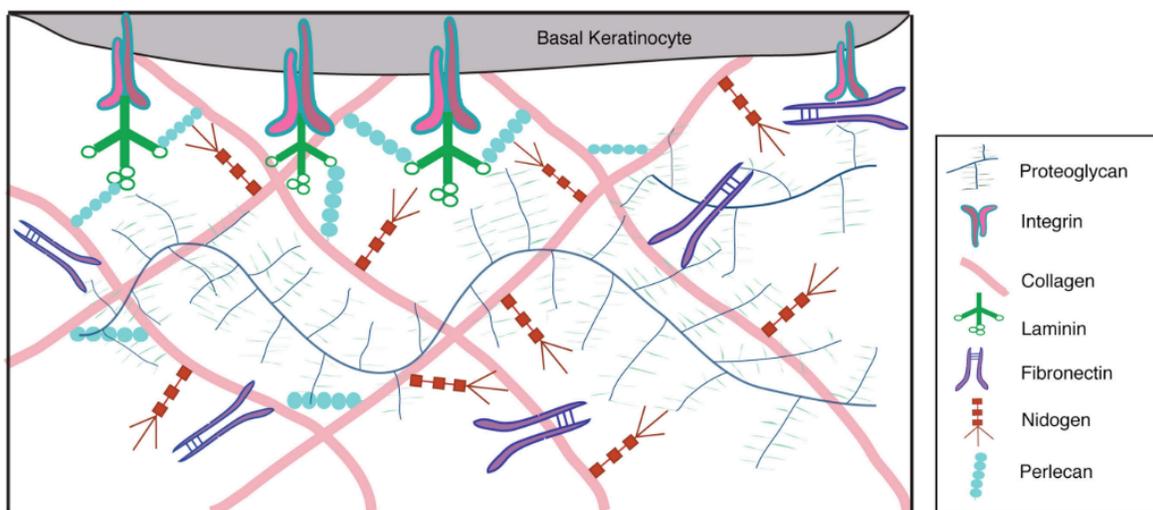
Figure 17. Schematic representation of the skin ECM depicting its main components. Figure taken from Bhattacharjee et al (2019)[131].

4.2.1   Composition

The major components of the ECM can be classified in six main groups, namely collagens, elastin, laminins, fibronectin, matricellular proteins and proteoglycans[128]. All of them can be

differentially expressed according to the physical structures of the tissue, as well as the cell signaling of health or disease states[128]. These components are briefly described hereunder:

4.2.1.1   Collagens

Collagens are the most abundant component of the ECM[128,132]. Their structure consists of triple helices formed by the interconnection of 46 polypeptide α chains, which are formed by the helical interaction of collagen polypeptide chains rich in proline and glycine[132]. Twenty-eight different collagens classified in 6 different groups according to their functionality[128]: (1) fibrillar, the most abundant and widespread (collagens I-III, V, XI, XXIV and XXVII); (2) network forming, which build more complex molecular structures (IV, VIII and X); (3) fibril-associated with interrupted triple helices, which regulate fibrillogenensis (IX, XII, XIV, XVI, XIX-XXII); (4) membrane associated with interrupted triple helices, which can act as surface receptors and play a role in cell adhesion and motility (XIII, XVII, XXIII and XV); (5) self-assembled collagens, which connect other components within the tissue (VI, VII, XXVI and XXVIII); and finally, (6) multiplexing collagens, which are characterized by a non-collagenous C-terminal and can mediate the interaction of the basal membrane with connective tissue[128,133].

4.2.1.2   Elastin

Elastin is the main component of continuous stretching tissues, providing elasticity via its intrinsically disordered structure[128]. Tropoelastin, its precursor, is rapidly assembled into complex structures upon secretion to the ECM. The high content of hydrophobic amino acid on its structure facilitates the assembly of elastin and constitutes a key aspect for the maintenance of elasticity on the tissue[134].

4.2.1.3   Laminins

Laminins are among the main components of the basal membrane and can initiate its assembly by binding to cells, other laminins or other basal membrane components, such as collagen IV[135]. In addition, they mediate anchoring of cells to the basal membrane via interaction with surface sulfated glycolipids, integrins and dystroglycan receptors that connect the extracellular matrix with the cytoskeleton[135]. Sixteen different combinations of α, β and γ chains interacting via their coil-coiled domain have been identified in vertebrates *in vivo*, assembled either in rod-, Y- or cross-shapes[128,135]. Altogether, laminins play an important role in cell differentiation,

adhesion and migration via their interaction with integrin and proteoglycan receptors in epithelial cells[136].

4.2.1.4   Fibronectin

Fibronectin is described as a fibril forming glycoprotein with ubiquitous localization[128]. It interacts with other components of the ECM (such as collagens and fibrin, as well as with glycosaminoglycans (GAGs) and integrins, providing a scaffold for matrix organization and playing an important role in cell-matrix interactions[128]. Such interactions facilitate growth and differentiation during development, as demonstrated by embryonically lethal fibronectin mouse models[136].

4.2.1.5   Matricellular proteins

This is a large group of non-structural matrix glycoproteins that localize both in the extra- and intracellular milieu[128]. Trombospondins, secreted protein acidic and rich in cystein (SPARC), Tenascins, Osteopontin and cartilage oligomeric matrix protein (COMP) constitute some of the most representative members of this group[128]. They mediate interactions between cells and the surrounding ECM acting as scaffolds for the binding of components such as small leucin rich proteoglycans (SLRPs), decorin and versican[137]. Some of the proteins in this group are essential for cancer progression by altering redox signaling and inducing a hypoxic environment around the tumor mass[137].

4.2.1.6   Proteoglycans

Proteoglycans (PGs) are a family of proteins with an amino acid core attached to a chain of GAGs of variable chain length[138]. PGs can be secreted, membrane bound or intracellular (Figure 18)[138]. Among the secreted PGs, two main subfamilies are present in the interstitial matrix: the hyalectans or aggrecans, which interact with hyaluronan (such as aggrecan, versican and brevican), and the small leucine-rich PGs (SLRPs), which are involved in matrix organization, collagen fibrillogenesis, inflammation and cell signalling (for example, decorin, syndecan and fibromodulin)[138]. The third group of secreted PGs, also known as modular or pericellular PGs (perlecan, agrin and collagens IX and VIII), are mainly components of the basal membrane and provide stability via interaction with integrins[138].

Transmembrane PGs are essential for cell migration and signaling[128]. This group is mainly represented by syndecans and glypicans[139]. Syndecans are molecules that actively participate in cell adhesion, migration and cytoskeletal organization by binding integrins and growth factor receptors[139]. Glypicans, on the other side, are GPI anchored proteins that play an essential role in signaling via regulation of associated receptors such as tyrosine kinase[128,138].
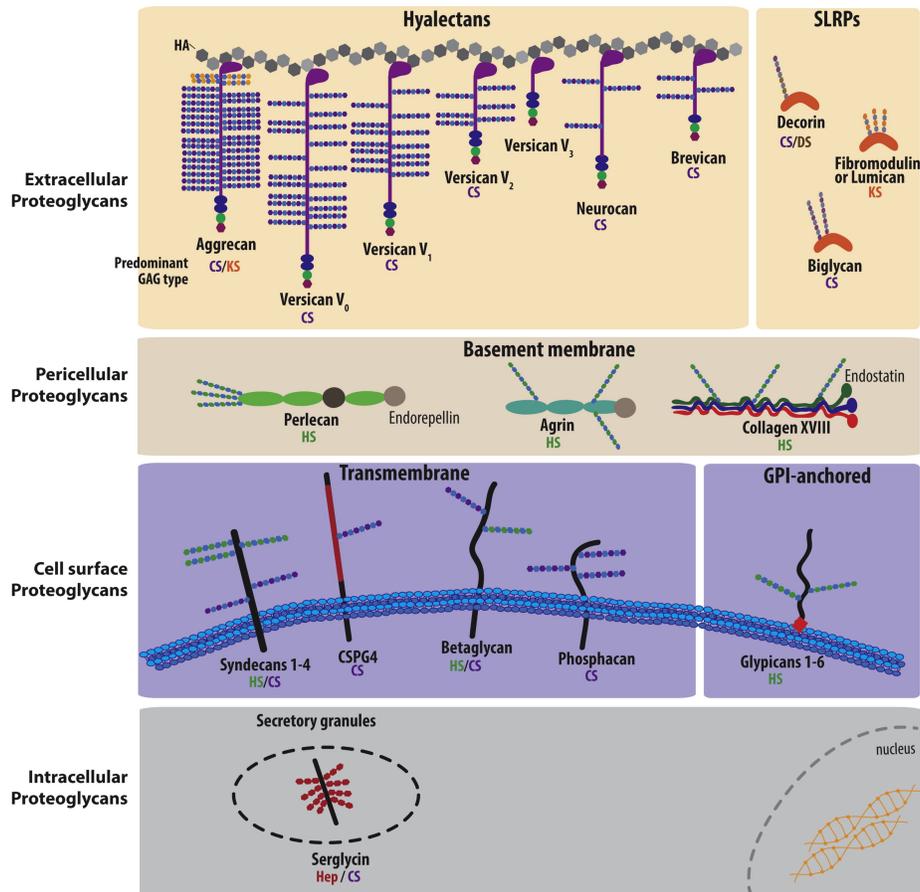
Figure 18. Diversity of PGs. Secreted PGs (upper 2 panels) are mainly involved in matrix organization and stability. Meanwhile, transmembrane PGs participate in signaling processes and intracellular PGs are involved in the formation of inflammatory granules. Figure taken from Teocharis et al. (2016)[140].

Currently only serglycin has been characterized as an intracellular PG in secretory compartments[128]. Serglycin is essential for the formation of secretory granules, as well as the packaging and secretion of growth factors and cytokines in hematopoietic cells, which are released upon stimulation during inflammation[140,141]. Furthermore, serglycin has been found

associated with CD44 in order to induce collagen type I adhesion and synthesis of matrix metalloproteases[141].

4.2.2 Cellular interactions with the ECM

Cells interact via different receptors with the ECM, namely: integrins, discoidin domain receptors (DDRs), cell surface PGs, hyaluronan (HA) receptors and Layilin (Figure 19)[129]. These receptors not only anchor the cellular cytoskeleton to the ECM, but can also initiate signaling cascades, direct cell migration and modulate the forces experienced by the cell[142]. The roles of these receptors in mediating cell to ECM interactions are briefly described hereunder.
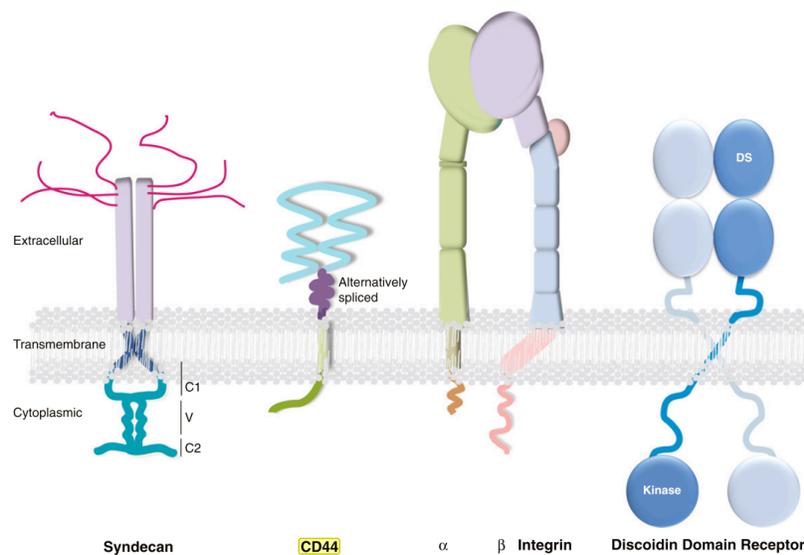
Figure 19.   Diagram of different ECM transmembrane receptors mediating cell anchoring to the matrix. Syndecan: transmembrane PG (see section 2.2.1.6); CD44: HA hyaluronan receptor. Figures taken from Multhaupt et al. (2016)[139].

4.2.2.1   Integrins

Integrins are heterodimeric receptors formed by the combination of 18 α-subunits and 8 different β-subunits that directly heterodimerize after synthesis at the ER[141,143]. They interact with the ECM either via an epitope in both subunits or a domain of the α-subunit[143]. Integrins can be regulated both biochemically (by a change in conformation from a bend to an extended state) as well as mechanically (by ligand-binding kinetics, integrin clustering, conformation and activation)[143,144].

The biochemical regulation can be generated by inside-out or outside-in mechanisms, according to the activating signal (Figure 20)[145]. Inside-out activation occurs via interactions with the integrin cytosolic domains, mainly mediated binding to talin, kindlin or focal adhesion kinase (FAK); this signal constitutes the first step in activation and allows the subsequent binding of other factors[143,146]. Conversely, outside-in activation occurs by interaction with specific ECM ligands, which generates force on the integrin cluster and induces recruitment of scaffold and adapting proteins, such as talin and vinculin, that couple the actin cytoskeleton to the integrin cluster[143,145,146].
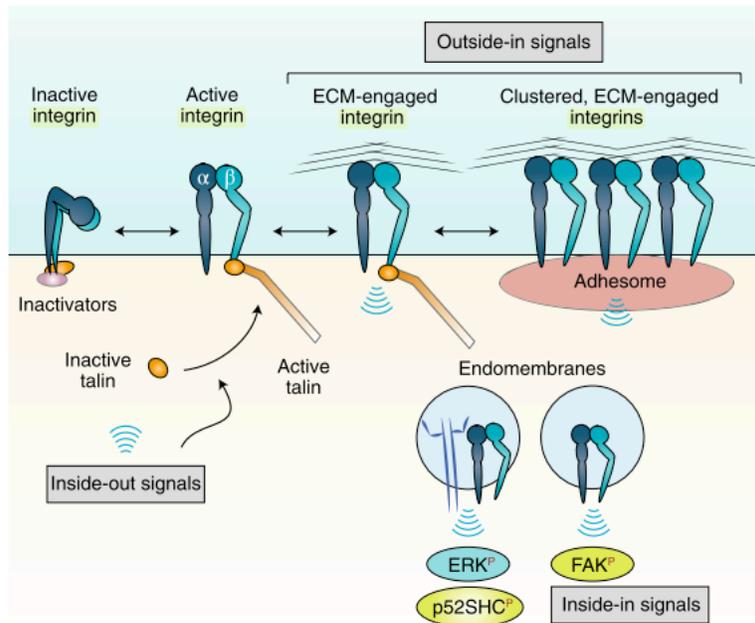
Figure 20. Integrin activation mechanisms. Inside-out activation occurs by binding of active talin to the β subunit of integrins, whereas outside-in activation is triggered upon binding of integrins to components of the extracellular matrix. Figure modified from Moreno-Layseca et al. (2019)[145].

Integrins mediate ECM interactions via focal adhesions (see section 4.2.3.1), therefore they experience constant force both from the ECM and the cytoskeleton[143]. In this scenario, integrins can form clusters to redistribute the force per integrin unit[143]. Integrins can the accumulate in cross-linked clusters bound to actin, where the recruitment of another integrin subunit will reduce the force per unit and stabilize the focal adhesion[143,145]. Integrins can also "diffuse laterally" according to the substrate and mechanics governing the interaction, or induce membrane bending by clustering in order to interact with the ECM[143]. Such is the case

of the glycocalyx, which has been shown to impose a steric barrier for integrin-ligand binding[143]. There, the membrane bending induces a "kinetic trap", where integrins that diffuse are closer to the substrate and can favorably interact with the substrate[143].

Overall, integrins are the main receptors mediating ECM interactions with cell cytoskeleton[139,143]. Their role as mechanical sensors, their ability to modulate the growth of FAs as well as their capacity to mediate cell-cell interactions allows them to promote directed cell migration[139,143,147,148].

4.2.2.2   Discoidin domain receptors (DDRs)

DDRs are tyrosine-kinase receptors (RTKs) that can spontaneously bind collagen[149]. They are type I membrane proteins containing a collagen-binding discoidin domain, an extracellular discoidin-like domain and a cytosolic tyrosine-kinase domain (TK)[149].
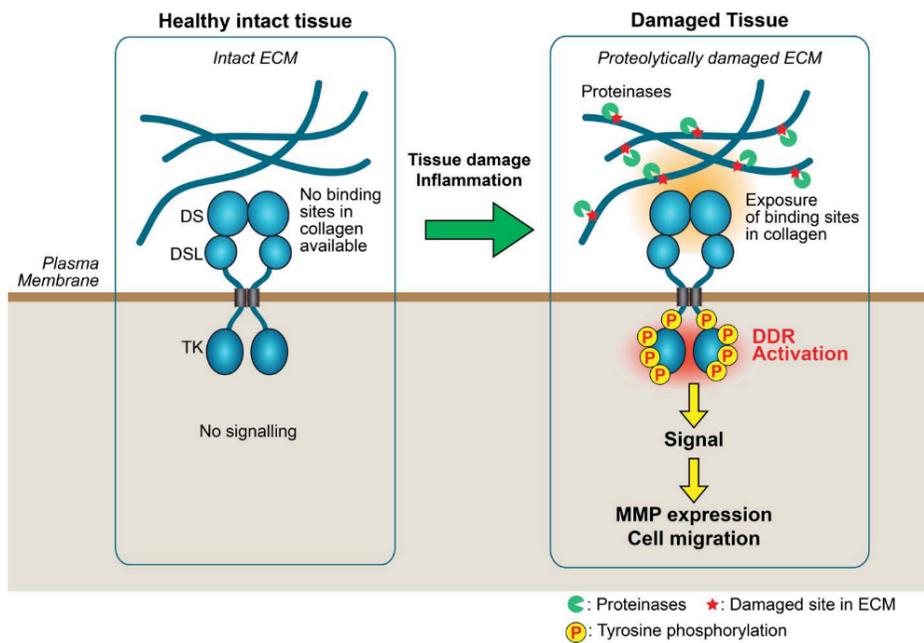
Figure 21.   DDRs in healthy and damaged tissue. In healthy tissue, DDRs cannot bind collagen, however, tissue injuries causing proteolytic damage, expose collagen and enables binding of DDRs. Binding to collagen activates DDRs, which in turn induce MMP expression and subsequent cell migration. Figure taken from Itoh (2018)[149].

Given that DDRs do not attach to a soluble substrate, their regulation is different from most RTKs in that their dissociation from collagen is usually mediated by ectodomain shedding[149].

This process is facilitated by ADAMT-10, (a disintegrin and metalloprotease with thrombospondin motif, further described in the next section)[149] and MMP14 (matrix metalloprotease 14, also known as MT1-MMP)[150].

Functionally, DDRs are very important in cell migration and as environmental sensors (Figure 21)[149]. In 3D cell migration, they can modulate matrix metalloprotease (MMPs) expression, as shown in smooth-muscle DDR1 knock out cells by Hou et al. (2002)[151]. As environmental sensors, they can activate the expression of MMPs upon collagen rupture due to tissue inflammation, which induces phosphorylation of their tyrosine-kinase domain and stimulates MMPs upregulation[149]. Given their impact on the regulation of migration processes, DDRs have been postulated as therapeutic cancer targets[149–152]. However, due to their heterogeneous expression in model cell lines, further investigation is required to provide specific solutions.

4.2.2.3   Hyaluronan receptors

Besides their role in the assembly of the ECM, proteoglycans can act as signaling receptors that initiate intracellular signaling cascades, as is the case for HA-receptors[153,154]. Hyaluronan (HA) is the only GAG synthesized outside the Golgi and it binds to proteoglycans via specific binding motifs, which allows the assembly of a wide range of molecular weight HA chains[153,154]. Although long HA aggregates promote anti-inflammatory responses, wound healing and tissue repair[141,154], short cleaved HA fragments generate pro-inflammatory signals that prevent ECM remodeling, impairing cell invasion and migration and subsequently stimulating pathological conditions[154–157].

HA plays a role in these processes mainly by triggering signaling cascades via interaction with several HA receptors[154]. Among them, CD44, is the main receptor and serves as an anchor for the cytoskeleton to the ECM[154,158]. Besides HA, CD44 binds also osteopontin, fibronectin, laminin, MMPs and collagens via its extracellular domain[154]. Via the interaction with signaling receptors such as Erb2 and EGFR, as well kinases of the Src family and RabGTPases, HA-CD44 can trigger pro-inflammatory signaling cascades and stimulate cell invasion and migration, as has been shown by several studies in cancer cells[156,157].

Recently, another HA receptor named layilin, aroused as an important receptor for adhesion and tumor invasion via HA binding[156]. Layilin can bind talin head via its intracellular domain and HA via a C-type lectin domain on the extracellular face[155]. Layilin localizes mainly in

membrane ruffles, actin-rich protrusions of the plasma membrane that are considered the step preceding cell migration in macrophages[159]. Also, it shares some similarities with CD44, such as the weak binding affinity with HA and the capacity to bind ERM molecules intracellularly. Finally, layilin has been catalogued as the main HA-induced effect receptor in the intestine given its role in directly influencing cell invasion in gastric cancers[155,156].

4.2.3 Dynamics

The ECM is an extremely dynamic environment that is in constant modification due to the synthesis, degradation and reassembly of its components[127]. The mechanisms involved in such rearrangements can be classified in six different processes: adhesion, contraction and alignment, degradation, internalization, deposition, and cross-linking (Figure 22)[129].
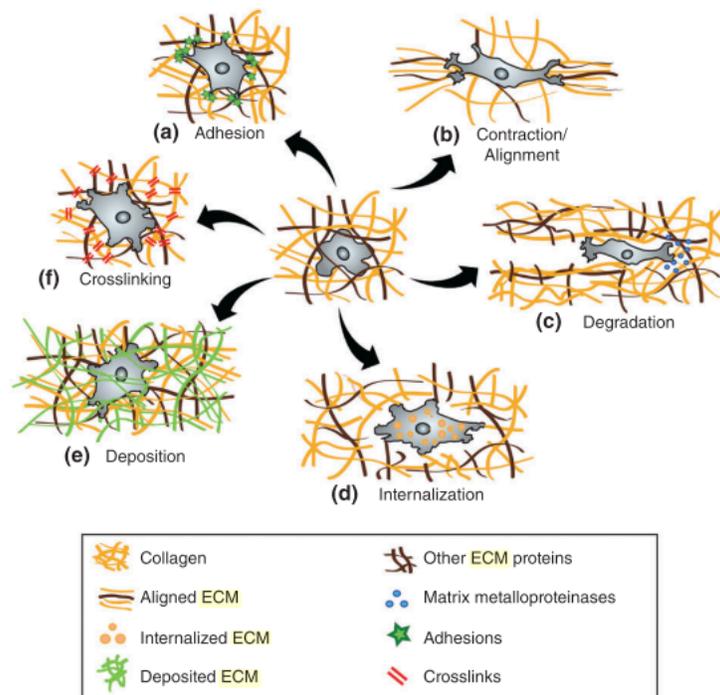
Figure 22. Mechanisms of ECM remodeling. Adhesion is mediated by integrins and focal adhesion proteins, conctraction and alignment by actomyosin, degradation by MMPs, internalization by endosomal internalization followed by lysosomal degradation, deposition by induced synthesis of ECM component s and crosslinking by post-translational modifications. Figure taken from Ford & Rajagopalan (2018)[129].

Together adhesion, contraction, alignment and degradation are processes that define the mechanical interaction of cells with the ECM and allow to maintain tissue homeostasis[127–129,160]. Furthermore, these processes shape the adequate environmental conditions for a cell to migrate and this migration can only take place once a cell adheres and is able to use its internal tension to move in a 2D environment, as rolling leukocytes on the endothelial cells, and in 3D scenarios, as transmigrating leukocytes through the endothelial monolayer, invasive macrophages in inflammatory conditions or cancer cells in metastasis[127–130]. For the purpose of the present study, this section will be focused on the first three processes.

4.2.3.1   Adhesion

Adhesion is an essential step in cell migration, a process occurring due to the simultaneous assembly and disassembly of these cellular structures[128,143,161]. Currently several kind of adhesive structures between cells and ECM have been described, e.g. focal adhesions, focal complexes, fibrillar adhesions and invadopodia[162]. However, these different structures can be organized in 2 main groups: focal adhesions and invadosomes (podosomes and invadopodia, see section 4.3.3.1)[162,163].
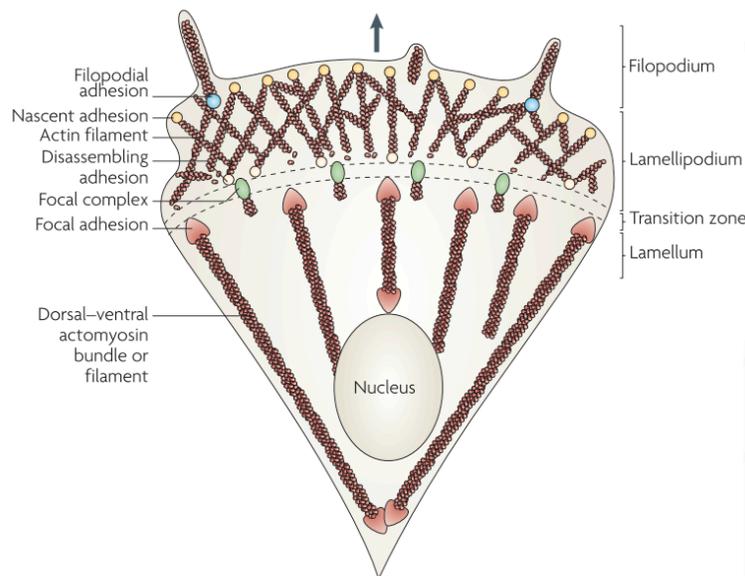
Figure 23. Scheme depicting the formation of cell adhesions. Figure taken from Parsons et al. (2010)[161].

Cell migration is first driven by the protrusion of the leading edge, which is stabilized by the proliferation of focal adhesions that subsequently stabilize the cell-ECM contact, generate tension and contraction forces to promote movement[161]. On the other hand, cells expressing podosomes move rather in a gliding way[162].

Focal adhesions are actin rich structures stabilized by integrins that localize in a tangential manner to the ECM and are mostly associated with matrix remodeling[161,162]. The formation of a focal adhesion initiates with the appearance of nascent adhesions, short-lived small structures, formed upon actin polymerization at the cell leading edge (Figure 23)[161]. They localize immediately behind the leading edge, after nucleation of 3 to 6 integrins, and are characterized by high turnover, of approximately 60 seconds[161,164]. According to increasing tension, nascent adhesions will mature into focal complexes, structures of around 0.5 to 1 μm diameter with a dot-like shape that are connected to the actin network via moderate tension[161,162].

As migration continues and the integrin cluster increases in size, focal adhesions are formed[161,164]. These structures have elongated shapes of around 2 μm wide and 3 - 10 μm long, are associated with stress fibers and disassemble at the rear once subjected to traction forces[161,162]. The assembly of focal adhesions in fibronectin matrices can give place to fibrillar adhesions, long-lived and highly elongated structures that are not prominent in migrating cells[161].

In this regard, contractile cells, such as fibroblasts, endothelial and smooth muscle cells preferentially express focal complexes and adhesions that help to stabilize in a longer term the cell-ECM interaction[161]. On the contrary, most of the migrating cells, e.g. cells belonging to the myeloid lineage, express preferentially small, short-lived structures such as nascent adhesions and invadosomes[161–163,165].

4.2.3.1.1   Adhesion dynamics

Two processes dictate the assembly or disassembly of adhesions, namely, actin polymerization and tension generated by myosin II[161]. Actin polymerization at lamellipodia (Figure 23) starts with the activation of the Arp2/3 complex, which is regulated by the Rho GTPases Rac1 and CDC42 that act via effectors from the WASP (Wiskott-Aldrich syndrome protein) and WAVE (WASP-family verprolin homologue, also known as SCAR) families of proteins[161]. Such

activation provokes actin nucleation and the formation of branch-like actin at the leading edge, which in turn generates a retrograde force due to the limitations imposed by the membrane in response to actin polymerization[161].

At the same time, actin bundles located in the lamellum, undergo retrograde flow but in a slower manner, generating a reorganization of actin into bundles at the transition zone[161]. Once these bundles grow thicker, they become stress fibers that start adhering to the ECM on the dorsal sides of the adhesion[161]. Then, ventral stress fibers arise from dorsal ones and anchor the cell to the ECM via FAs in both ends (Figure 23)[161]. These ventral stress fibers also connect to the so-called transverse acts: not anchored actin bundles that start forming by annealing of myosin II bundles and Arp2/3-nucleated actin in lamella[161].

Actin polymerization in nascent adhesions is mainly regulated by focal adhesion kinase (FAK), which recruits the Arp2/3 complex in the first place[161,164]. The activation of FAK, as well as paxillin, induces talin binding to the cytosolic tails of integrins[164]. Talin, as well as kindlin, stimulates Rac1 activity, which in turns inhibits Rho GTPase and induces actin polymerization[164].

4.2.3.2   Contraction and alignment

The antagonist process resulting after adhesion is contraction[129]. Here, the force exerted at the stabilized FA will generate such a tension that, upon surpassing a threshold, will make the cell contract[129]. In this regard, non-muscular myosin II (referred here as myosin II) is the primarily source for contraction (Figure 24)[161,166]. Upon binding to the ECM, actin filaments containing myosin IIa elongate and can generate mechanical tension by myosin IIa induced sliding of the filaments, creating contractile forces[161,166].

Myosin II contraction activity and tension influence only mature adhesions by mediating the contraction of actin stress fibers[161]. Nascent adhesion formation does not depend on myosin II activity, however, as long as the adhesion elongates, talin and vinculin bind active integrins to actomyosin via a mechanical linkage denominated "the molecular clutch"[164]. This engagement is first triggered by the exposure of a talin actin binding site (ABS, ABS3 usually), which enables F-actin binding and induces "stretching of the talin rod", subsequently exposing a vinculin binding site (VBS)[164]. Upon vinculin binding, talin is able to engage with F-actin via ABS2 to increase the force transmission[164]. This in turn unfolds helical structures at the talin

rod, making available more VBSs and further consolidating the recruitment of F-actin and stabilizing the FA[164].

a **Actomyosin**

Actin filament
Essential light chain
Non-helical tail
Coiled coil
Head (motor ATPase) domain
Regulatory light chain

b **Migrating cell**

Maturing adhesion (in protrusions)
Actin filament
Myosin IIA
α-actinin
Maturing adhesion

Mature adhesion (retracting)
Myosin IIA
α-actinin
Myosin IIB
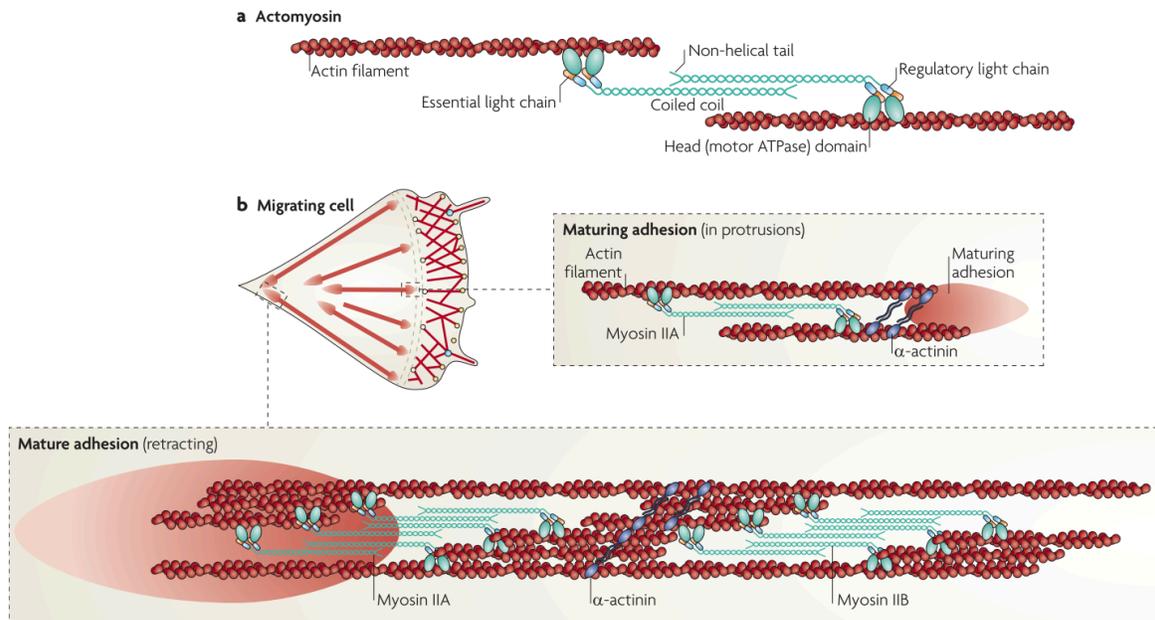
Figure 24. Myosin II structure and role in maturing adhesion during cell migration. (a) scheme of myosin II conformation depicting the regulatory light chains (RLC). (b) During migration myosin II acts mainly in mature FAs where it mediates retraction and disassembly at the rear end. Figure taken from Parsons et al. (2010)[161].

Myosin II activity is regulated by the phosphorylation of regulatory light chains (RLC), and can also influence FA retraction and disassembly during migration at the rear end (Figure 24)[161]. Combining adhesion and contraction not only controls the formation of focal adhesions, but also aligns components of the ECM, which in turn facilitates directed cell migration and force transmission[129]. In addition, the realignment of ECM components modifies physical properties of the matrix, such as stiffness, facilitating 3D matrix invasion as well as tissue organization[129].

4.2.3.3   Degradation

The cleavage of ECM proteins is generally referred as degradation[129]. However, Apte and Parks (2015) suggest to subdivide the ECM proteolytical degradation in three categories: the turnover, which constitutes the regular physiological breakdown and replacement of ECM proteins; the remodeling itself, which encompasses the breakdown and clearance of tissues

under transformation, like resorption during development; and the degradation, which they suggest, should be applied only to the uncontrolled ECM proteolysis seen in disease contexts[160]. In general, all the processes described above require the breakdown of ECM components by secreted proteases, their cellular internalization and their subsequent degradation in the lysosomes[129].

The proteases of the metzincin family, a group of zinc-dependent proteases that possess a methionine-turn sequence, are the main enzymes responsible for ECM proteolysis[160,167,168]. They can be secreted or membrane associated, and are synthesized, mostly, as pre-pro-polypetides that require activation[127,160]. There are 6 families of metzincins, among these the most relevant for mammalian ECM degradation are: astacins, adamalysins and matrix metalloproteases (also known as matrixins), which are the main focus of this study and will be thoroughly described further below[127,160,168].

4.2.4 The metzincin family of proteases

As mentioned previously, metalloproteases are the most important proteases during ECM remodeling. Although their catalytic regions are highly conserved, other domains are greatly variable, which explains the versatility of these proteins and their capacity to influence cellular processes independent of ECM remodeling[160].

Traditionally MMPs have been considered the only participants in the ECM remodeling, however, studies performed in the last two decades have challenged this assumption[127,169,170]. Other metalloproteases such as ADAMTs, Meprins and BMP1/tolloid-like proteinases are also crucial for the maintenance and turnover of ECM[160]. These main groups of ECM remodelers are described below, with the exception of MMPs, which are widely described in the next section and constitute a central topic of the present study.

4.2.4.1   Astacins

This group of metalloproteases is only present in animals and bacteria[168]. Interestingly, some parasite nematodes, like Hydra, express astacins during development and also secrete them as zymogens to their host ECM in order to move through it[168]. Among vertebrates, astacins are represented by three subgroups: egg hatching enzymes, (bone morphogenetic protein) BMP-tolloid proteases, and meprins[168,171]. In particular, humans express 7 different astacins encoded by six genes[172]:

- BMP-1, mammalian tolloid (mTld), tolloid-like 1 (Tll-1) and 2 (Tll-2) are involved in dorsal/ventral patterning during embryogenesis.

- Ovastacin, responsible of preventing polyspermy during fertilization.

- Meprin-α and meprin-β, proteases that stimulate the maturation of fibrillar collagen.

BMP-1 is a zinc metallopeptidase that was for long time erroneously categorized in the BMP family, a group of bone modifier enzymes that belong to the TGF-β growth factor superfamily[173,174]. Its structure is characterized by a conserved metalloprotease catalytic domain followed by a Ca^{2+}-binding EGF domain and up to five CUB (complement component C1r/C1s, urinary EFG, BMP-1) domains[173,174]. Only three proteins, besides BMP-1, belong to this family in humans and all of them have been catalogued as orthologues of *Drosophila* tolloid, a protein involved in the dorso-ventral patterning during development[174]. During ECM assembly they cleave the C-termini of procollagen I and II, enabling fibril formation[173,174]. Also, by cleavage of the Latent TGF-β Binding Protein (LBTP-1) and release of active TGF-β, tolloids regulate the cellular response to inflammation and fibrosis[174].

Meprin-α is among the largest secreted proteins found in nature given its capacity to build complexes up to 6MDa[168,171,172]. The main difference between the α and β subunits of meprin is that meprin-α is secreted due to its "I-domain", a protein sequence that is recognized by Furin at the ER-to-Golgi compartment and cleaved in order to release the N-terminus of the α subunit to the secretory pathway, while the C-terminal transmembrane fraction remains bound to the membrane[172].

Meprin-β in turn is the only membrane bound member of the astacin family, although it can be shed at the cell surface by ADAM-10 or ADAM-17[172]. Meprins are highly glycosylated and promote the fibril formation of collagen I + III *in vivo* by cleaving their globular pro-peptides[168,172]. Studies with knock-out (KO) mice have shown that meprins are required for collagen maturation together with BMP-1[172]. Therefore, in chronic pathologies involving fibrinogenesis and tumor invasion, such as breast cancer and colon carcinoma, meprins are found to be upregulated[171,172].

4.2.4.2   A Disintegrin And Metalloprotease with Thrombospondin type-1 repeat (ADAMTS) family

ADAMTS are secreted proteases characterized by a variable thrombospondin type-1 repeat region (TSR)[175,176]. Structurally, ADAMTS highly resemble the ADAM family of proteins, however, the 2 main differences between them are that all ADAMTs have protease activity and that they are highly glycosylated[175,176].

The basic structure of ADAMTS proteases consists of a signal peptide, followed by a pro-peptide domain, a metalloprotease catalytic domain, a characteristic disintegrin-like domain, and the ancillary domain, comprised by a central TSR domain, a cysteine rich region and a spacer domain (Figure 25)[167,177,178].
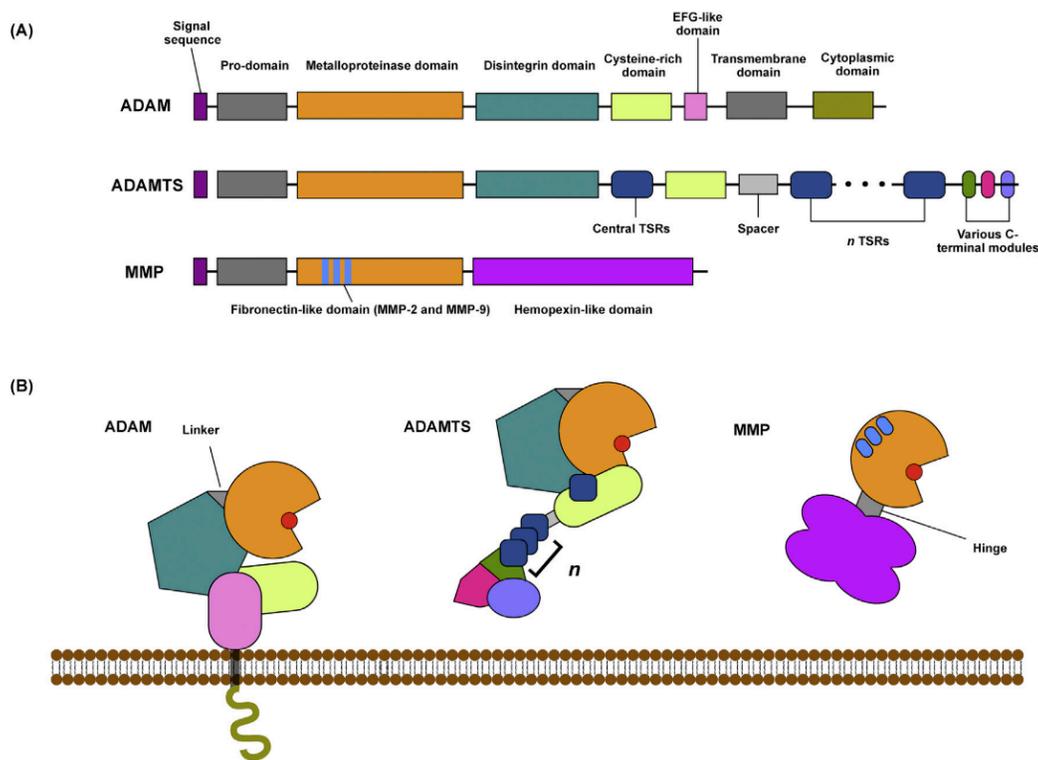
Figure 25.   Schematic representation of ADAMTs structure and comparison with ADAMs and MMPs. (A) depicts the characteristic domain for each group of proteins whereas (B) illustrates their topography. Taken from Yang et al. (2017)[179].

The association between the ADAMTS disintegrin-like domain and the substrate-binding pocket provides great variability and therefore, high substrate specificity for each ADAMTS

protein, making them excellent therapeutic targets to treat diseases such as Ehlers-Danos syndrome, thrombotic thrombocytopenic purpura and Weill-Marchesani syndrome[167,178,180].

Physiologically, ADAMTS participate in several cellular processes but depending on the species, cell type and environmental conditions, they can be expressed either constitutively or in an induced manner[178]. Overall, ADAMTS are involved in homeostatic processes such as tissue regression during development[181], cleavage of cartilage and tendon in bone maturation[178] and fertility[169,178], as well as in pathological ones, as is the case for cancer angiogenesis[178,180].

4.3   Matrix metalloproteases (MMPs)

MMPs are amongst the most thoroughly studied members of metzincins[182]. Since their discovery in 1962 by Gross and Lapiere[183], they have been the focus of research on therapeutic targets for inflammation, cancer and tissue remodeling[127,182,184,185]. MMPs have a highly conserved structure (Figure 26) consisting in a signal sequence, followed by a ~80 amino acids propeptide, a metalloprotease catalytic domain (~170 amino acids), a linker region and a hemopexin domain (~200 amino acids)[186,187].

MMPs have been traditionally classified according to homology with MMP1 (with exception of MMP7, -23 and -26 lacking the linker region and hemopexin domain)[167]. They share the cysteine switch motif in the propeptide region (PRCGXPD) that controls MMP activation, and a motif in the catalytic domain (HExxHxxGxxH), where the three histidines bind the Zn^{2+} ion necessary for their catalytic activity[127,160,186,188–190].

Although the cleavage of the propeptide is not absolutely necessary for their activation, most MMPs reach the active state after its removal[188,191,192]. The propeptide can be removed either by cleavage (mostly by another active MMP, but also peptidases such as trypsin or plasmin), by chemical agents, such as mercurial and disulfide compounds, chaotropic agents, oxidants and alkylating agents[188], or by conformational changes triggered by nitric oxygen (NO), reactive oxygen species (ROS) and hypoxia processes[193].

The regulation of MMPs takes place also at the transcriptional level via control of gene expression, transcript stability, epigenetic variations and promotor polymorphisms[182]. In this regard, some aspects are common to all MMPs: they possess a TATA box, an AP-1 binding site and a PEA3[182]. MMPs can also be regulated post-transcriptionally by miRNAs, as has been

shown for MMP2 and -9, which expression levels can be controlled by miRNA-29 in breast cancer, whereas miRNA-9 can modulate metastasis, invasion and angiogenesis in neuroblastoma by regulating MT1-MMP activity[127,194].
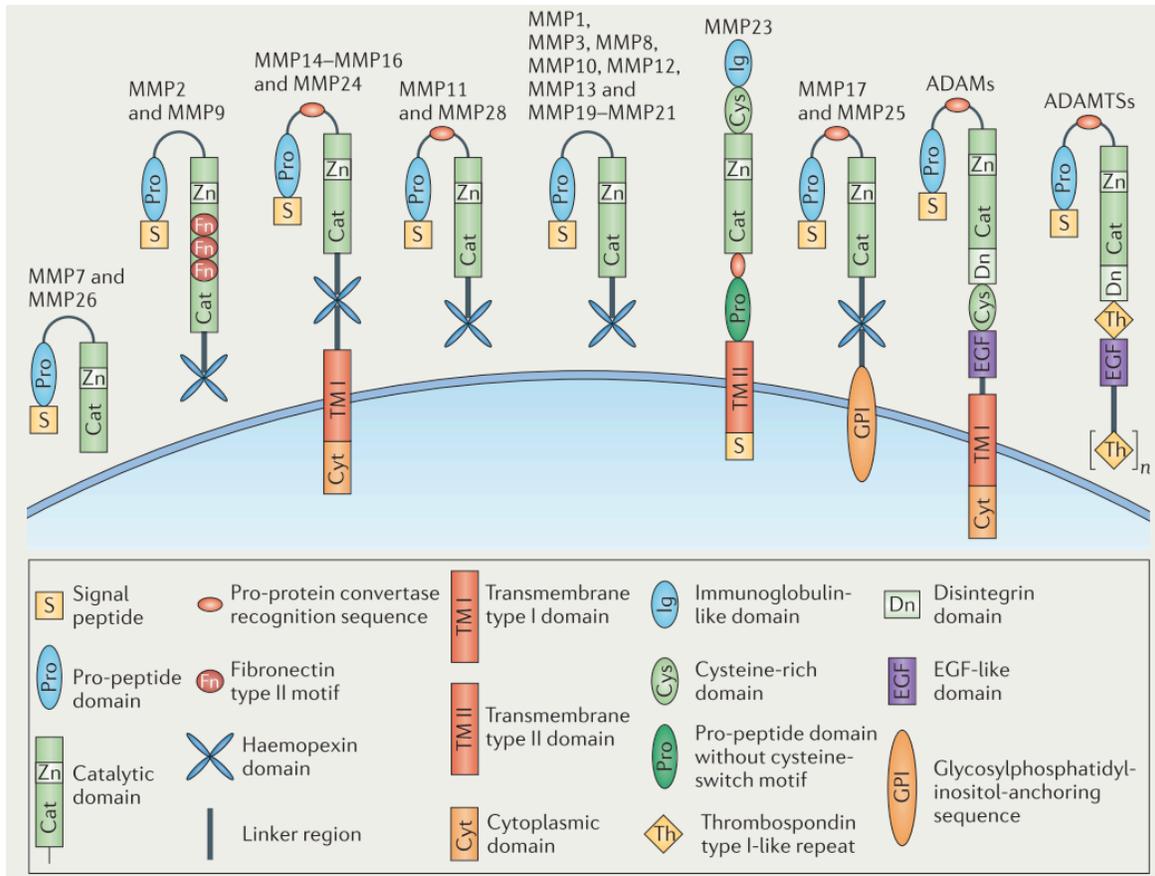
Figure 26. Diversity of MMPs. Schematic representation of known human MMPs and their characteristic domains. Adapted from Khokha et al. (2013)[167].

Although ubiquitously located, the expression of MMPs is tissue and cell dependent[186,190]. Fibroblast and leukocytes, though, are main sources of MMPs, in particular of MMP2[186]. Also, platelets highly express MMP1, -2, -3 and MT1-MMP[186]. Given their role in ECM remodeling and the high turnover rate of the vascular tissue, MMPs are highly expressed in endothelial and vascular smooth muscles cells[186].

MMPs can be both soluble or membrane-anchored, and proteins belonging to this latter group have, in addition to the described domains, a transmembrane domain of variable length, and a short cytoplasmic domain important for intracellular trafficking, activity regulation and

recycling[187]. Besides MMP-23, which is a type-II membrane protein with an immunoglobulin-like domain and a cysteine (Cys)/proline (Pro) rich region at the C-terminus, trans-membrane (TM) MMPs are further classified in two classes: type-1 transmembrane MMPs (also known as MT-MMPs, including MMP-14, -15, -16 and -24) and GPI-anchored MMPs (MMP-17 and -25)[182,186,195].

All the MT-MMPs possess a Rx[R/K]R motif at the end of their propeptide domain that is recognized and cleaved by proconvertases such as Furin, and leads to the intracellular activation of membrane bound MMPs (Figure 27)[189,195]. In addition, type-1 MT-MMPs have a unique feature in their catalytic domain: an 8-9 amino acid insertion named the MT-loop that has been described to be relevant for proper localization and is not found in any other member of the MMP family[195–197].
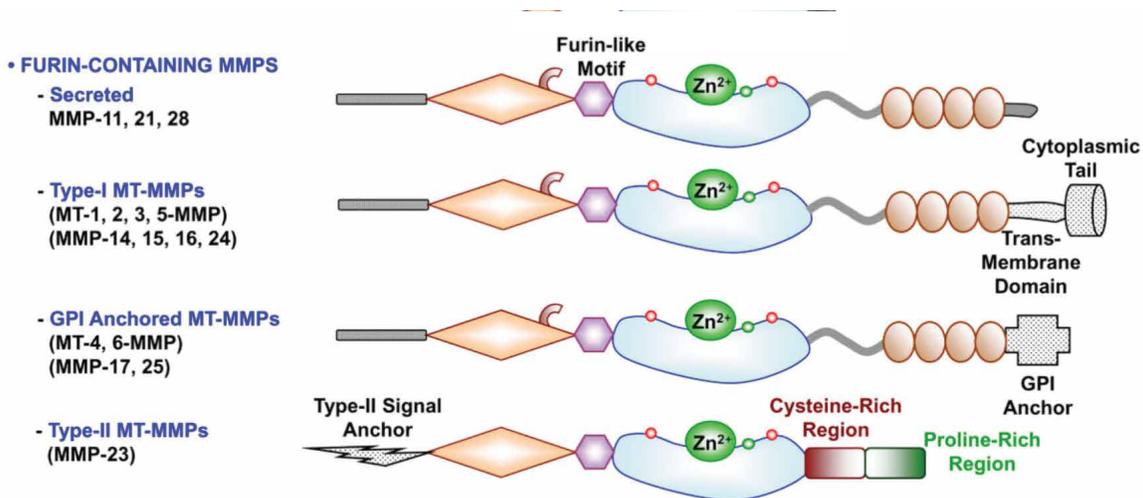
Figure 27. MMPs containing Furin cleavage sites. Figure taken from Cui et al. (2017)[186].

Altogether, twenty eight MMPs have been identified in vertebrates and twenty three are expressed in humans, among which fourteen are expressed in the vascular system[186]. Structurally, soluble MMPs can also have additional domains relevant for their proteolytic activity, for example, MMP2 and -9, the so-called gelatinases, possess three repeats of a fibronectin-like motif that enhances the interaction between the MMP and collagen[186].

4.3.1 Classification of soluble MMPs

MMPs have been initially classified according to their substrate, however, research from the last 20 years has shown that their broad spectrum of substrates is not limited to ECM

components[198]. Cytokines, chemokines, cell surface ligands, receptors and antimicrobial peptides constitute also critical substrates for cell signaling and transcriptional regulation of the expression of other MMPs[167,182,187,188,190]. Although MMPs can also degrade intracellular substrates[167,187,198], the following description focus on their extracellular roles.

4.3.1.1   Collagenases

This was the first group of MMPs identified and is represented by MMP1, -8, -13 and -18, which hydrolyze collagen type I, II and III (interstitial collagens) in their native triple helical structure[182,187,188,199,200]. Their function has been directly associated with fibrosis resolution, wound healing and restoration of the ECM after injuries[187]. MMP1, known as the interstitial collagenase and the first MMP that had been described, can degrade both collagen and gelatin, and activate MMP9 by proteolytical cleavage[186]. It has been reported to be upregulated in inflammatory conditions and autoimmune disorders as well as during osteoarthritis[186].

Meanwhile, MMP-8, also known as the neutrophil collagenase, also cleaves interstitial collagens and is recognized as the first collagenase appearing in wound healing processes[167,186]. It is secreted in a "free" form, meaning it traffics intracellularly in an inactive form and is only activated in the extracellular space by MMP3 and -10[186]. The other collagenases, MMP13 and -18 (the latter only expressed in *Xenopus laevis*), are mainly involved in bone resorption by cleavage of collagen and aggrecan (MMP13)[186,201], and   control of axonal growth (MMP-18). Notably, both MMP13 and -18 are also highly expressed in migrating cells, either cancerogenic (MMP13)[186] or macrophages during *Xenopus* embryonic development (MMP18)[202].

4.3.1.2   Stromelysins

Although MMPs belonging to this group are structurally similar to the collagenases, stromelysins cannot degrade interstitial collagen[186,199]. Stromelysins bind to a varied set of substrates, such as collagen IV and IX, laminin, fibronectin, elastin and proteoglycans, with different affinities corresponding to the tissue where the protein is expressed[187]. Three MMPs belong to this group (MMP3, -10 and -11) although only the first two are soluble and secreted, extracellularly activated by other MMPs and actively degrade ECM components[186,189,199]. MMP11 differs from MMP3 and -10 in that it is activated by Furin and its capacity to degrade ECM is limited[186]. Particularly, MMP3 can activate other MMPs (such as MMP9) and has a catalytic pocket that can degrade substrate using cobalt, manganese, cadmium and/or nickel

instead of Zn^{2+}[186,203]. As mentioned, MMP11 is distantly related and its role in migration is controversial, having both promoting and inhibiting roles in cancer metastasis depending on the cancer type and the stage[186,204].

4.3.1.3   Matrilysins

Matrilysins are characterized by the lack of hemopexin domain[186,205]. Only two MMPs belong to this group: MMP7 and -26. MMP7 has been shown to be key in ECM remodeling and immune system modulation[187]. It cleaves the FAS-ligand, controls programmed cell death and, by upregulation of TNFα, initiates the apoptotic response[189,190,206]. Moreover, MMP7 can also cleave E-cadherin, elastin, Pro-α defensins and syndecan-1 modulating cell-to-cell interactions and plays an important role in wound healing[190,199]. On the other hand, MMP26 has only been reported in human and some primates' genomes[199]. It has been associated with remodeling of embryonic tissue during development and promotion of angiogenesis and cancer metastasis under stimulation of granulocyte-macrophage colony-stimulating factor (GM-CSF)[186].

4.3.1.4   Elastases

MMP12 is the main elastin degrading MMP[186]. It is highly expressed in macrophages and, contrasting with most of the members of the family, exerts a protective function on the tissue by translocating to the nucleus, binding IκBα and promoting INFα secretion from host cells in virus infection events[186,199,207]. Additionally, Marchant et al. (2014) suggested that MMP12 can attenuate the subsequent inflammatory response by clearing systemic INFα: after infection, extracellular MMP12 can cleave the plasma INFα, avoiding long term toxicity by negative feedback[207].

4.3.1.5   Enamelysin

MMP20 is found in teeth and its expression is upregulated in the process of new enamel formation, cleaving matrix enamel proteins such as ameloblastin, amelogenin and enamelin[186].

4.3.1.6   Gelatinases

Gelatin is denatured type I collagen and gelatinases bind it via their fibronectin-like III-repeat motif on the catalytic domain[160,167,182,186,188,189,199,208]. Two MMPs possess such a motif: MMP2

and MMP9, and their roles in inflammation[209–211], cancer[212–214] and endothelial transmigration have been thoroughly studied[167].

As with most MMPs, knockout mice have been generated for gelatinases although no remarkable phenotype has been observed in steady state[167]. Nevertheless, alterations in the mice response to inflammation denote a phenotype that is only evidenced upon challenging[215]. In this regard, Song et al. (2015) showed in a murine double knock out model (MMP2^{-/-} + MMP9^{-/-}) that MMP2 and MMP9 are required to modulate the chemotactic signals of astrocytes at the blood-brain-barrier and that such activity is restored only when either MMP2 or MMP9 were re-expressed[210].
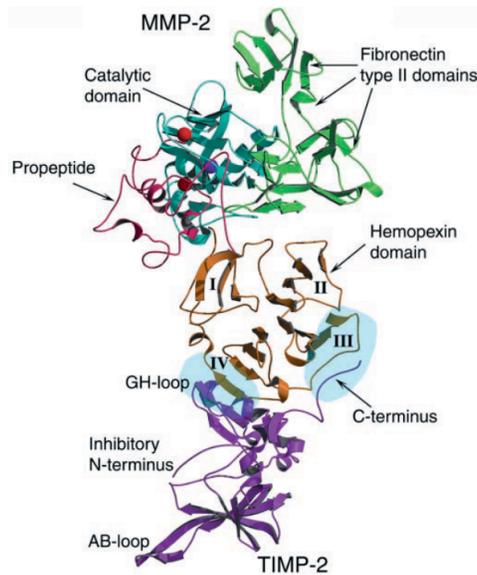
Figure 28. Structure of the complex formed between MMP2 and its inhibitor TIMP2. Figure taken from Morgunova et al. (2002)[192].

MMP2, which is the focus of this study, is constitutively expressed in monocytes, fibroblasts, keratinocytes, endothelial cells, and chondrocytes[199]. In general, MMP2 has been strongly associated with processes involving cell migration[212–214,216]. In particular, several studies have documented upregulation of MMP2 in cancer invading cells, where upregulation of MMP2 activation promotes cell invasion[192,212].

In this regard, Packard et al. (2009) showed that MMP2 and MMP9 localized at the leading edge of migrating tumors[217]. Also Shaverdashvili et al. (2014) showed that MT1-MMP induced

cell migration of melanoma cells by upregulating MMP2 activity[213]. Moreover, Jacob et al (2016) evidenced that Tks5-mediated active delivering of MMP2 and MMP9 in Rab40b vesicles to the invadosome enabled focal ECM degradation and cancer cell invasion[216].

Interestingly, Matsumura et al. (2005) have demonstrated that MMP2 inhibition can be beneficial for the survival rate of myocardial infarction by protecting the tissue against cardiac rupture[218]. In this scenario, a reduction in the cleavage of fibronectin and laminin delays macrophage migration and tissue proteolysis without affecting scar formation and agiogenesis[218].

MMP2 is also a key regulator of inflammation[185,211,219]. T-cells, Th1 in particular, secrete MMP2 in order to further stimulate MMP2 secretion in macrophages[167]. In dendritic and Langerhans cells, MMP2 and MMP9 aid in cell transmigration and the presentation of antigens[131]. MMP2 can also induce the production of CXCR3 receptor antagonists, such as CCL7, as well as inactivate chemokines such as CXCL12[130].
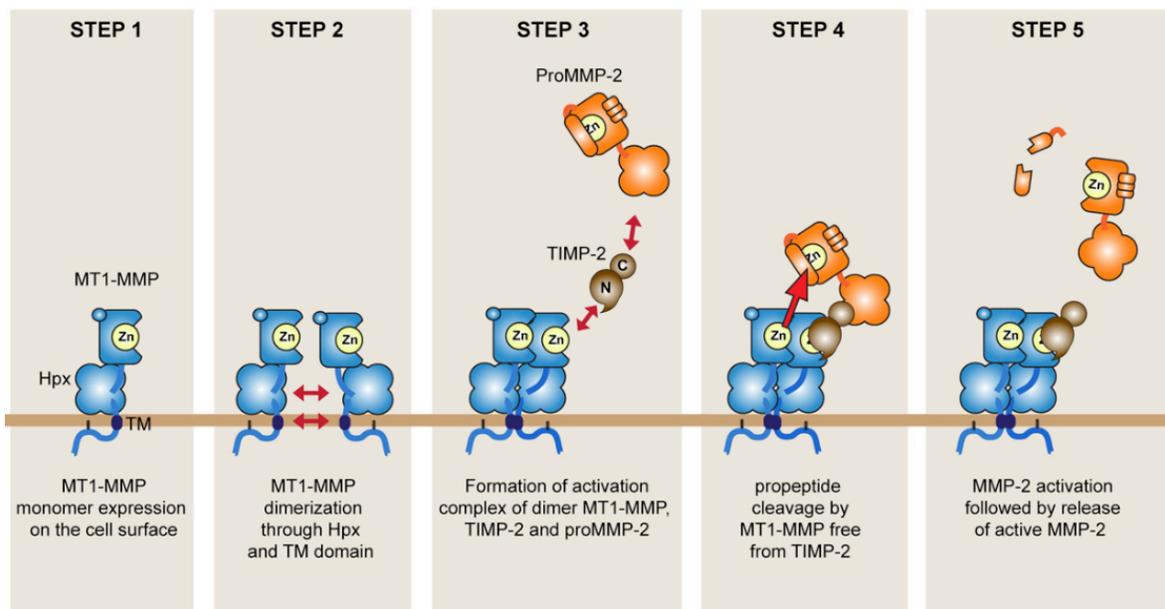
Figure 29. MT1-MMP-mediated activation of MMP2. Figure taken from Itoh (2015)[195].

Given its multiple roles in cancer and inflammation, MMP2 is tightly regulated[214]. In this context, it can be regulated in 5 different ways: (1) by transcriptional control[199], (2) by extracellular cleavage after secretion, (3) by MT-MMPs[195,213,214,220], (4) by internalization from

the cell surface (i.e. by indirect binding to LRP-1 via trombospondin-1 or TIMP1 or -3) or (5) by tissue inhibitors of matrix metalloproteases (TIMPs)[214].

Among these, the best described mechanism is the one activating MMP2 at the cell surface by MT-MMPs[192,221]. In principle any MT-MMP can cleave MMP2 propeptide, but it has been shown that MT1-MMP does it with higher efficiency –MT4-MMP does not interact with MMP2 and, MT2- and MT3-MMP do it with lower affinity, whereas MT5-MMP binding to MMP2 has not yet been confirmed *in vivo*[195,214]. MMP2 activation initiates with the homodimerization of MT1-MMP via the hemopexin domain[195,221]. Then one of the MT1-MMP units in the homodimer is inhibited by binding of the MMP2-TIMP2 complex (Figure 28) via TIMP2 N-terminus, while the other free MT1-MMP is able to cleave MMP2 propeptide (Figure 29)[195,214,221]. Although any of the 4 identified TIMPs can inhibit MMP2, only TIMP2 mediates its activation at the plasma membrane[214].

4.3.1.7   Other MMPs

Some MMPs share the characteristic structure features common to their counterparts, but because of differences in substrate degradation or lack of characteristic features common to a group, are not classified in any of the mentioned groups[190,222].

One of the most relevant MMPs in this group is MMP19, which structurally resembles the stromelysins (has been named by some authors as stromelysin-4) but unlike members of this group, it can degrade collagen IV[186,223]. Its catalytic activity is not limited to collagen, instead, MMP19 can degrade a wide variety of ECM substrates such as laminin, nidogen, fibronectin and type I gelatin (in vitro)[186,223].

4.3.2   Transmembrane MMPs

As mentioned before, MT-MMPs are classified in 2 groups, the TM-MMPs, containing a transmembrane domain, and the GPI-anchored type, without it (Figure 30)[195]. Although all MT-MMPs intervene in cell migration and matrix invasion processes, TM-MMPs anchor to the membrane after being transported in vesicles from the TGN[195]. The GPI-anchored-MMPs, instead, are directly associated with GPI moieties containing 2-3 fatty acids directly at the ER lumen[195].

Up to date, MT1-MMP is the only TM-MMP that promotes migration in collagen matrices[195,224]. Such a role explains the enriched localization of MT1-MMP at the leading edges of cells in structures such as lamellipodia, filopodia and invadopodia[195,225,226].

MT1-MMP is one of the most studied MMPs[195,225]. It has been associated mainly with tumor invasion, although it plays also roles in inflammation (by cleavage of TNF-α) and cell migration (by cleavage of syndecan)[186,227]. MT1-MMP is mainly localized in fibroblasts, vascular smooth muscle cells, brain, uterus and plays an important role in angiogenesis[186]. Although MT1-MMP is mostly activated by Furin at the TGN, a small portion can be transported in its inactivated form[147].
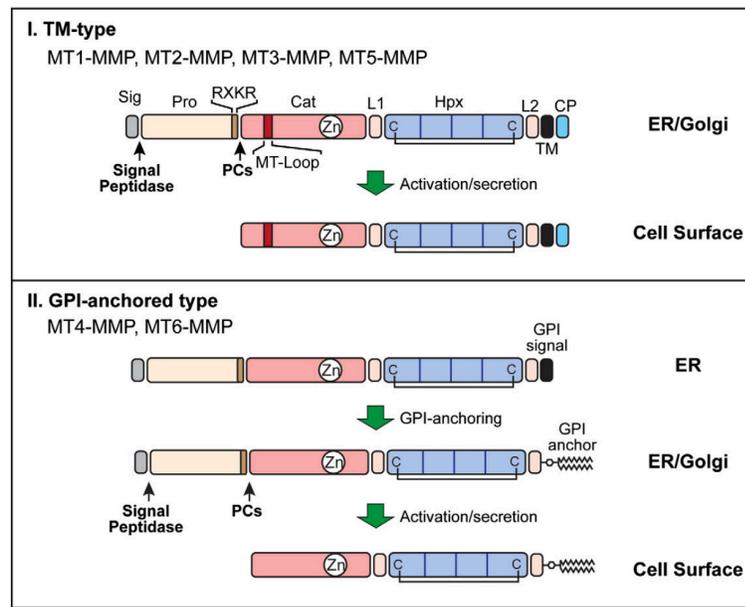
Figure 30. Structural differences between TM and GPI anchored MT-MMPs. Figure taken from Itoh (2015)[195]

Deryugina et al (2004) found that MT1-MMP can act as an integrin convertase by cleavage of pro-αv when associated with αvβ3 integrin; this enhances FAK phosphorylation and subsequent cell migration[147]. Furthermore, Takino et al (2010) demonstrated that MT1-MMP induces ERK pathway activation and subsequent cancer cell proliferation in 3D collagen matrices[224].

It has been shown that MT1-MMP accumulation is necessary to initiate invadosome formation, defining a "pre-invadosome" stage[228]. In order to maintain a pool of MT1-MMP

that is easily and rapidly available upon stimulation, and also that copes with the formation and maintenance of new invadopodia, MT1-MMP is kept in an intermedial endosomal compartment after its synthesis and trafficking through the secretory pathway[225,228,229]. From there is transported in Rab8 vesicles to the plasma membrane and from there can be recycled both via clathrin-dependent or -independent mechanisms (Figure 31)[228].
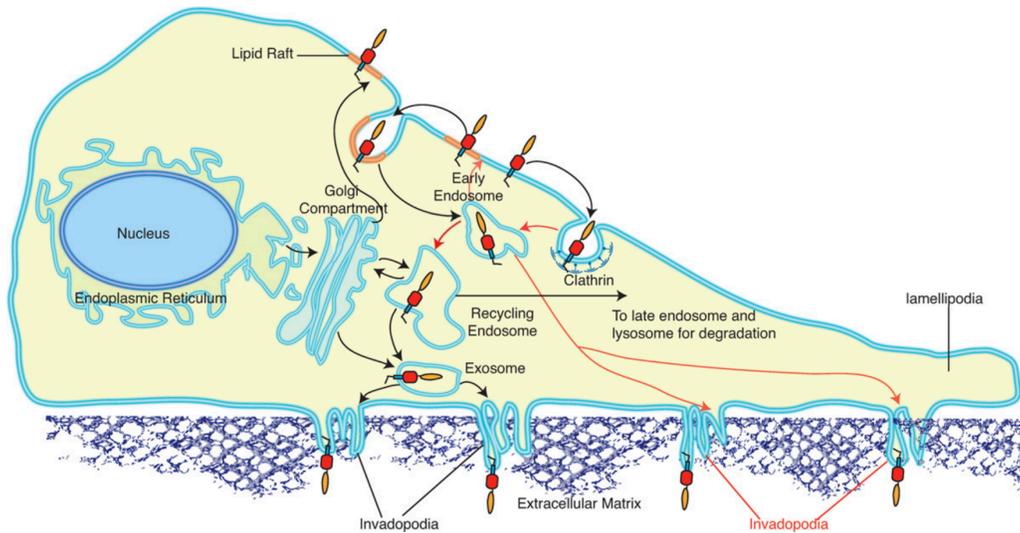
Figure 31. Membrane trafficking of MT1-MMP and its delivery to invadopodia. Upon Furin activation at the Golgi, MT1-MMP is transported to the plasma membrane. Black arrows indicate directed polarized secretion of MT1-MMP from Golgi or exosomes guarantees the confined activation of MT1-MMP. Recycling occurs via clathrin- or caveola-mediated endocytosis to the recycling endosome, from where a small fraction undergo degradation upon transportation to the lysosomes. The red lines represent routes for the confined delivery of MT1-MMP "in response to motogenic stimuli". Figure taken from Frittoli et al. (2011)[228].

4.3.3   MMPs and cancer

Almost all MMPs participate in tumor angiogenesis by degrading capillary basal membrane (Figure 32)[182]. In particular, MMP9 has been shown to modulate angiogenesis by stimulation of CXCL5, 6 and 8 release and of fibroblast growth factor (FGF) and vascular endothelial growth factor (VEGF)[182]. Indeed, the increased expression of VEGF can also be triggered by MMP2 and MT1-MMP and VEGF cleavage is promoted by MMP1, -3, -7, -16 and -19, increasing the angiogenic potential of tumor cells[182].

Tumor invasion occurs either by mobilization of a group of cells or by cell migration, where the migrating cell moves in an amoeboid or mesenchymal manner and mimics the epithelial-to-mesenchymal transition (EMT) characteristic of embryonic development and invasive cancer[206,230]. In this regard, MMP2, -9 and MT1-MMP have been involved in tumor cell extravasation[206]. Afterwards, MMPs create the metastatic niche for tumor cells to grow by promoting angiogenesis, modulating apoptosis and preventing inflammatory cell chemotaxis by cleavage of chemokines such as CXCL12 and IL-1β[130,206].
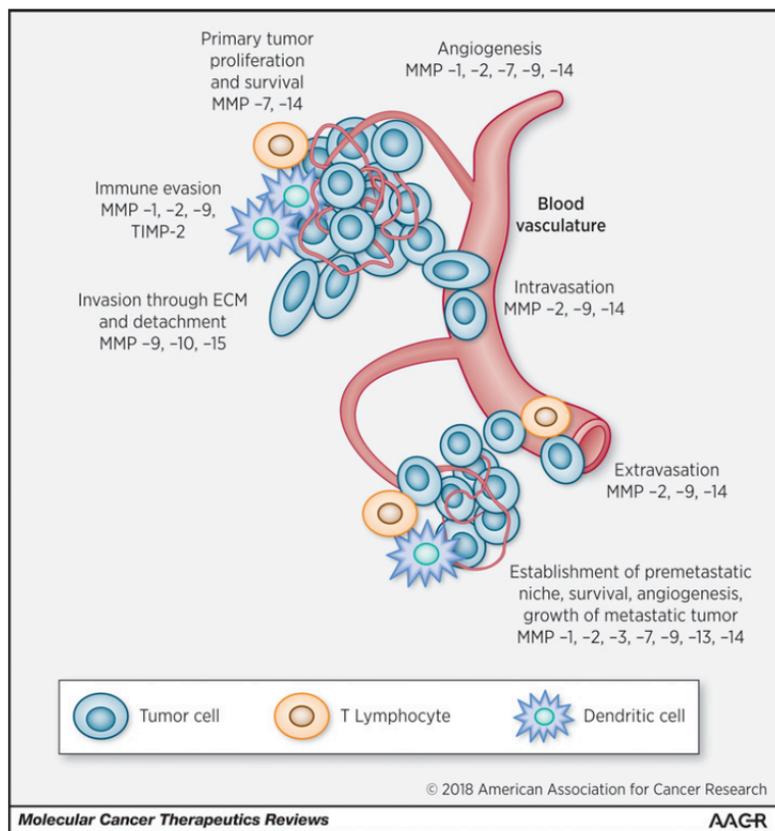
Figure 32. MMPs in cancer. Differential expression of MMPs in tumor growth, proliferation, invasion, intravasation, extravasation and angiogenesis. Figure taken from Winer et al. (2018)[206].

Angiogenesis is mainly regulated by MMP1, -2, -7, -9 and MT1-MMP, whereas apoptosis is reduced in tumor cells by MMP7-mediated cleavage of the Fas ligand at the cell surface of tumor cells, restricting Fas death receptor stimulation[206]. In terms of inflammatory response caused by chemotaxis inhibition, MMP1, -2 and -9 can downregulate interleukin receptor availability on the cell surface and promote tolerance to cancer[130,206].

Given their multiple roles in promoting cancer progression, MMPs were initially used as a therapeutic target for cancer treatment[206,231]. The design of several inhibitors initiated in the late 1980s with Batimastat, however, due to its high toxicity was not further developed[206]. Some other inhibitors targeted to several MMPs moved to phase III clinical trials but were cancelled without successful results, probably due to the fact that MMPs are very similar, particularly in the area close to the active site, therefore, targeting only a specific group of MMPs results challenging[206,231]. Nowadays, a strategy addressing selective MMPs with inhibitors targeting MMP1, -2, -3, -9 and MT1-MMP is ongoing and several of these inhibitors are being tested in preliminary phases of clinical trials[206].

4.3.4 MMPs and cell migration

As mentioned before, MMPs actively participate in cell migration[158,185,202]. Cell migration occurs as a cyclic process where cells polarize at one end, extend protrusions in that direction and stabilize by forming adhesions with the ECM[232]. The extension of such protrusions requires actin polymerization and depending on the type of protrusion, such extensions could be branching-like (as in lamellipodia), parallel organized bundles (in filopodia)[232] or punctual cores (in podosomes and invadopodia)[233].
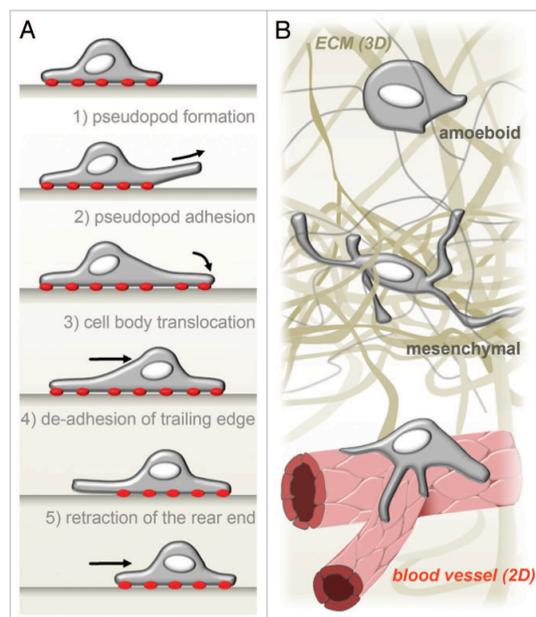
Figure 33. Migration in 2D (A) and 3D (B) environments. Figure taken from Wiesner et al. (2014)[234].

Migration can happen in 2 dimensions: in 2D cells slide along the matrix, whereas in 3D cells can penetrate it (Figure 33)[165,234,235]. Although the ECM represents a 3D environment, some cells, like leukocytes, could be exposed to 2D environments when, for example, they need to crawl on top of endothelial layer, preceding transmigration of blood vessels[236].

In 3D environments, cells can move either in an amoeboid manner, where cells maintain a spherical shape, generate short protrusions and migrate with higher velocity; or in a mesenchymal manner, where they acquire a more extended shape and generate longer protrusions at the cost of reduced velocity[234]. Both migration modes happen in parallel and depend mainly on the ECM network surrounding the cells[128,129].

Two structures are crucial for MMP secretion to ECM degradation areas: podosomes, in cells of the hematopoietic system, and invadopodia in cancer cells[237]. Their structures are described in more detail below.

4.3.4.1   Podosomes and invadopodia

The structure defining both podosomes and invadopodia constitutes an F-actin core surrounded by a "ring" of actin regulators –such as cortactin, N-WASP, Tsk5 and Arp2/3– that are recruited to the ECM via integrins, and plaque proteins –such as paxillin, vinculin and talin[158,216,237,238]. Although initially thought as a surrounding structure, nowadays it is known that the plaque ring is formed by discontinuous clusters of plaque proteins[239].

Both podosomes and invadopodia localize on the contact site between the cell membrane and the substrate in a perpendicular way and display a characteristic dot-like structure (Figure 34)[158,162,234,239]. Although structurally similar, podosomes are associated with migrating albeit non-malignant cells, such as macrophages, whereas invadopodia is mainly associated with cancer cells[163,165].

The main differences between both structures lie in their number (podosomes are more numerous, 20-100/cell vs. 1-10/cell), their size (invadopodia are bigger, 8x5 μm^2 vs. 1x0.4 μm^2), their life time, (podosomes have a high turnover rate) and their ability to degrade matrix (higher in invadopodia)[240]. In this regard, one of the main characteristics of invadosomes is their degrading capacity[237]. Contrary to FAs, where their presence is mostly associated with matrix reorganization and fibrillogenesis, invadosomes actively secrete matrix metalloproteases and ADAMs in order to degrade underlying ECM and move throughout the tissue[237].
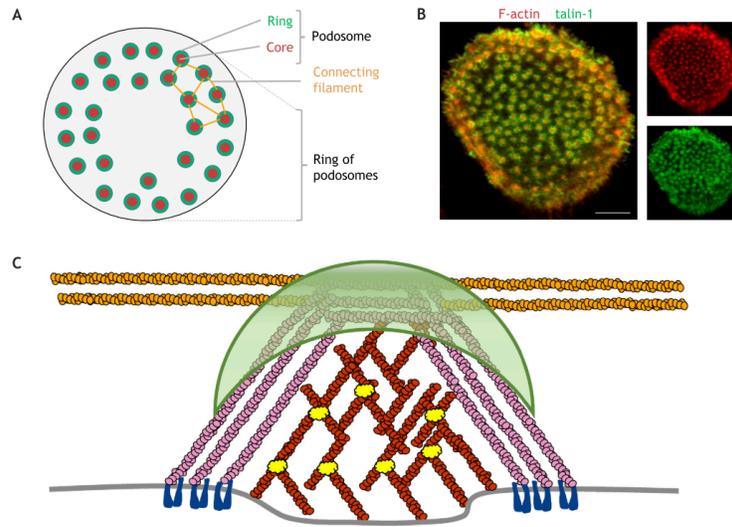
Figure 34. Podosome structure. (A) Scheme depicting podosome organization in clusters. (B) Confocal microscopy image of a primary human macrophage stained for F-actin (red, Phalloidin-Alexa564) and talin (green, primary antibody + Alexa 488). (C) Scheme of podosome substructure with the connecting filaments in orange, the cap in green, the lateral filaments in pink, the F-actin core in red, the Arp2/3 complex in yellow and integrins in dark blue color. Figure taken from van den Dries et al. (2019)[239].

Although invadopodia has a higher degrading capacity, probably due to a longer lifetime, podosomes numbers allow leukocytes to degrade a larger area[165]. In particular, podosomes in monocyte cells recruit membrane-bound type I matrix metalloprotease (MT1-MMP, see section 4.3.2) to the plasma membrane in a microtubule-dependent manner mediated by the motor proteins kinesin-1 and -2 and RabGTPases such as Rab8[226,241]. Noticeably, such recruitment is not relevant for the podosomes assembly, but for its proteolytic activity[165,226].

4.4   Intracellular transport of MMPs

MT1-MMP has been described as the major proteolytic enzyme in invadopodia[225,226,228,229], although it has also been observed in podosomes on human macrophages[241,242]. Monteiro et al. (2013) showed that WASH and Arp2/3 were required for the formation of invadopodia extensions and, together with the exocyst complex, for the docking of MT1-MMP positive endosomes to the plasma membrane[229]. This in turn recruited MT1-MMP and promoted basal membrane rupture and the subsequent invasion of tissue[229].

Vesicle transport is essential for MT1-MMP secretion[195]; therefore, research efforts have focused on elucidating the machinery that brings MT1-MMP to the plasma membrane. In this regard, Bravo-Cordero et al. (2007) demonstrated that MT1-MMP transport to the invasive structures was mainly dictated by regulated exocytosis[243]. Moreover, they identified colocalization between Rab8 and MT1-MMP, strongly indicated that the GTPase activity is necessary for MT1-MMP exocytic transport[243]. Altogether, they propose the existence of a permanent pool of intracellular MT1-MMP that can rapidly distribute this MMP to the plasma membrane upon stimulus[243].

Further studies from the Linder and Scita groups elucidated a network of at least 4 different GTPases controlling the delivery of MT1-MMP to podosomes in macrophages, with Rab8a regulating MT1-MMP delivery from Golgi to plasma membrane, and Rab5, Rab22a and Rab14 involved in its endosomal recycling[226,228,242,244]. In cancer cells, MT1-MMP trafficking is rather regulated by Rab2a, Rab4 and Rab5, which control its availability from the endosomes to the plasma membrane[226,245].

Although MT1-MMP trafficking has been intensively studied in the last years, the trafficking of soluble MMPs requires more investigation. Initially, studies on neurons from Sbai et al. (2008) evidenced for the first time that MMP2, MMP9 and TIMP1 were trafficking in vesicles from the secretory pathway, based on observations of a secretion impairment in BFA treated cells[246]. Later on, the same group demonstrated that MMP2 and MMP9 were delivered in different vesicles that were distributed along microtubules and transported by kinesin and myosin V[247]. In parallel, Kean et al. (2009) showed in cancer cells, that MT1-MMP, but not MMP2 and MMP9, required syntaxin-13 for proper delivery to the cells surface[248]. Furthermore, they revealed that SNAP23 and VAMP3 are required for MMP2 and MMP9 secretion[248].

Recently, Jacob et al. (2013) identified the requirement of Rab40b for proper delivery of MMP2/9 to invadopodia. Moreover, they observed that Rab40b silencing reduced matrix degradation down to 50%, suggesting that MT1-MMP, which was already shown to be transported in different vesicle carriers, may compensate for the impaired delivery of MMP2/9[212].

In conclusion, the transport of MMPs to either podosomes or invadopodia is mediated by vesicular carriers, which seem to be different among MMPs[246]. These carriers are transported from the TGN –or intermediate endosomal compartments in the case of MT1-MMP– via

motor proteins towards the plasma membrane[241,249]. Although new investigations are contributing to the elucidation of MMP trafficking pathways, the intracellular mechanism driving their transport through the secretory pathway remains unknown. And this question is the core of the present thesis.

5. Aims and scope

MMPs play a crucial role in tissue homeostasis[129,160,185,211,234]. During the last 20 years these proteins were the focus of many researchers looking for a mechanism that could control their function and, in this way, develop therapies against cancer[185,250,251]. However, the moonlighting functions of MMPs, as well as their highly conserved catalytic domain, contributed to the failure of many of these efforts[206].

Although the literature covering MMPs function is abundant, the intracellular trafficking of these proteins remains poorly understood. Some studies have made an effort to describe their trafficking in neurons[246,247], cancer[212,216], and olfactory cells[249], however, the machinery involved has not been yet elucidated. Therefore, the principal aim of this thesis was to identify the molecular mechanism of intracellular trafficking of MMPs, with particular focus on MMP2. For this purpose, this thesis addressed the following goals:

I. To identify MMP2 potential interacting candidates that could influence its intracellular trafficking.

II. To evaluate their impact in MMP2 intracellular trafficking using single-cell cargo sorting assays.

III. To examine the physiological relevance of MMP2 trafficking in the absence of identified candidate(s).

6. Materials and methods

All the methods marked with an asterisk (*) are included on the paper *Nucleobindin-1 regulates ECM degradation by promoting intra-Golgi trafficking of MMPs*, at the moment under revision for publication on the Journal of Cell Biology (JCB). Specific methods from other labs are also indicated in brackets.

6.1 Molecular biology methods

Expression vectors were generated using either a general cloning approach (as follows) or the Gibson assembly method[252]. Unless otherwise indicated, all the restriction enzymes were purchased from New England biologicals (NEB, Ipswich, USA) and used according to manufacturer's recommendation. For the PCR reactions, a Mastercycler Nexus Gradient (Eppendorf, Hamburg, Germany) was used.

6.1.1 Polymerase Chain Reaction (PCR)

Plasmid DNA was amplified using 20 ng of template vector, 200 µM dNTPs, 0.5uM of primers (reverse and forward, see Table XX) and 0.01 units of Phusion High Fidelity DNA Polymerase (Thermo Fischer, Waltham, USA) in the provided 1X HF buffer and completed with Gibco™ sterile distilled water (Thermo Fischer, Waltham, USA) up to a final volume of 50 µL.

Samples were then incubated for 5 min at 95°C to denature DNA strands, then incubated in 35 cycles of 30 sec at 95°C and incubated for annealing 30 sec at temperatures ranging from 52 to 67°C according to the annealing primer pair. Finally, elongations cycles of 30 sec/500 bp at 72°C were performed with a final elongation cycle of 10 min at 70°C before cooling at 4°C.

6.1.2 sgRNA annealing and insertion into pX vectors for CRISPR cell line generation

The annealing of sgRNAs was performed using 100 µM top and bottom oligo nucleotides. These were mixed with 10 units of polynucleotide kinase in 1X T4 ligase provided buffer and incubated as follows: 30 min at 37°C + 5 min at 96°C + 1 min incubation at 95°C + 5 min at 85°C + 1 min at 80°C + 0.1 C/sec until reaching 70°C. The annealed oligo nucleotides were

then stored at 4°C and posteriorly digested with BbsI to create compatible ends for cloning in pX vector.

6.1.3 Agarose gel analysis and DNA purification

DNA amplification was analyzed using 1% agarose gels stained with SYBR Safe (Thermo Fischer, Waltham, USA) in 1% TAE buffer. Samples were mixed with 10X DNA loading dye and ran for 30 min at 100V. Confirmation of PCR products was performed evaluating correspondence to the expected molecular weight using a marker (8 µL) from Thermo Scientific (Waltham, USA). Correct bands were cut and digested with mi-Gel extraction Kit (Metabion, Martinsried, Germany), according to the provider instructions.

6.1.4 Restriction digest

After PCR purification, products and vectors were digested overnight (ON) at 37°C with the enzymes indicated in Table XX. Then the enzymatic components were removed using the mi-PCR purification Kit from Metabion (Martinsried, Germany) and ligated into backbone vectors.

6.1.5 Ligation

The DNA amounts used for digestion were calculated using the NEBBioCalculator webtool (nebiocalculator.neb.com/#!/ligation) or keeping a ratio fragment to vector of 3:1 or 7:1 depending on the length of the fragment. For all reactions, 100 ng of vector was used. The reaction was carried out for at least 1h at room temperature (RT) with 10 units of T4 ligase in the corresponding buffer (CutSmart, 2.1 or 3.1) and completed with water to a final volume of 20 µL.

6.1.6 Gibson assembly

This cloning and ligation strategy was performed as previously published[252] using the Gibson Assembly master mix provided by the Core Facility of the Max Planck Institute of Biochemistry. Primers are listed in Table XX. The mixture of fragments was done keeping a fragment to plasmid ratio 3:1 and using at least 25 nmol plasmid per reaction. DNA amount for each reaction was calculated using the Promega webtool (**https://www.promega.de/resources/tools/biomath/**).

6.1.7 Transformation into *E. coli* bacterial cells

10 – 20 μL of ligated DNA were transformed into at least 30 μL of *E. coli* chemically competent OmniMAX 2Tl cells by incubation for 30 min on ice, followed by a heat shock of 90 sec at 42°C and recovery for at least 1h at 37°C with constant shaking. After this time, cells were plated in agar LB plates containing ampicillin or kanamycin (100 μg/mL) and incubated ON at 37°C.

6.1.8 Single clone isolation and sequencing validation

After ON incubation, colonies were picked and cultured in 4 mL LB medium containing ampicillin / kanamycin (100 μg/mL) and incubated again ON at 37°C with constant shaking. Then, plasmid DNA was purified using the NucleoSpin Plasmid EasyPure Kit (Macherey-Nagel, Düren, Germany) and DNA concentration was determined with a Nanodrop ND-1000 Spectrophotometer (PEQLAB Biotechnologie GmbH, Erlangen, Germany). To confirm the correct insertion, DNA was evaluated by sequencing using the SmartSeq Kits from Eurofins Genomics (Ebersberg, Germany).

6.1.9 Mutagenesis for introduction of single point mutations

This methodology was developed and performed by Birgit Blank as previously documented[253]. Briefly, PCRs were performed as described above with the following modifications: 400 μM dNTPs and 0.6 μM primers were used. The number of cycles was reduced to 16 and after confirmation of correct PCR product by agarose gel electrophoresis, the DNA was digested with DpnI for 1h at 37°C to destroy the template DNA. Finally, 2.5 μL of the treated DNA were transformed into 50 μL competent *E. coli* cells.

6.1.10 Generation of chemically competent *E. coli*

E. coli Omnimax 2Tl culture (2 mL) were incubated ON in 100 mL LB growth medium at 37°C with permanent shaking until they reached OD 0.5. Cells were then collected to 4°C and centrifuged 15 min at 3000 rpm (4°C). After discarding the SN, the pellet was resuspended in 10 mL TSS buffer with 2.5mL of 87% glycerol and aliquots were snap frozen and stored at -80°C.

6.1.11 Plasmids, primers and restriction enzymes

All restriction enzymes used in this study were purchased from New England Biolabs Inc. (Ipswich, MA, USA). Primers were purchased to Metabion International AG (Planegg, Germany).

Table 1. List of plasmids used in this work.

Backbone plasmid	Insert	Publication	Cloning method	Restriction enzymes	Primer Forward 5' - 3'	Primer Reverse 5' - 3'
pLPCX	ssHRP-Flag	von Blume 2012[107]	N/A			
pLPCX	LyzC-Flag-EGFP	This work	RC	EcoRI / BamHI	CCGGAATTCCGGATGAAGGCTCTCATTGTTCTGGGGC	CGCGGATCCGCGCTTGTCATCGTCATCCTTGTAATCGATGTCATGATCTTTATAATCACCGTCATGGTCTTTGTAGTCCACTCCACAACCTTGAACATACTGACGG
				BamHI / NotI	CGCGGATCCGTGAGCAAGGGCGAGGAG	TTTTCCTTTTGCGGCCGCTTACTTGTACAGCTCGTCCATGC
pIRESneo 3	Str-KDEL-LyzC-FLAG-SBP-EGFP	Deng et al., 2018[96]	N/A			
pLPCX	hsMT1MMP-pHluorin-HA	This work	RC	EcoRI / Not1	CCGGAATTCATGTCTCCCGCCCCAAGAC	TTTTCCTTTTGCGGCCGCTCAAGCGTAATCTGGAACATCGTATGGGTAGACCTTGTCCAGCAGGGAACG
pIRESneo 2	Str-KDEL-SS-SBP-EGFP	This work	RC	AscI / EcoRI	TTGGCGCGCCATGGCTACAGGCTCCCGGAC	CCGGAATTCCCGGATAAGGGAATGGTTGGGAAGG
pIRESneo 3	Str-KDEL_SS-SBP-EGFP-HA-Cathepsin D	Deng et al., 2018[96]	N/A			
pIRESneo	Str-	This work	RC	AscI /	TTGGCGCGCCATGGCTACAGGCTCC	CTTATCGTCGTCATCCTTGTAAT

4	KDEL_SS-SBP-EGFP-HA-MMP2nSS			EcoRI	CCGGAC	CGGATAAGGG AATGGTTGGGA AGGC
					GCCTTCCCAACC ATTCCCTTATCC GATTACAAGGAT GACGACGATAA G	CCGGAATTCCC CAGCGTAATCT GGAACATCGTA TG
pIRESneo 3	Str-KDEL-SBP-MT1MMP-mCherry	This work, kind gift from Franck Perez Lab	RC	AscI / EcoRI	AAGTGGCGCGC CATGTCTCCCGC CCCAAGA	GCGCGAATTCG CTCCGCCCTCCT CGTCCA
				FseI / SfiI	AGATGGCCGGC CATTAGGCGGG GCGGTGAGCG	AATCGGCCCTC GAGGCCTCAGA CCTTGTCCAGC AGGG
				BsrGI / SbfI	MCHERRY CODING SEQUENCE WITH THE MENTIONED RESTRICTION SITES	
pLPCX	SS-EGFP	This work	RC	EcoRI / XhoI	CTGGGCCCATAA AGCTTATACGAA TTCATGGCTACA GGCTCCCGGAC	CTCCTCGCCTTT GCTCACCATGG AATTCCCGGAT AAGGGAATGG
pLPCX	GFP-HA	This work	RC	BamHI / EcoRI	CGTGGATCCATG GTGAGCAAGGG CGC	GCAGAATTCTT AAGCGTAGTCT GGGACGTCGTA TGGGTACTTGT ACAGCTCATCC ATGCCG
pLPCX	SS-Flag-MMP2-HA-eGFP	This work	GA	EcoRI / XhoI	GGGCCCATAAAG CTTATACGAATT CCATGGCTACAG GCTCCCGGAC	TCCTCGCCTTTG CTCACCATAGC GTAATCTGGAA CATCGTATGGG TA
					TACCCATACGAT GTTCCAGATTAC GCTATGGTGAGC AAAGGCGAGGA	GCGGCCGCTTG TCGACACTCGA GTTAAGGCCGG CCCTTGTACAG
pLPCX	GoD1cpv	Deng et al., 2018[96]	N/A			
pLPCX	NUCB1 tagless	This work	RC	EcoRI / Not1	INSERT FROM PCMV6-AC-NUCB1-TURBOGFP (ORIGENE: RG201786)	
pLPCX	NUCB1-myc	This work	GA	HindIII / BamHI	GATCTGGGCCCA TAAAGCTTCCAT GCCTCCCTCTGG GC	CGACACTCGAG TATGGATCCTC ACAAGTCTTCTT CAGAGATGAGT TTCTGCTCCAG ATGCTGGGGCA CCTCAAC
pBT-PAF	NUCB1-myc	This work	RC	HindIII / NotI	INSERT FROM PLPC-NUCB1-TAGLESS	
pLPCX	NUCB1-EQ1-myc	This work	SDM	HindIII / NotI	CGGACTCAGATC TGGGCCCATAAA GCTTCCATGCCT CCCTCTGG	GTGCCTCCAGC TGCTGCTCATC C
					GGATGAGCAGC AGCTGGAGGCA	CCCCTTTTTCTG GAGACTAAATA

					C	AAATCTTTTATT TTATCGATGTA TATGCTCACAA GTCTTCTTCAG AGATGAGTTTC TGCTCC
pLPCX	NUCB1-EQ2-myc	This work	SDM	HindIII / NotI	CGGACTCAGATC TGGGCCCATAAA GCTTCCATGCCT CCCTCTGG	GCGAGGAACTG CTCCAGGGTC
					GACCCTGGAGCA GTTCCTCGC	CCCCTTTTTCTG GAGACTAAATA AAATCTTTTATT TTATCGATGTA TATGCTCACAA GTCTTCTTCAG AGATGAGTTTC TGCTCC
pLPCX	NUCB1-EQ1+2-myc	This work	RC	BamHI / SphI	INSERT FROM PLASMID PLPCX-NUCB1-EQ1-MYC REPLACED IN PLPCX-NUCB1-EQ2-MYC	
pLPCX	dPro-peptide-Flag-MMP2-eGFP	This work	GA	EcoRI / XhoI	GCCCATATATGG AGTTCCGCGTTA C	GGGCTTGCGAG GGAAGAAGTTG TAGCTACCGCC TCCACCCTTATC G
					CGATAAGGGTG GAGGCGGTAGC TACAACTTCTTCC CTCGCAAGCCC	CCTCGCCTTTG CTCACCATGCA GCCTAGCCAGT CGGATTTG
					CAAATCCGACTG GCTAGGCTGCAT GGTGAGCAAAG GCGAGG	GCGGCCGCTTG TCGACACTCGA GTTAAGGCCGG CCCTTGTACAG
pLPCX	dCatalytic Domain_Flag-MMP2-eGFP	This work	GA	EcoRI / XhoI	GGGCCCATAAAG CTTATACGAATT CCATGGCTACAG GCTCCCGGAC	CAGCTCCTCGC CTTTGCTCACCA TGAGCTCCTGA ATGCCCTTGAT GTC
					GACATCAAGGGC ATTCAGGAGCTC ATGGTGAGCAAA GGCGAGGAGCT G	GCGGCCGCTTG TCGACACTCGA GTTAAGGCCGG CCCTTGTACAG
pLPCX	dHpex-Flag-MMP2-eGFP	This work	GA	EcoRI / XhoI	GGGCCCATAAAG CTTATACGAATT CCATGGCTACAG GCTCCCGGAC	CAATGTCAGGA GAGGCCCCATA GTTGGCCACAT CTGGGTTGCC
					GGCAACCCAGAT GTGGCCAACTAT GGGGCCTCTCCT GACATTG	CCTCGCCTTTG CTCACCATGCA GCCTAGCCAGT CGGATTTG
					CAAATCCGACTG GCTAGGCTGCAT GGTGAGCAAAG GCGAGG	GCGGCCGCTTG TCGACACTCGA GTTAAGGCCGG CCCTTGTACAG

Vector	Construct	Source	Method	Restriction sites	Primer 1	Primer 2
pLPCX	MMP2-Prop-CtoA-eGFP	This work	SDM		SINGLE MUTAGENIC PRIMER: GGCCACATCTGGGTTGCCGGCGCGTGGCTTCCG	
pLPCX	nSS-Flag-MMP2-Propeptide-truncation-HA-eGFP	This work	GA	EcoRI / XhoI	AGCGTAATCTGGAACATCGTATGGGTAGTTGGCCACATCTGGGTTGC	GGGCCCATAAAGCTTATACGAATTCCATGGCTACAGGCTCCCGGAC
					GCAACCCAGATGTGGCCAACTACCCATACGATGTTCCAGATTACGCT	GCGGCCGCTTGTCGACACTCGAGTTAAGGCCGGCCCTTGTACAG
pLPCX	GPP130-Twitch5	This work	RC	MluI / NotI	CACACGCGTGTGAGCAAGGGCGAGGAG	CACGCGGCCGCTCAATCCTCAATGTTGTGACGG
				HindIII	CCCAAGCTTATACGAATTCATGGGAAACGGGATGTGCTC	CCCAAGCTTAGAATCTTGCCTTCCTTTGTTCAGTG
pBT-PAF	NUCB1-His	This work	RC	NheI / NotI	GGCGGCCATCACAAGTTTGTACAGCTAGCCATGCCTCCCTCTGGGC	GCGGCCGCTTGTCAGTGATGATGATGGTGATGACCGCCTCCACCCAGATGCTGGGGCACCTCAAC
pBT-PAF	His-Sumo-MMP2	This work	GA	HindIII / NotI	CATTCCCTTATCCTCGGGAACAAAGCTTCATCACCATCATCATCACGGGTCC	CTTATCGTCGTCATCCTTGTAATCGCATTCACCTCCAATCTGTTC
					GAACAGATTGGAGGTGAATGCGATTACAAGGATGACGACGATAAG	GATCAGTTATCTATGCGGCCGCTCAGCAGCCTAGCCAGTCGGATTTG
pBT-PAF	NUCB1_EQ1+2-His	This work	RC	NheI / NotI	GGCGGCCATCACAAGTTTGTACAGCTAGCCATGCCTCCCTCTGGGC	GCGGCCGCTTGTCAGTGATGATGATGGTGATGACCGCCTCCACCCAGATGCTGGGGCACCTCAAC
pLPCX	NUCB1-cyto	This work	RC	HindIII / NotI	CCATAAAGCTTATACATGGTCCCCCTGGAGCGAGGG	TTATCGATGTATATGCGGCCGCG

RC: recombinant cloning; GA: Gibson assembly; SDM: site directed mutagenesis.

6.2 Cell culture methods

6.2.1 General culture conditions

HeLa and HEK293T cells were cultured in Dulbecco's Modified Eagle Medium (DMEM), high glucose, GlutaMAX supplemented with 1% Penicillin/Streptomycin and 10% fetal bovine serum (FBS). MDA-MB-231-MT1-MMP-mCherry were a kind gift from Dr. Angelika Haußer and were cultured in Leibowitz 15 medium supplemented with 15% FCS and 0.5 mg/mL gentamycin (G418). Unless indicated otherwise, all cell culture reagents, including DNA/RNAse free water were from Gibco (ThermoScientific, Waltham, USA). Plasticware (well plates and petri dishes) were purchased from Corning Inc. (Corning, USA).

HeLa and HEK293T cells were kept at 37°C and 5% CO_2, whereas MDA-MB-231-MT1-MMP-mCherry cells were maintained at the same temperature but with only 1% CO_2. To passage the cells, first they were washed with DPBS, then incubated for 2-5 min with 1X trypsin/EDTA and resuspended in cell culture media. Then cells were centrifuged for 5 min at 1000 rpm, supernatant was discarded, and cells were resuspended in growth medium. Afterwards, cells were count (only for seeding) or directly transferred to a new dish with growth medium (amount adjusted according to the desired cell density).

6.2.2 Freezing and thawing

Cells destined to be kept for long term were detached as mentioned before for passaging and after centrifugation and discarding supernatant, resuspended in a solution of FCS with 1% DMSO, transferred to cryo-freezing units and frozen at -80°C. After freezing was complete, they were transferred to a liquid nitrogen tank at -196°C. For thawing, cells were briefly incubated at 37°C in a water bath and then resuspended in growth media (twice their volume). After 5 min centrifugation at 1000 rpm, supernatant was discarded, cells were resuspended in 5 mL growth medium, mixed with additional 15 mL fresh medium and transferred to a 15 cm petri dish. Once 70-80% confluence was reached, cells were used for experiments.

6.2.3 siRNA tranfection

Cells were silenced using 1.5 μL of 20 μM siRNA with 12 μL HiPerfect® (Quiagen, Venlo, The Netherlands) diluted in 100 μL OptiMEM. After vortexing and RT incubation, the mixture was added dropwise to cells seeded in 6-well plates. For MDA-MB-231-MT1-MMP-mCherry cells the amount was escalated to silence 10 cm dishes.

The oligonucleotides used for silencing were purchased from Life Technologies, with the following epitopes:

siNUCB1-1:   5'-UCAUGCAGUAUGAAGAAGGUCUUGG-3′

siNUB1-2:   5'-GAGCUGGAGAAAGUGUACGACCCAA-3′

siMMP2-1:   5'-AGUAGAUCCAGUAUUCAUUCCCUGC-3′

siMMP2-2:   5'-CCAGAUGUGGCCAACUACAACUUCU-3′

6.2.4   Plasmid transfection

HeLa and HEK293 transfections were done using polyethylenimine (PEI) in growth medium. Once HeLa cells reached around 50-60% confluence, a mixture of 2 μg DNA and 1.25mg/mL Polyethylenimine (PEI, Alfa Aesar Chemicals, Shanghai, China) in OptiMEM® was added dropwise to cells in culture and incubated for 24 h. For MT1-MMP-mCherry RUSH transfection, the same concentration of Lipofectamine LTX was used instead of PEI.

6.2.5   Single clone isolation

Cells were trypsinized as described above, counted by the Countess II system (Thermo Fisher Scientific, USA), diluted and seeded in a concentration of 100 cells in 15mL. Cells were incubated in 15 cm dishes until they were big enough to be distinguishable by naked eye. Then cells were manually scratched off with a pipette tip and transferred to a 96 well plate. Cells were incubated again until reaching at least 70% confluence.

6.2.6   Generation of stable cell lines

HeLa cells stably expressing MMP2-eGFP or any of its variants were transfected by VSV-G pseudotyped retroviral particles produced in transiently transfected HEK293T cells, as described by Pfeifer et al. (2000)[254]. Viral particles were concentrated from cell culture supernatants and used for infection. The next day, HeLa cells were selected in 2 μg/ml puromycin (Sigma-Aldrich, Munich, Germany) for 24 h and frozen or used for experiments.

6.2.7   Generation of CRISPR cell lines

HeLa cells were transfected with pSpCas9 vectors encoding at least 3 designed gRNAs and using PEI as a transfection reagent. Selection was performed using puromycin (2 μg/ml) for at

least 24 h. Then single clones were isolated (see above), expanded and analyzed by western blotting and immunofluorescence microscopy. For sequencing, genomic DNA was isolated by GenElute Mammalian Genomic DNA Miniprep Kit according to manufacturer's protocol (Sigma-Aldrich, Munich, Germany). More details are given in section 7.3.

6.2.8 qRT-PCR (Haußer Lab)*

RNA isolation from cells was performed using the NucleoSpin® RNA kit (Macherey-Nagel) according to the manufacturers' instructions. The real-time PCR reaction was performed using the QuantiTect SYBR Green RT-PCR Kit (Qiagen) and 100 ng of RNA. qRT-PCR was performed with a Cfx96 device (Bio-Rad) using a Power SYBR Green RNA-to-Ct 1-Step kit (Applied Biosystems). To amplify MMP2 (Hs_MMP2_1_SG) and Peptidylprolyl Isomerase (PPIA; Hs_PPIA_4_SG), QuantiTect Primer assays (Qiagen) were used, and changes in the relative expression levels were determined using the 2–ΔΔCt method (Bio-Rad CFX Manager software 3.1).

6.3 Biochemical methods

6.3.1 SDS PAGE and Western blotting

10% homemade acrylamide gels or NuPAGE 4%–12% gradient gels were used for SDS-PAGE. For Western blotting, transfer of samples to nitrocellulose membranes was performed for 75 min. Then membranes were blocked in 5% BSA in Tris-buffered saline (TBS) for at least 1 h at room temperature. After this time, membranes were incubated overnight with primary antibody in a shaker at 4 °C, washed for 1 h with TBS + 0.1% Tween-20 (TBS-T) and incubated with secondary antibody for 2 h at 4 °C. Previous to documentation in ChemiDoc Imaging System (Bio-Rad®), ImageQuant LAS 4000 series (GE Healthcare Life Sciences, Pittsburgh, PA, USA) or Amersham Imager 600 (GE Healthcare Life Sciences, Pittsburgh, PA, USA), membranes were washed for half an hour with TBS-T.

6.3.2 Protein expression and purification*

Stable HEK293 cells lines expressing His-SUMO-MMP2, rNUCB1-His or rNUCB1-mEF1+2-His were generated by transfecting of 1.2 µg of the pBT-PAF vector encoding the correspondent sequence of interest (see Table 1), 0.8 µg pB-RN vector and 0.8 µg pBase vector with PEI (see section 6.2.4). After selection, 2 pools of positively transfected cells were

frozen. HEK293T cells were incubated with DMEM serum-free media supplemented with 1 µg/mL doxycycline and 1 µg/mL aprotinin for at least 20 h to induce protein production. Upon this time, cell supernatants were collected and purification initiated.

For His-SUMO-MMP2 and rNUCB1-His a purification column packed with cOmplete His-tag purification resin from Roche (Mannheim, Germany) was used, as described by Crevenna et al., (2016) was used[95]. For the purification of rNUCB1-mEFh1+2- cell supernatants were collected, concentrated 100X using centrifugal filter units (Amicon Ultra, Ultracel 10K), transferred to an Eppendorf tube containing previously equilibrated Protino® Ni-NTA agarose beads (His-binding buffer) and incubated for 2 h at 4ºC with rotation. Afterwards, the protein-bound-beads were washed by centrifugation cycles (3400 xg, 5 min each), incubated with His-elution buffer and finally, eluted samples were dialyzed overnight in His-reconstitution buffer at 4°C.

6.3.3 Maleimide protein labelling*

Recombinant His-SUMO-MMP2 was labeled with Cy®3-NHS-Ester according to the manufacturer instructions (Sigma-Aldrich, St. Louis, MO, USA). After labeling, the protein was dialyzed in 20 mM Tris + 100mM NaCl, pH7.0 to remove excess of free dye.

6.3.4 Visualization of NUCB1 EF-hand motifs*

The nuclear magnetic resonance structure of NUCB1 [1SNL, Research Collaboratory for Structural Bioinformatics Protein Data Bank (RCSB PDB)] were visualized using the UCSF Chimera software [developed by the Resource for Biocomputing, Visualization, and Informatics at the University of California, San Francisco, with support from NIH P41-GM103311][255]. The rotamer that is shown was selected according to the highest probable candidate from the Dunbrack backbone-dependent rotamer library Shapovalov and Dunbrack (2011), and the pictures were adapted from the available model 1SNL de Alba and Tjandra (2004) in RCSB PDB using the UCSF Chimera software[108,255,256].

6.3.5 Immunoprecipitation assays*

HeLa cells (3×10^5 cells/mL) were seeded in 15-cm plastic dishes (2 per sample), incubated overnight, transfected with 15 g DNA per dish using PEI (ratio: 2 µg DNA / 7.5 µL PEI) and incubated for 20 h. Thereafter, the cells were washed twice with 1X PBS, scraped, and centrifuged for 3 min at 3400 rpm. Supernatants were removed and pellets were washed two

more times. After washing, 300 μL lysis IP buffer were added to the samples and these were incubated for 30 min on ice. After this time, samples were filtered through a 27G needle and centrifuged at >13,000 rpm, 4°C for 5 min. Then, supernatants were placed in a new Eppendorf tube and centrifuged once more for at least another 20 min, >13,000 rpm, 4°C. Afterwards, total protein was estimated using Bradford assay and normalized to the lowest protein concentration. To incubate with the beads, a volume of 27 μL per sample was taken, mixed with 9 μL 4× Laemmli buffer and labeled as input sample (10% input). Samples were then mixed with 35 μL GFP beads, previously equilibrated with the lysis IP buffer, and incubated in an end-to-end rotator at 4°C for 1 h. After incubation, samples were centrifuged at 3400 rpm, 4°C for 3 min, supernatants were discarded, and pellets washed with 1 mL lysis IP buffer. This step was repeated twice, and after the last removal of supernatant, 35 μL oh 4X Laemmli buffer was added to the samples, incubated at 95°C for 10 min and centrifuged at maximal speed (room temperature –RT°–). Finally, supernatants were collected and labeled as IP sample for loading in 10% SDS gel.

For the immunoprecipitation experiments using rNUCB1-His, approximately 100 μL of the recombinant protein were dialyzed overnight using the Pur-A-Lyzer™ mini dialysis Kit (Sigma-Aldrich, St. Louis, MO, USA) was used to dialyze approximately 100 μL of the recombinant protein in 500 mL IP buffer without protease inhibitor. After overnight dialysis, protein concentration was determined via absorbance measurement at 280 nm using a Nanodrop ND-1000 Spectrophotometer (PEQLAB Biotechnologie GmbH, Erlangen, Germany) was used to determine protein concentration via absorbance measurement at 280 nm. Then, protein concentrations were normalized and samples were incubated for 2 h (on rotator at 4ºC) with previously equilibrated Protino® Ni-NTA agarose beads (Macherey-Nagel, Duren, Germany; equilibration buffer: IP buffer without protease inhibitor). During the incubation time, Golgi preps (see section 3.4.1) were lysed by incubation with 50 μL lysis IP buffer for 15 min on ice and centrifuged at 13200 rpm for 10 min to remove lipid membranes. Upon incubation, beads were washed 5X with lysis IP buffer and centrifuged at 3400 rpm, 4ºC for 3 min each time. The lysed Golgi preps were added to the beads and incubated for 2 h with rotation at 4ºC. After incubation, samples were centrifuged at 3400 rpm at 4ºC for 3 min. The beads were transferred to a new tube in the last step. Then, 35 μL Laemmli buffer 4× was added to the samples and they were incubated at 95°C for 10 min. Samples were centrifuged at

maximal speed (room temperature), the supernatants were collected, labeled as IP sample and loaded in a NuPAGE™ 4–12% Bis-Tris protein gel.

6.4 Cell Biological methods

6.4.1 Isolation of Golgi membranes (Golgi preps)

The following procedure was adapted from the one described by von Blume et al. (2012)[107]. At least 15 x 15 cm plastic dishes containing HeLa control cells (3×10^5 cells/mL) were seeded and incubated overnight. Then they were washed 2x with PBS, cells were trypsinized (see cell culture section) and pooled in a falcon plus 10mL 1X PBS. Samples were centrifuged at 1000 rpm for 5 min, supernatant was discarded and pellets were placed on ice. From here on, all the procedure is made on ice. Cells were resuspended in 1 mL breaking buffer and centrifuged at 900 rpm, 4°C for 10 min. Supernatants were then discarded and pellet was resuspended in homogenization buffer (1:5 sample:buffer ratio). Samples were then transferred to an EMBO homogenizer with a 0.8 cm sphere and pushed 10-15 times through, caring about not introducing bubbles during the procedure. Afterwards, few μL of the sample were stained with trypan blue and evaluated by light microscopy to check for cell plasma membrane disruption.

When >80% of the cells were disrupted, homogenization buffer was added to the samples up to a final volume of 7.5 mL. Then the homogenate for the sucrose gradient was prepared by adding 7mL of 62% sucrose buffer and 150 μL of 100 mM EDTA pH 7.4. Refracted indexed was checked and, if necessary, adjusted to ~37% (+/- 0.5%). To prepare the gradient, 11.6 mL of 29% sucrose buffer were added at the bottom of a 30mL ultracentrifugation tube. Then, using a long needle, 15 mL of 35% sucrose buffer were poured very slowly on the bottom of the tube, caring about not mixing both sucrose solutions.

Finally, the homogenate sample was poured with a long needle in the bottom of the tube, keeping the gradient. Samples were then centrifuged at 28000 rpm for 2.5 h and 4°C (acceleration: 7/10). Afterwards, a 20G or 21G needle was used to take the cloudy fraction located in the upper part of the tube below the meniscus. This sample was transferred to a new ultracentrifugation tube, filled up to ¾ with breaking buffer and centrifuged again for 30 min, 28000 rpm at 4°C with maximal acceleration. Finally, supernatant was discarded, pellet

resuspended in ~150 μL and samples snap frozen in liquid nitrogen. These samples were stored at -80°C.

6.4.2   Secretion assays*

The Retention Using Selective Hooks (RUSH) secretion assay was performed according to the protocol described by Deng et al. (2018)[96]. Briefly, HeLa and NUCB1-KO cells (1×10^3 cells/mL) were seeded in 6-well plates, incubated overnight and transfected with SS-Flag-MMP2-SBP-eGFP or LyzC-Flag-SBP-eGFP using PEI. After 24h incubation, the cells were washed 3 times with 1X PBS and incubated in DMEM serum-free media for 45 or 60 min. After this time supernatants were collected and concentrated 20X using Centrifugal Filters (Amicon Ultra, Ultracel 10K). The cells were then lysed using 1× PBS + 0.05% Triton A-100, and the total protein was quantified. All samples were normalized to the corresponding lysate protein concentrations and Laemmli buffer was added to a final concentration of 1× for subsequent evaluation via SDS–PAGE and Western blotting.

The HRP transport and secretion assay was performed according to a previously described protocol[93,94,107]. Twelve-well plates were seeded with 125,000 HeLa or NUCB1-KO cells stably expressing SS-HRP-FLAG and incubated for 24 h. HeLa Brefeldin A (BFA) samples were pre-incubated with 10 μg/μL BFA in medium for 1 h previous to start the HRP secretion. Cells were then washed 5× with PBS and incubated in medium with or without BFA for 4 h. Cell culture supernatants were harvested and filtered. Cells were lysed in 0.5% Triton X-100 in PBS. The HRP activity was assessed by mixing 50 μL of medium or whole cell lysis with 50 μL Liquid Substrate System solution (2,2'-Azino-bis (3-ethylbenzothiazoline-6-sulfonic acid), Sigma-Aldrich, A3219) and absorbance measurements on a Magellan™ plate reader (Tecan Group Ltd., Switzerland) at 405 nm. The ratio of absorbance between secreted HRP and cellular HRP was then normalized to HeLa control samples, set to 100% and the normalized data from three independent experiments were plotted as mean ± SD. Significant differences with p-values < 0.05 were analyzed using the non-parametric Kruskal–Wallis test with Dunn's multiple comparison test.

Endogenous MMP2 secretion assays were performed using MDA-MB-231 cells stably expressing MT1-MMP-mCherry. Here cells were seeded into 6-well plates, incubated overnight and silenced afterwards using the described siNUCB1-1 (see section 6.2.3). Cells were incubated until 80% confluence was reached, washed with 1X PBS and incubated in 2 mL

Leibowitz L15 serum-free media for 16–20 h. After this time, supernatants were collected and concentrated 20× using centrifugal filter units (Amicon Ultra, Ultracel 10K). Cells were then lysed using 1× PBS + 0.05% Triton X-100, and total protein was quantified and normalized by the corresponding cell lysate protein concentration. Samples were then analyzed via SDS–PAGE and Western blotting.

Following the protocol described by Deng et al. (2018)[96], a semi-quantitative analysis of band intensities was performed using Fiji (ImageJ), and normalized data from at least two independent experiments were plotted as the mean ± SD. Significant differences were analyzed using the non-parametric Kruskal–Wallis test with Dunn's multiple comparison test (p-values < 0.05).

6.4.3   Zymography*

Gel Zymography experiments were performed as described by Toth et al. (2012)[257]. For this purpose, HeLa or NUCB1-KO cells (1.5 × 10^5 cells/mL) were seeded in 10-cm petri dishes, incubated overnight and thereafter transfected with either SS-Flag-MMP2-SBP-eGFP or LyzC-Flag-SBP-eGFP using PEI. After 24 h incubation, cells were washed carefully and starved by incubating in serum-free medium containing 40 μM biotin for 45 or 60 min, accordingly. Supernatants were collected and concentrated 20× using centrifugal filter units (Amicon Ultra, Ultracel 10K), whereas cell lysates were incubated with 300 μL Zymography lysis buffer on ice for 15 min and centrifuged at maximal speed for 20 min.

Samples were prepared by adding 1× Zymography sample buffer and evaluated using a Novex™ 10% Zymogram Plus (Gelatin) gel. For electrophoresis, zymography running buffer was used and samples ran at 150 V for 80 min. After this time, gels were briefly washed with distilled water and incubated with 100 mL 1X renaturing solution for at least 3 h. Then, gels were washed 3× with distilled water, incubating each time with at least 100 mL distilled water for 10 min. After the last washing step, water was replaced with 100 mL 1X developing solution and incubated for 30 min at room temperature. Upon this time, buffer was replaced with new 1X developing solution and incubated for at least 20 h at 37ºC on a shaker. Finally, the gels were briefly washed with water and stained with zymography staining solution until completely dark blue. Bands appeared as sharp clear areas. If necessary, gels were briefly (< 5 min) de-stained in zymography destaining solution. Semi-quantitative analysis was performed with Fiji (ImageJ).

6.4.4 Invasion assay (Haußer Lab)*

50 µL growth factor-reduced Matrigel (BD Biosciences, Bedford, MA, USA) diluted 1:20 in L-15 medium containing 0.5% FCS was used to coat Transwells (pore size 8 µm; Costar®; Corning Inc., Corning, NY, USA) on the upper side and then allowed to polymerize for 1 h at 37°C. Transfected cells (5×104 cells/mL) were seeded in Transwells in 100 µL of L-15 medium containing 0.5% FCS. L-15 medium supplemented with 10% FCS was placed in the bottom chamber of the Transwell. After 24 h of invasion, cells on the bottom of the membrane were fixed and stained with crystal violet. Quantification of six independent fields at a 10× magnification was performed using Image J (v1.49s).

6.4.5 Matrix degradation of MDA-MB-231 cells (Haußer Lab)*

Using Oregon488-conjugated gelatin (1 mg/mL; Invitrogen), coverslips were coated and crosslinked with 0.5% glutaraldehyde (Carl Roth GmbH, Karlsruhe, Germany). Transfected cells (5 × 104 cells/mL) were seeded on these coverslips and incubated for 5 h at 37 °C. At this time, cells were fixed and nuclei counterstained with 4′,6-diamidino-2-phenylindole (DAPI). A confocal laser scanning microscope LSM 710 (Carl Zeiss GmbH) equipped with a Plan-Apochromat 20×/0.8 was used for imaging and 40 confocal images per condition were acquired using identical settings for 488 and DAPI channels. Quantification of gelatin degradation was performed using the CellProfiler software version 3.0.0. Relative degraded area was defined as the measured area normalized by the average area of siControl in each experiment.

6.4.6 2D gelatin degradation assay of human primary macrophages (Linder Lab)*

NHS Rhodamine (Thermo Fisher Scientific) fluorescent gelatin (from swine; Carl Roth GmbH) was prepared according to the method described by Chen and Ko (1994). Rhodamin-labelled gelatin was then used to coat coverslips by fixation in 0.5% glutaraldehyde (Carl Roth GmbH), and washing in RPMI and culture medium. Seventy-two hours after siRNA transfection, cells were reseeded on coated coverslips (5 x 10^4 cells), fixed and permeabilized at 4, 6, and 8 h after seeding. Later on, fixed cells were stained with Alexa Fluor-488–phalloidin and coverslips were mounted on Mowiol (Calbiochem) containing 1,4-diazabicyclo[2.2.2]octane (25 mg/mL; Sigma-Aldrich). Quantification of matrix degradation was determined by counting the degradation sites/cells of different conditions using ImageJ

software. For comparison, laser intensity was not changed between measurements. Two donors of independent experiments were analyzed, with at least eight fields of view (400–1000 cells) per condition.

Images were acquired using confocal laser scanning microscopes (Leica DMi8 confocal point scanner equipped with a 20× HC PL APO IMM/CORR CS2 and oil immersion 63× HC PL APO Oil CS2 objective and 3× HyD, 2× PMT, 1× Trans-PMT detector). Acquisition and processing were performed using the Leica LAS X SP8 confocal software (Leica Camera AG, Wetzlar, Germany) and/or Volocity 6.1.1 software (Perkin-Elmer, Waltham, MA, USA) and ImageJ software.

6.5 Physical methods

6.5.1 Mass spectrometry (MS)*

Samples were processed at the core facility of the Max Planck Institute of Biochemistry (Martinsried, Germany). SDS gel lanes were digested with trypsin using in-gel digestion protocol, and peptides were extracted and purified via C18 StageTips. Afterwards, they were analyzed in a Q Exactive HF machine with a data-dependent acquisition scheme using higher-energy collisional dissociation fragmentation. Raw data were processed using the MaxQuant computational platform, and the peak lists were searched against a human reference proteome database from Uniprot. All identifications were filtered at 1% false discovery rate and label-free quantitation. Proteomic data were analyzed with the Perseus 1.5.5.3 software Tyanova et al., (2016), and results from a t-test using Perseus were plotted as logarithmic ratios against logarithmic p-values[258]. The final selection of positive hits was done by filtering out potential contaminants, reverse sequences, and hits identified only by site.

6.5.2 Circular Dichroism (CD)*

CD measurements were performed as described previously[95] with the following modifications: measurements were performed at 4°C using a His-reconstitution buffer. The mean of four independent spectra (from 198 to 250 nm with 0.1 nm spacing) was recorded and used for CONTIN analysis, which was performed with CDPro. CONTIN decomposes the CD signal into six secondary structural elements: regular α-helical, distorted α-helical, regular β sheet,

distorted β sheet, turn, and unordered[259]. Reported values in the main text for the α-helical and β sheet content were the sum of regular and distorted fractions for each secondary element.

6.5.3 Analytical Ultracentrifugation (AUC)*

Sedimentation velocity experiments were performed on an Optima XL-I analytical ultracentrifuge (Beckman Inc., Palo Alto, CA, USA.) using an An 60 Ti rotor and double-sector epon center pieces. The proteins were added to a 20 mM Tris + 100 mM NaCl buffer at 0.6 mg/mL and 1.6 mg/mL for His-SUMO-MMP2 and NUCB1-His, respectively. Buffer density and viscosity was measured using a DMA 5000 densitometer and an AMVn viscosimeter, respectively (both by Anton Paar, Graz, Austria). Fluorescently labeled protein concentration distribution was monitored at 544 nm at 50,000 rpm and 20°C. Time-derivative analysis was computed using the SEDFIT software package, version 12.1b (Schuck, 2000), resulting in a c(s) distribution and an estimate of the molecular weight M_f (from the sedimentation coefficient and the diffusion coefficient, as inferred from the broadening of the sedimentation boundary, assuming all observed species share the same frictional coefficient $f/f0$).

6.6 Microscopy methods

6.6.1 Immunofluorescence and confocal microscopy*

Samples were prepared by seeding HeLa cells (3×10^4 cells/mL) into six-well plates with two glass slides per well. Cells were incubated for 24 h, transfected (see section 6.2.4) and incubated for no more than 24 h. Then, cells were washed 3 times with 1X PBS, fixed with 4% PFA for 10 min and permeabilized with 0.2% Triton X-100 and 0.5% SDS in PBS for 5 min (if no co-staining was needed, cells were directly mounted after fixation). In between fixation and permeabilization, cells were washed 3–5 times with PBS. For co-staining, cells were incubated with 5% BSA in PBS overnight at 4°C. After this time, primary antibody was added, incubated either overnight at 4°C or 1 h at RT°, washed 3–5 times with 1X PBS and secondary antibody was added. After 1 h incubation at RT°, cells were mounted in glass slides using ProLong™ Gold antifade reagent (Invitrogen) and evaluated using confocal microscopy.

Images acquisition was performed at 22°C on a Zeiss laser scanning LSM780 confocal microscope (Carl Zeiss GmbH, Jena, Germany) equipped with a 100× (NA, 1.46 oil) objective.

To detect AlexaFluor, the 488-nm laser line was used. Pictures were acquired using Leica software (ZEN 2010) and processed, merged, and gamma adjusted in ImageJ (version 1.37).

6.6.2 RUSH assays*

RUSH cargo sorting assays were performed as previously described Deng et al. (2018)[96]. Briefly, HeLa or NUCB1-KO cells were cultured on sterile glass slides in 6-well dishes, transfected using pIRESneo3-SS-Str-KDEL-Flag-MMP2-SBP-HA-eGFP, pIRESneo3-SS-Str-KDEL-acGFP-HA, pIRESneo3-SS-Str-KDEL-LyzC-SBP-eGFP, or pIRESneo3-SS-Str-KDEL-MT1MMP-SBP-mCherry alone or together with NUCB1-WT, NUCB1-WT-myc, or its EF-hand mutants for 16 h. Afterwards, cells were washed with 1X PBS and incubated with DMEM complete medium supplemented with 40 µM D-biotin (SUPELCO, 47868). Time point 0 cells was defined as incubation with complete medium without D-biotin to confirm reporter retention. After biotin incubation, cells were washed 2 x in 1X PBS, fixed, mounted and evaluated by immunofluorescence microscopy, as described in section 6.6.1. Only cells showing proper reporter transport to the Golgi after biotin addition were processed, whereas those showing ER signal after biotin addition were discarded. To cover the whole volume of the cells, typically 8–16 z-stacks with a step size of 0.39 µm were acquired for each field of view.

6.6.3 Vesicle quantification*

A custom-made ImageJ macro previously described Deng et al. (2018)[96] was used to evaluate cellular vesicle numbers. In this macro, ImageJ's rolling ball background subtraction algorithm is used together with the enhance contrast function, and maximum z-projection of the RUSH reporter channel to cover all vesicles of the cell volume in a 2D image. After using a median filter, suitable cells were selected via polygon selection and a binary image was generated using the Threshold function, using the threshold algorithm "Yen" was used as default and adjusting threshold by manual correction for low-intensity images. The vesicle objects in the binary images were compared with the original image and controlled via visual inspection. In the binary image, vesicle objects with sizes 4–20 pixels were quantified using the Analyze Particles function. All macros used for image analysis are available at https://github.com/MehrshadPakdel.

6.6.4   RUSH live cells trafficking assay*

Live cell dishes (μ-Dish 35 mm, high Glass Bottom from ibidi, Gräfelfing, Germany) were seeded with HeLa control or NUCB1-KO cells (3 x 104 cells/mL), incubated overnight and transfected with the SS-SBP-MMP2-eGFP RUSH construct for 24 h. Upon incubation, cells were washed with 1X PBS and incubated in DMEM, high glucose, HEPES, no phenol red (Gibco™, Thermo Fischer, Waltham, USA). Image acquisition was performed using GE DeltaVision Elite microscope at intervals of 1 min per frame. DMEM + 40 μM Biotin was added to the cells at t = 0 min. Images were acquired using softWoRx 5.5 software (GE Healthcare).

6.6.5   Live-cell vesicle image analysis*

The quantification of cytoplasmic vesicles per frame was performed using a custom-made ImageJ macro based on RUSH vesicle analysis, as formerly described by Deng et al. (2018)[96]. In this macro, ImageJ's rolling ball background subtraction algorithm is used, followed by a mean filter to smooth edges of the objects. A binary image was generated by the Auto Threshold function using the "Minimum" algorithm for frames 1–25, and the "Moments" algorithm for frames 26–45 to optimize image thresholding for ER-like objects and then for Golgi and vesicular structures. A comparison between vesicle objects in the binary images and the original image was performed and controlled via visual inspection. Lastly, the Analyze Particles function was used to quantify vesicle objects with sizes ranging between 4 and 40 pixels. Seventeen HeLa and 22 NUCB1-KO cells from two independent experiments were evaluated and plotted as median ± interquartile range. Significant differences with p-values < 0.05 were analyzed using the non-parametric Kruskal–Wallis test with Dunn's multiple comparison test.

6.6.6   Live-cell ER–Golgi cargo transport analysis*

Custom-made ImageJ macros were used to quantify normalized Golgi area over time. The first part of the macro used a median filter to smooth the edges of objects. A binary image was produced for the first frame of the movie to extract the ER signal of RUSH reporter using the Threshold function of ImageJ and to manually extract the ER object and the ER area was measured using the Analyze Particles function with pixel sizes 50–Infinity. The second part of the macro was optimized for extracting Golgi objects for each frame and quantifying their

area. This macro used ImageJ's rolling ball background subtraction algorithm followed by a median filter. A binary image was generated for each frame with the Auto Threshold function using the "Moments" algorithm and areas of binary Golgi objects were then quantified for each frame with the Analyze Particles function using pixel sizes 15–Infinity. The normalized Golgi area was calculated as the ratio of Golgi area at each frame and the ER area at the first frame. Normalized Golgi area for 15 control and NUCB1-KO cells were plotted for each time point as the median ± interquartile range. Significant differences at t = 22 min with p-value < 0.05 were analyzed using the non-parametric Mann–Whitney test.

6.6.7 Ca2+ influx assays*

To measure Ca2+ entry into the TGN or *cis*-Golgi two fluorescent Ca2+ sensors were used: Go-D1-cpv, which targets the TGN, or GPP130-Twitch5, which targets the *cis*-Golgi, following the methodologies previously described by Deng et al., (2018)[96] and Lissandron et al., (2010)[49], respectively. Changes in Ca2+ concentration in the TGN by the Go-D1-cpv sensor were observed as changes in FRET efficiency between CFP and YFP fluorescent proteins linked by a modified calmodulin and calmodulin-binding domain, whereas changes in Ca2+ concentration in the *cis*-Golgi were evaluated as FRET efficiency between enhanced CFP and Citrine fluorescent proteins linked by a modified C-terminal domain of *Opsanus tau* troponin C[260].

Go-D1-cpv or GPP130-Twitch5 alone or together with NUCB1-WT or NUCB1-EFh1+2 mutant were transfected to HeLa or NUCB1-KO cells. After 24 h incubation, Ca2+ entry into the TGN or cis-Golgi were measured upon Ca2+ depletion (cells were previously incubated for 1 h at 4°C in HBSS buffer supplemented with 1 μM ionomycin (Abcam, Cambridge, MS, USA) and 0.5 mM EGTA)[93,96]. Upon 2x washing steps with HBSS + 0.5 mM EGTA followed by 2x washing steps with HBSS only, images were acquired using the GE DeltaVision Elite (GE Healthcare Life Sciences) as described above. Excitation filter (430/24), dual-band Sedat CFP/YFP beam splitter (Chroma Technology Corp., Bellows Falls, VT, USA), and emission filters (535/25 for FRET and 470/24 for CFP) were rapidly changed using an external filter wheel controlled by a motorized unit to generate the images.

Fluorescent signals reflecting TGN or *cis*-Golgi Ca2+ concentration were presented as $\Delta R/R0$, where R0 is the value obtained before the addition of 2.2 mM $CaCl_2$ to the cell's bathing solution. The softWoRx 5.5 software (GE Healthcare Life Sciences) was used for image

acquisition and image analysis was conducted using a custom-made ImageJ macro based on ratiometric FRET analysis, as described before[94,96,261]. The macro uses ImageJ's rolling ball background subtraction algorithm followed by a mean filter to smooth out the edges of the objects. A binary image is generated by the Auto Threshold function using the "Moments" algorithm. FRET and CFP channel images were multiplied by the "ImageCalculator" plugin with their respective binary images, resulting in images that show 0 intensities outside of the threshold Golgi region while retaining intensities within the Golgi. Then, a ratio image of FRET/CFP was generated using the "Ratio Plus" plugin. The Golgi objects were detected using the "Find Maxima" function and added to the region of interest (ROI) manager. Mean intensities of each ROI were measured in the ratio image for each frame. Ratio values of each frame were then subtracted with those in the first frame. These values were normalized to the first frame and presented as percentage $\Delta R/R0$ to obtain the normalized ratio values before the addition of $CaCl_2$.

6.7   Statistical analysis

Data were first evaluated for normality fit. Most of the time, the data did not follow a normal distribution, therefore Kruskal–Wallis test with Dunn's comparison was used for most statistical significance evaluations, unless otherwise stated, using the GraphPad PRISM software (GraphPad Software, Inc., San Diego, CA, USA). For the evaluation of statistical differences in $Ca2+$ influx assays, the Mann–Whitney test was used.

6.8   Other reagents

6.8.1   Antibodies

MMP-2 antibody was purchased from Abcam [rabbit (ab92536)] (Cambridge, MA, USA), NUCB1 and β-actin antibodies were obtained from Sigma-Aldrich [rabbit (HPA008176) and mouse (A5441), respectively], ERGIC53 was acquired from ENZO Life Sciences Inc. [mouse (ENZ-ABS300); Farmingdale, NY, USA], GM130 antibody was purchased from BD Bioscience (mouse (610822); San Jose, CA, USA] streptavidin–HRP antibody was from Cell Signaling [3999S; Danvers, MA, USA]; TGN46 antibody was obtained from AbD Serotec (sheep (AHP500G); Oxford, UK). MMP-14 (MT1-MMP) antibody was purchased from

Millipore (mouse (MAB3328); Burlington, MA, USA) and GFP antibody [rabbit (sc8334)] as well as the horseradish peroxidase (HRP)-coupled secondary antibodies [anti-rabbit IgG, anti-mouse IgG, and anti-sheep IgG] were purchased from Santa Cruz Biotechnology Inc. (Santa Cruz, CA, USA). Anti-rabbit HRP antibody used with primary macrophages was purchased from Cell Signaling [7074; Danvers, MA, USA]. The AlexaFluor secondary antibodies used for immunofluorescence (alexaFluor-488, alexaFluor-594, alexaFluor-633, and Phalloidin-alexaFluor-488) were purchased from Thermo Scientific (Carlsbad, CA, USA).

6.9   Buffers

Table 2.   List of buffers used in this work.

Buffer	Composition
His-binding buffer	50 mM NaP, pH 8.0, 500 mM NaCl.
His-Elution buffer	50 mM NaP, pH 8.0, 500 mM NaCl, 250 mM Imidazole
His-reconstitution buffer	20 mM Tris, 500 mM NaCl
IP buffer	50 mM Tris + 150 mM NaCl + cOmplete Tablets, Mini EDTA-free, EASYpack protease inhibitor tablets (Roche Diagnostics GmbH, Mannheim, Germany)
Lysis IP buffer	50 mM Tris + 150 mM NaCl + 0.1% Triton X-100 + cOmplete Tablets, Mini EDTA-free, EASYpack protease inhibitor tablets (1 per 15mL buffer; Roche Diagnostics GmbH, Mannheim, Germany)
GolgiPrep – breaking buffer	250mM sucrose in 10mM Tris pH 7.4
GolgiPrep – homogenization buffer	Breaking buffer + 3 cOmplete Tablets, Mini EDTA-free, EASYpack protease inhibitor tablets (Roche Diagnostics GmbH, Mannheim, Germany)
GolgiPrep- 62% sucrose buffer	62% w/w sucrose in 10mM Tris pH 7.4
GolgiPrep - 35% sucrose buffer	35% w/w sucrose in 10mM Tris pH 7.4
GolgiPrep - 29% sucrose buffer	29% w/w sucrose in 10mM Tris pH 7.4
HBSS buffer	20 mM HEPES, Ca2+/Mg2+-free HBSS (Gibco by Life Technologies, Grand Island, NY, USA) + 2 g/L glucose + 490 μM MgCl2 + 450 μM MgSO4. 300 mOsmol/L, pH 7.4.
Coomasie solution	40 % v/v methanol, 10 % v/v acetic acid, 0.1 % w/v Coomassie Brilliant Blue R
Destain solution	40 % v/v methanol, 10 % v/v acetic acid
DNA-loading dye	3 % glycerol, 0.15 % OrangeG
Laemmli buffer	200 μM Tris pH 6.8, 4 μM EDTA, 84.5 % glycerol, 8 % SDS, 4 % b- mercaptoethanol, 0.05 % bromophenol blue

Freezing medium	90 % FBS, 10 % DMSO
LB growth medium	1 % w/v Trypsin-Peptone, 1 % w/v NaCl, 0.5 % w/v yeast extract
PBS	10 mM Na2HPO4, 1.7 mM NH2PO4 pH 7.4; 2.6 mM KCl, 137 mM NaCl
PEI solution	1.25 mg/ml PEI in sterile water; pH 7.4
Permeabilization solution	0.2 % TritonX-100 and 0.5 % SDS in 4 % BSA in PBS
Running buffer	25 mM Tris pH 7.4, 190 mM glycine, 0.1 % SDS
Separating gel (10%)	119 mM Tris pH 8.8, 10% v/v acrylamide, 0.1 % w/v SDS, 0.01 % v/v APS, 0.0015 % v/v TEMED
Stacking gel (5%)	125 mM Tris pH 6.8, 5 % v/v acrylamide, 0.1 % SDS, 0.01 % v/v APS, 0.001 % v/v TEMED
Transfer buffer	25 mM Tris pH 7.4, 192 mM glycine, 20 % v/v methanol
TAE buffer	40 mM Tris, 1 mM EDTA, pH 8.3
TBS buffer	25 mM Tris pH 7.4, 150 mM NaCl
Trypsinization solution	10 % Trypsin-EDTA in PBS
TSS buffer	1 % tryptone-peptone, 0.5 % yeast extract, 100 mM NaCl, 10 % PEG (MW3000/3500), 5 % DMSO, 50 mM MgCl2, pH 6.5
Zymography lysis buffer	25 mM Tris, 100 mM NaCl, 0.1% NP-40
Zymography running buffer	Running buffer with 5% SDS instead of 0.1%
Zymography sample buffer	Zymography running buffer, 35% Glycerol, 8% SDS, 1 mg/mL Bromophenol Blue
Zymography 10× renaturing solution	25% v/v Triton X-100 in distilled water
Zymography 10× developing buffer	500 mM Tris-HCl (pH 7.8), 2 M NaCl, 50 mM CaCl2; and 0.2% Brij 35
Zymography staining solution	0.5% Coomassie blue R-250, 5% methanol, 10% acetic acid
Zymography destaining solution	5% methanol, 10% acetic acid

7. Results

The majority of the results shown in this section correspond to the paper *Nucleobindin-1 regulates ECM degradation by promoting intra-Golgi trafficking of MMPs*, at the moment under revision for publication on the Journal of Cell Biology (JCB). The mentioned paper was a collaborative effort between the von Blume group in Munich and Yale, the Haußer group in Stuttgart and the Linder group in Hamburg. Each section in which experiments were performed by any of the collaborators of this study is pointed out.

The first aim of this thesis was to identify potential candidates involved in the trafficking of MMP2. Initially, an evaluation and optimization of suitable systems for the study of MMPs trafficking was assessed, choosing the Retention Using Selective Hooks (RUSH) system (see next section) to better dissect cargo transport through the secretory pathway. To enrich cargos specifically in the Golgi compartment, the RUSH system was combined with a mass spectrometry approach to identify new interacting partners involved in trafficking. The identified candidates were later phenotypically analyzed using the RUSH system on a single-cell level. As a main finding, this study identified nucleobindin-1 (NUCB1) as a crucial component of the intra-Golgi trafficking machinery of MMP2, opening the path for future investigations to elucidate new components of such machinery, as well as identify new regulatory pathways that modulate the intracellular trafficking of MMPs.

7.1   MMP2 follows the secretory pathway

To evaluate the trafficking behavior of MMP2, the RUSH system[262] was used (Figure 35A). In this system, cells are transfected with a construct expressing two proteins at the same time: one is streptavidin bound to an anchor protein localizing the complex in a donor compartment, and the other is the protein of interest, tagged with a fluorophore and bound to a streptavidin binding peptide (SBP)[262]. The method is based on the strong affinity between streptavidin and biotin, therefore once biotin is added to the cell culture media, the binding of SBP to streptavidin is lost, and the cargo is released to the acceptor compartment[262] (Figure 35A).
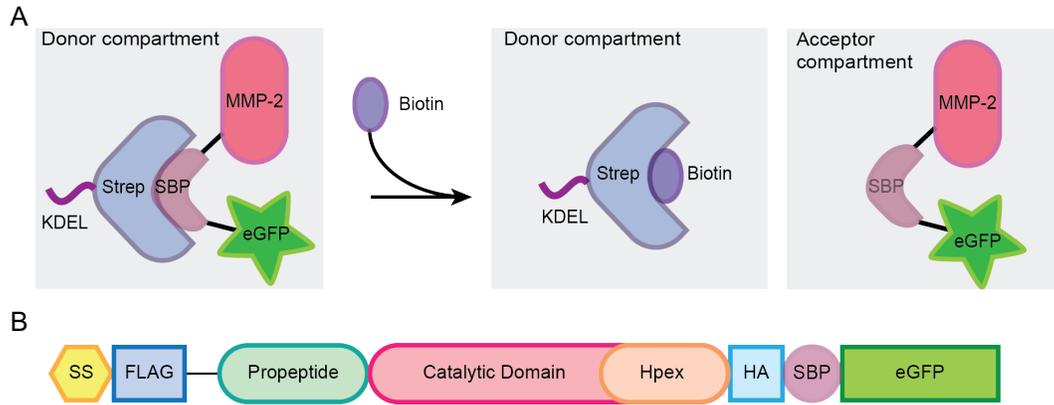
Figure 35. Schematic representation of the RUSH assay used in this study. (A) Scheme representing the Retention Using Selective Hooks (RUSH) system. Adapted from Boncompain et al. (2012)[262]. SS-Flag-MMP2-HA-SBP-eGFP was used as a reporter and streptavidin-KDEL as an endoplasmic reticulum (ER) retention hook. (B) Schematic representation of the MMP2 RUSH protein used as cargo in this study, illustrating the domains of MMP2.

In this study, HeLa cells were transfected with a RUSH construct containing streptavidin bound to a KDEL sequence to act as a hook and keep streptavidin in the ER, and MMP2-SBP-eGFP (Figure 35B) as cargo. Confocal imaging of fixed cells after 0, 15, 30 and 45 min of biotin incubation, as well as colocalization with ER and Golgi markers evidenced the trafficking of MMP2 through the secretory pathway (Figure 36).
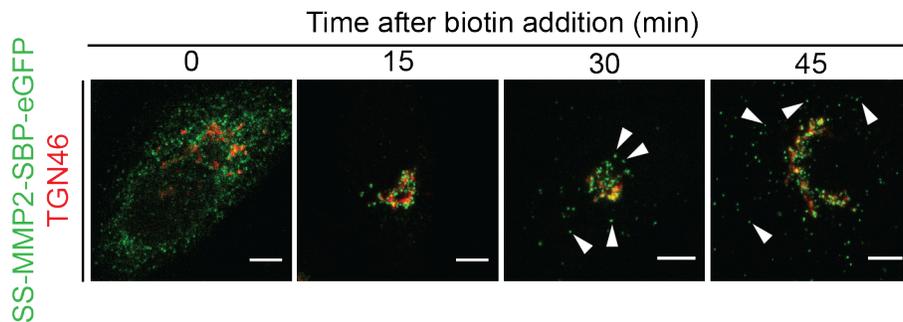
Figure 36. MMP2 traffics through the secretory pathway. Fluorescence images show HeLa cells expressing MMP2-SBP-eGFP and co-stained with a TGN46 (red) antibody. In the absence of biotin, MMP2-SBP-eGFP is retained in the ER (0 min). MMP2 reaches the Golgi 15 min after biotin addition and is sorted into vesicles (arrowheads) after 30 and 45 min of biotin incubation, respectively. Scale bars, 5 μm.

These results showed that MMP2 reaches the Golgi apparatus after 15 min of biotin incubation, is released in vesicles after 30 min and after 45 min of biotin incubation cytoplasmic vesicles are released in the extracellular space (Figure 36). It is important to note that in comparison with other reported cargoes analyzed using the same system (such as LyzC[96], or E-cadherin[262]) only a small fraction of MMP2-eGFP remains in the Golgi at 45 min after biotin addition.

7.2 Identification of potential candidates involved in the trafficking of MMP2

In order to identify potential Golgi localized protein candidates involved in the intracellular trafficking of MMP2, a novel mass spectrometry (MS) approach was used (Figure 37A). Here, HeLa control cells were transfected with 2 different constructs: the described RUSH MMP2 and, as a control, a RUSH construct containing only the signal sequence of human Growth Hormone (hGH, from now on SS) coupled to eGFP.
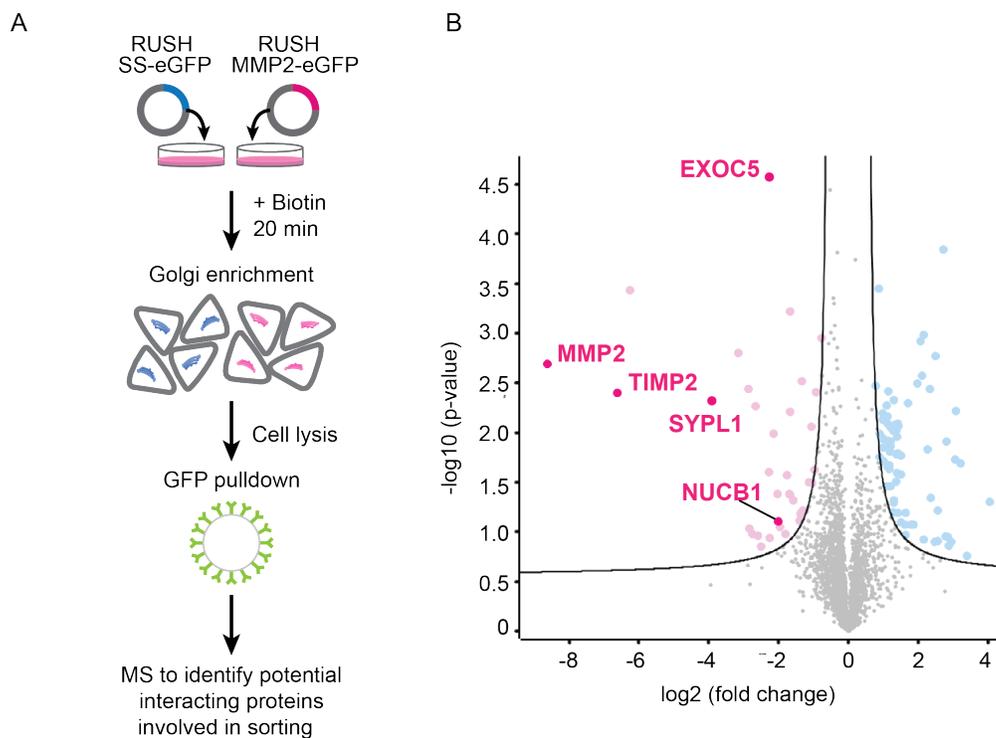
Figure 37. Mass spectrometry approach to identify candidates involved in the intracellular trafficking of MMP2. (A) Schematic representation of the MS-RUSH protocol used to identify

specific MMP2 interacting partners in the Golgi complex. HeLa cells were transfected with MMP2-SBP-eGFP or SS-SBP-eGFP and incubated for 20 min with biotin to enrich reporter proteins at the Golgi. Cells were then lysed, and reporter proteins were pulled down using GFPtrap®. The samples were loaded on an SDS gel and analyzed using mass spectrometry for identification of interactors (n = 3). (B) Volcano plot of identified candidates highlights significantly enriched MMP2 interactors in pink. Forty-two sorting-related candidates were found. Among them were tissue inhibitor of metalloproteinase 2 (TIMP2), a known inhibitor of MMP2; nucleobindin-1 (NUCB1), a major calcium regulator at the cis-Golgi; exocyst 5 (EXOC5) a component of the Exocyst complex; and synaptophysin-like protein 1 (SYPL1), predicted to be a transmembrane component of cytoplasmic vesicles. Significance was assessed using a two-sample t-test. FDR = 0.3, s0 = 0.5. X-axis represent the t-test difference in mean values between groups and y-axis the –Log of the p-value for the t-test.

Biotin was added to the medium 24 h after transfection, cells were incubated for 20 min to accumulate cargo in the Golgi and lysed directly afterwards. Then, protein pull downs were performed using GFPtrap® on whole cell lysates and samples were loaded on an SDS gel. Finally, the bands were excised and the proteins were digested and analyzed by mass spectrometry.

MS results were analyzed using the Perseus software[258] and 42 MMP2 interacting candidates were identified (Table 3). As expected, TIMP2, an inhibitor known to bind MMP2 early on its trafficking to the plasma membrane, was found, validating the accuracy of the assay and serving as positive control for the MS experiment (Figure 37B).

Among the other proteins found, three were considered particularly relevant for MMP2 trafficking given their roles in *cis*-Golgi Ca2+ homeostasis (nucleobindin-1, NUCB1), vesicle tethering at the plasma membrane (exocyst complex component 5, EXOC5) and as a component of cytoplasmic vesicles (synaptophysin-like protein 1, SYPL1). They are described with more detail below.

Table 3.   List of protein interactors found with the described MS approach.

Protein name	Gene name
72 kDa type IV collagenase;PEX	MMP2
Cystatin-B	CSTB
p53-induced death domain-containing protein 1	PIDD1
Metalloproteinase inhibitor 2	**TIMP2**

Arginase-1	ARG1
Bleomycin hydrolase	BLMH
Gasdermin-A	GSDMA
Exocyst complex component 5	**EXOC5**
Tubulin-specific chaperone A	TBCA
Dynein heavy chain 2, axonemal	DNAH2
ATP-binding cassette sub-family A member 10	ABCA10
Protein CASC5	CASC5
Keratinocyte proline-rich protein	KPRP
Histidine ammonia-lyase	HAL
Integrin β-8	ITGB8
Nicotinamide N-methyltransferase	NNMT
Small proline-rich protein 3	SPRR3
Hemoglobin subunit β	HBB;HBD
A-2-macroglobulin-like protein 1	A2ML1
Protein NipSnap homolog 1	NIPSNAP1
Protein FAM32A	FAM32A
RNA polymerase-associated protein LEO1	LEO1
Synaptophysin-like protein 1	**SYPL1**
Prefoldin subunit 1	PFDN1
Nucleobindin-1	**NUCB1**
Transmembrane protein 14C	TMEM14C
Thymidylate kinase	DTYMK
NADH dehydrogenase [ubiquinone] 1 β subcomplex subunit 9	NDUFB9
Protrudin	ZFYVE27
ATP-dependent RNA helicase SUPV3L1, mitochondrial	SUPV3L1
Testis-specific Y-encoded-like protein 1	TSPYL1
Epithelial splicing regulatory protein 2	ESRP2
Dehydrogenase/reductase SDR family member 7B	DHRS7B
Neuropathy target esterase	PNPLA6
Chromodomain-helicase-DNA-binding protein 3	CHD3
Collagen α-1(XII) chain	COL12A1
60S ribosomal protein L11	RPL11
Armadillo repeat-containing protein 6	ARMC6
Quinone oxidoreductase	CRYZ

E3 ubiquitin-protein ligase RNF220	RNF220
Mediator of RNA polymerase II transcription subunit 24	MED24
Mediator of RNA polymerase II transcription subunit 31	MED31

7.2.1 NUCB1

NUCB1 is a 63 kDa Ca2+ binding protein mainly localized at the *cis* compartment of the Golgi[104,106,112,263]. NUCB1, also known as NUC or CALNUC is encoded by a gene located in the chromosome 19 (19q13.33) and is conserved from *Drosophila* to humans[264]. Although its function is not completely understood, up to date, most of the studies on NUCB1 have shown an effect on the activation of the α subunit of the G-protein[113,116,117], the control of the biogenesis and folding of amyloid-β precursor in Alzheimer's disease[88,118,265] and a role in the regulation of endosomal trafficking of lysosomal receptors[120,121].
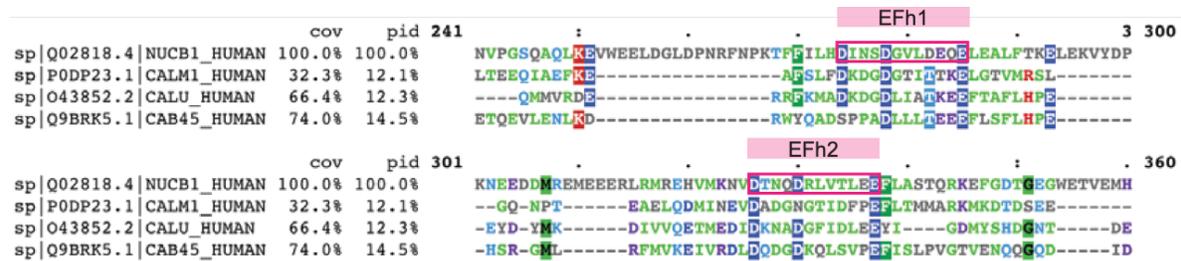
Figure 38. Protein sequence alignment of human NUCB1 (Q02818, amino acids 241–360), calmodulin (P0DP23), calumenin (O43852) and Cab45 (Q9BRK5). Pink boxes highlight the EF-hand domains of NUCB1. Color scheme: CLUSTAL by group (MView 1.63, Copyright © 1997–2018 Nigel P. Brown).

NUCB1 belongs to the EF-hand family of proteins. Proteins in this family share a helix-loop-helix 29 amino acid motif (the EF-hand motif) that binds Ca2+[22,86,109,110]. Among them, a group of soluble proteins, known as CREC (**C**ab45, **R**eticulocalbin, **E**R-55 and **C**alumenin), is mostly, although not exclusively, distributed throughout the secretory pathway[22]. They play a role as Ca2+ sensors and therefore participate in signaling cascades involving molecular chaperoning (calumenin, reticulocalbin-3[22]), and cargo sorting (Cab45[95,96]).

Although all the members of this family possess a conserved EF-hand domain region, the rest of the sequence is considerably different[22,110]. The alignment between NUCB1 and 3 other EF-

hand proteins (2 of them belonging to the CREC family) shows the highly conserved E residue at the end of the sequence motif and the similarities between the EF-hand sequences of NUCB1 EF-hand motifs 1 and 2, and the calumenin motifs 4 and 5, and Cab45 motifs 3 and 4, respectively[22] (Figure 38).

Among the CREC proteins, Cab45 is the only one residing in the Golgi[103,111], although it has been shown that calumenin can also partially localize at the Golgi before being secreted[21]. Moreover, Cab45 has been shown to play a critical role in protein sorting by close interplay with SPCA1, the unique Ca2+ ATPase pump at the TGN[94–96,107]. Though the mechanism is not fully understood, it is known that after Ca2+ influx, Cab45 oligomerizes and promotes cargo sorting in sphingomyelin rich vesicles[96]. In addition, NUCB1 and Cab45 are described as the only soluble Ca2+-binding proteins present in the lumen of the Golgi[103,104,266], suggesting that, as well as Cab45, NUCB1 could be playing a role in protein trafficking at an early stage in the Golgi.

7.2.2 EXOC5 and SYPL1

Exocyst component 5, previously known as Sec10, is a 81 kDa component of the exocyst complex that helps to stabilize the attachment of TGN derived vesicles and their tethering to the plasma membrane[267]. Together with WASH, the exocyst complex has been identified as a crucial component for the "polarization and tethering of MT1-MMP-positive endosomes at the plasma membrane"[229].

Synaptophysin-like protein-1 is a scantily studied protein that resembles the neuronal Synaptophysin-1[268]. The latter is a known transmembrane component of synaptic vesicles that has been proposed to regulate the formation of SNARE complexes via interaction with VAMP2 and VAMP3[269,270]. Studies on SYPL1 have identified it as a component of cytoplasmic vesicles in non-neuronal cells and partially associated with GLUT4 in adipocyte cytoplasmic vesicles[269].

Their roles in vesicle tethering and SNARE complex formation suggest that both proteins might be necessary for MMP2 post-Golgi transport to the plasma membrane. However, the scope of this study will be limited to the understanding of the early trafficking of MMP2 and therefore further investigation on the role of EXOC5 and SYPL1 should be the focus of future studies.

7.3   Generation of CRISPR NUCB1 KO cells

In order to establish tools to study the role of NUCB1 in MMP2 trafficking, a commercially available antibody was tested by confocal microscopy and Western blotting. For this purpose, HeLa cells were fixed and stained with NUCB1 antibody and the Golgi markers GM130 and TGN46. The images showed a strong co-localization between NUCB1 and the *cis*-Golgi marker GM130 but not the TGN marker TGN46, confirming the intracellular localization previously documented[104,106] (Figure 39A). Also, HeLa cells were transfected with either a commercial NUCB1 siRNA (siNUCB1) or a mock siRNA (siControl) and evaluated for NUCB1 expression by Western blotting, which evidenced a decreased NUCB1 expression after double silencing for 48 h (Figure 39B). Given the moderate knock-down efficiency in HeLa cells, NUCB1-KO cell lines were generated (see below).
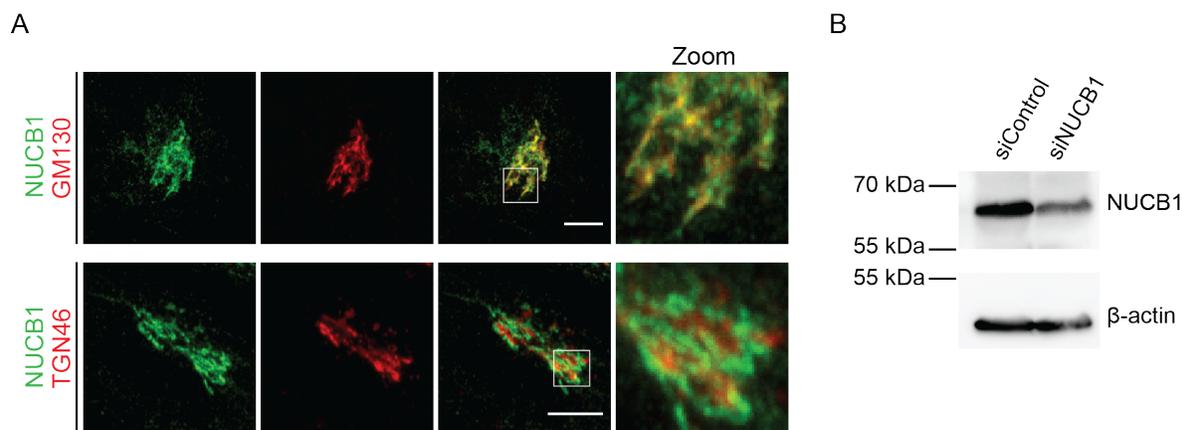
Figure 39.   Immunofluorescence and Western blot evaluation of NUCB1 antibody. (A) Confocal microscopy images show HeLa cells labeled with endogenous NUCB1 (green) and co-stained with the Golgi markers GM130 or TGN46 (red). NUCB1 colocalizes with the *cis* (GM130) but only partially with the *trans* (TGN46) fraction of the Golgi, as previously reported[104]. The square highlights the zoomed area. Scale bars: 5 μm. (B) HeLa cells were transfected with a commercial siRNA (siNUCB1) and analyzed by Western blotting after 48 h. A reduction in the expression of NUCB1 was observed in the silenced cells when compared to HeLa cells transfected with an siRNA mock (siControl). B actin was evaluated as loading control.

To evaluate the role of NUCB1 in the trafficking of MMP2, a CRISPR strategy to generate stable KO cells lines was used (Figure 40, for more details see materials and methods).
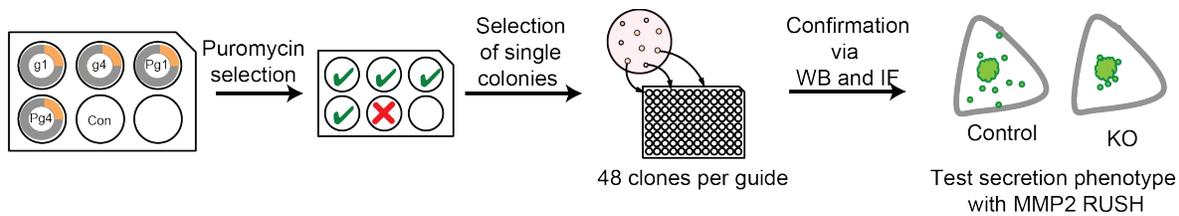
Figure 40. Evaluation of CRISPR candidates. The CRISPR-Cas9 system was used to generate CRISPR-KO cells of each candidate (NUCB1, EXOC5 and SYPL1) and selected clones were evaluated by Western blot and immunofluorescence. Once selected, MMP2 trafficking was analyzed in the positive KO clones using RUSH assays.

sgRNAs targeting NUCB1 were designed to generate HeLa CRISPR KO cells using the platform from the Zhang Lab (not available online anymore[271]). Three different sgRNAs were selected according to a score value reporting the reliability of the sgRNA. Table 4 encompasses the selected sgRNAs, with their corresponding targeting sequence, as well as the score calculated by the Zhang Lab algorithm or the online available tool CRISPOR (http://crispor.tefor.net). A minimal score of 81 was accepted for selection.

Table 4.　　sgRNAs used for the generation of CRISPR KO HeLa cells

Gene	Gene name	Guide No.	sgRNA sequence	Score	No. of Off-targets
NM_006184.6	NUCB1	1	AGTCACCAAGAACGCACCGG	93	73
		2	GCTCCTGCTTCGCGCCGTGC	92	80
		3	AAGGACCTCCGGTGCGTTCT	94	38

After cloning each oligonucleotide pair in a pSpCas9 vector and its subsequent transfection in HeLa cells, positive single clones were selected and evaluated by Western blot. Three positive NUCB1-KO clones were found using the sgRNA No. 2 (Figure 41A). These were later confirmed by immunofluorescence (Figure 41B) and clone g2-2-2 was selected as the NUCB1-KO cell line to perform all the experiments presented in this work.
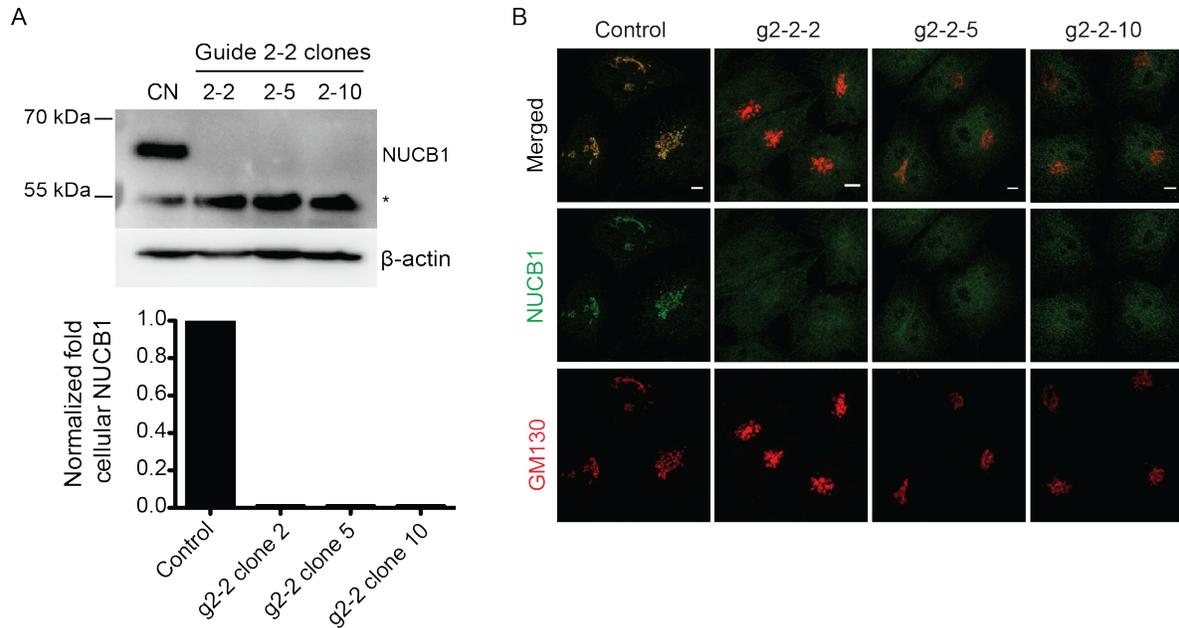
Figure 41. Confirmation of three NUCB1-KO clones in HeLa cells by Western blotting (A) and immunofluorescence (B). *: unspecific band. KO: HeLa KO cells, CN: HeLa control. The semi-quantitative analysis of the Western blot shows the expression level of NUCB1 normalized by β-actin. Scale bars: 5 μm.

7.4   NUCB1-KO delays the trafficking of MMP2

In order to examine the role of NUCB1 in MMP trafficking, RUSH experiments were performed using Hela control and NUCB1-KO cells. Briefly, cells were transfected with RUSH MMP2 constructs, incubated for 24 h, washed and incubated with biotin for 0, 15, 30 and 45 min. Afterwards, cells were fixed, co-stained with NUCB1 antibody and evaluated using confocal microscopy (Figure 42A). The quantification of cytoplasmic vesicles showed a reduced vesicle number in NUCB1-KO cells at 30 min after biotin addition (median: 8, interquartile range: 3–26) when compared with HeLa control cells (median: 29 interquartile range: 17–52.75), indicating a delay in the trafficking of MMP2 when NUCB1 is absent (Figure 42B). Importantly, this trafficking delay was rescued when cells re-expressed NUCB1-WT, showing similar cytoplasmic vesicle numbers as those observed for HeLa control cells (median: 36.5, interquartile range: 17–51.75; Figure 42B).
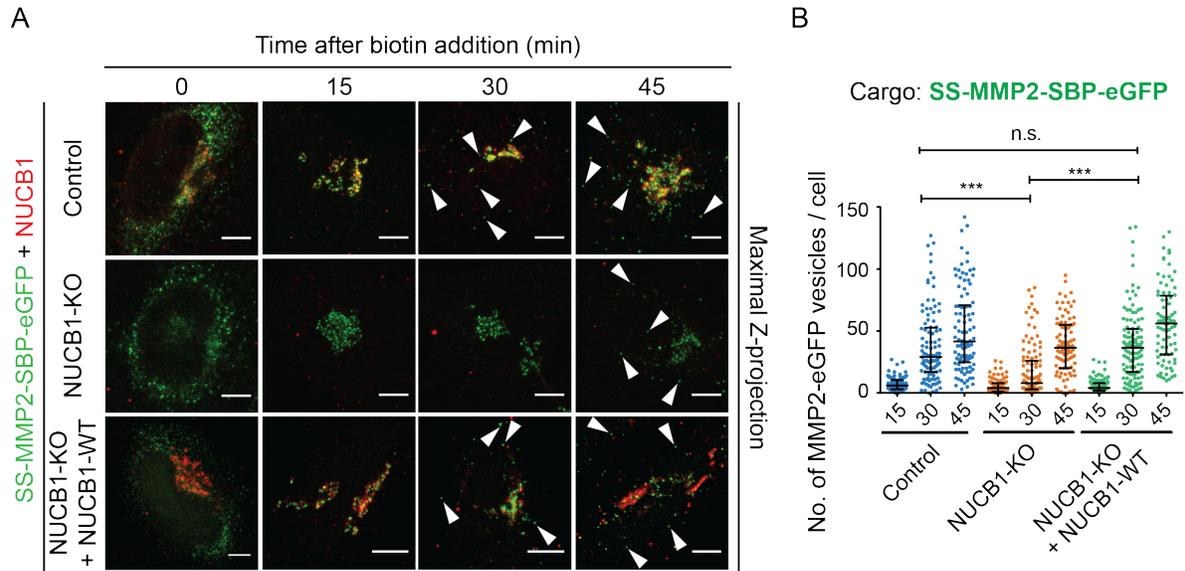
Figure 42. Intracellular trafficking of MMP2 is delayed in NUCB1-KO cells. (A) HeLa or NUCB1-KO cells transfected with SS-MMP2-SBP-eGFP with or without NUCB1-WT were co-stained with NUCB1 (red). Fluorescent images were captured after fixing cells at 0, 15, 30, and 45 min of biotin incubation. Arrowheads point to cytoplasmic vesicles. Scale bars, 5 μm. (B) Cytoplasmic vesicle counts from at least 90 cells per condition are plotted as number of vesicles per cell. The medians of two independent experiments (±interquartile range) are plotted. Significant differences at $p < 0.05$. X-axis: time after biotin addition in minutes. $*p < 0.05$; $**p < 0.01$; $***p < 0.001$.

To investigate the specificity of NUCB1 depletion on protein trafficking, the same experiment was performed using another cargo: RUSH LyzC. LyzC is a soluble protein cargo known to traffic through the secretory pathway and is sorted at the TGN in a Cab45-dependent manner[95,96]. Given the differences in trafficking kinetics, cells were incubated for 0, 20, 40 and 60 min with biotin and subsequently fixed and analyzed by confocal microscopy (Figure 43A). LyzC reached the Golgi after 20 min of biotin addition in HeLa control cells and is sorted in cytoplasmic vesicles after 40 min. When the number of LyzC cytoplasmic vesicles was compared between HeLa control and NUCB1-KO cells, no significant difference was found (Figure 43B).
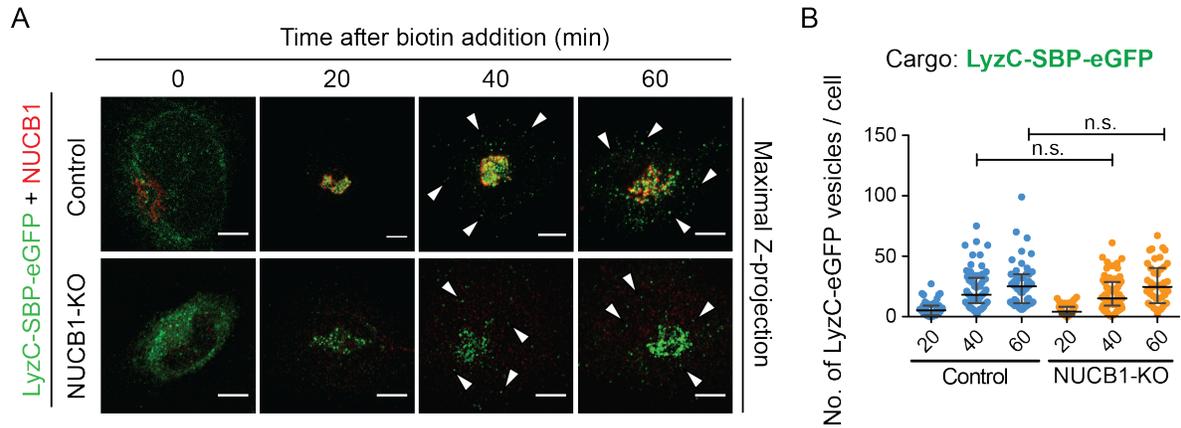
Figure 43. NUCB1 does not alter the intracellular trafficking of LyzC. (A) HeLa or NUCB1-KO cells were transfected with LyzC-SBP-eGFP, fixed, co-stained with a NUCB1 antibody (red) and evaluated by confocal microscopy at 0, 20, 40, and 60 min after biotin addition. Arrowheads point to cytoplasmic vesicles. Scale bars, 5 μm. (B) Cytoplasmic vesicle counts from at least 42 cells per condition. The medians of two independent experiments (± interquartile range) are plotted. X-axis: time after biotin addition in min. n.s.: non-significant.

Furthermore, RUSH experiments using Cathepsin D (a lysosomal hydrolase) showed also no differences in vesicle numbers between NUCB1-KO and HeLa control cells (Figure 44), suggesting a specific role for NUCB1 in the anterograde trafficking of MMP2.
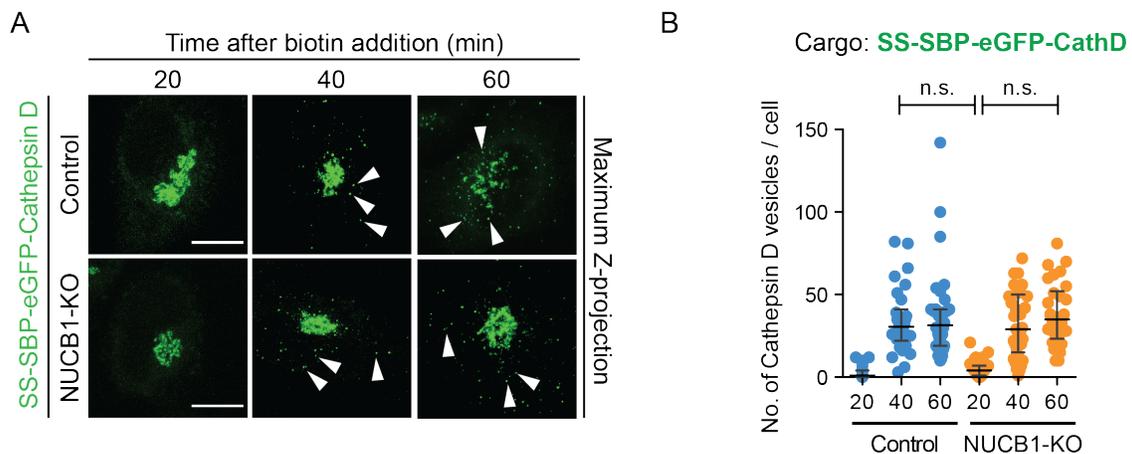
Figure 44. Cathepsin D trafficking is not affected by the absence of NUCB1. (A) HeLa or NUCB1-KO cells expressing SS-SBP-eGFP-Cathepsin D were fixed after 20, 40 and 60 min of biotin incubation and acquired by confocal microscopy. Representative maximum Z-projection images show Cathepsin D trafficking from the Golgi to cytoplasmic vesicles (arrowheads). Scale

bars: 10 μm. (B) Quantification of cytoplasmic Cathepsin D vesicles from cells shown in (A). Data from more than 30 HeLa and NUCB1-KO cells per time point from two independent experiments were plotted as mean ± SD. Statistical analysis was performed using a non-parametric Kruskal-Wallis test with Dunn's multiple comparison test. No significant differences with p-values < 0.05 were detected.

Additionally, RUSH MMP2 secretion assays were performed in order to evaluate if such a delay in MMP2 trafficking could also influence the delivery of the protein to the extracellular milieu. For these experiments, HeLa control and NUCB1-KO cells were transfected with RUSH MMP2 or RUSH LyzC, washed after 24h and incubated with biotin for 0 and 45 min (RUSH MMP2 cells) or for 0 and 60 min (RUSH LyzC cells). A reduction in the amount of MMP2 was observed on the supernatant of NUCB1-KO cells when compared to HeLa control at 45 min after biotin incubation (Figure 45A, 45B). Moreover, the evaluation of secreted LyzC showed no reduction in the amount of protein detected on supernatants of both NUCB1-KO and HeLa control cells (Figure 45A, 45C), corroborating that LyzC trafficking is not affected by the absence of NUCB1.
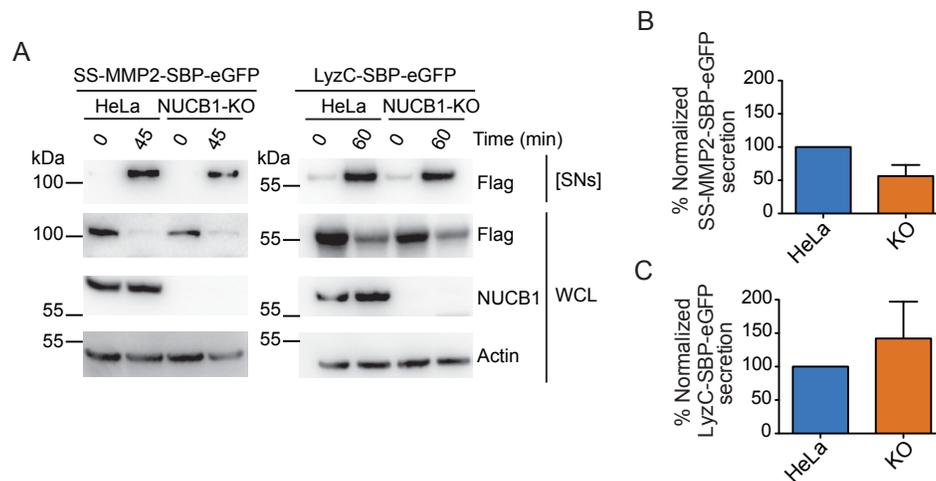
Figure 45. MMP2 secretion is reduced in NUCB1-KO cells. (A) Secretion assay using HeLa or NUCB1-KO cells transfected with SS-MMP2-SBP-eGFP or LyzC-SBP-EGFP and incubated with biotin for 45 or 60 min, respectively. Numbers on the left side of the blots indicate molecular weight in kDa. WCL: whole cell lysates. [SNs]: 10X concentrated supernatants. The supernatant band intensities were normalized by the lysates and a semi-quantitative analysis from three independent experiments is depicted in (B) for MMP2 and (C) for LyzC.

Another cargo widely studied in the trafficking field is horse radish peroxidase (HRP)[272,273]. In order to evaluate if NUCB1 could have an effect on the trafficking of additional cargo,

secretion experiments were performed using Hela control and NUCB1-KO cells stably expressing SS-HRP-Flag. For this purpose, cells were first plated in 12-wells and incubated for 24h. As positive control, a sample was incubated Brefeldin A (BFA, an inhibitor of anterograde protein trafficking) for 1h prior to the secretion assay. Afterwards, all samples were washed and incubated with fresh medium for 4h with (positive control) or without (HeLa control and NUCB1-KO cells) BFA. Finally, supernatants and lysates were evaluated by Western blot (Figure 46A) and HRP activity was quantified using a chemiluminescence assay (Figure 46B). These results showed no difference in SS-HRP secretion between HeLa control and NUCB1-KO cells, suggesting a specific effect on the trafficking of MMPs.
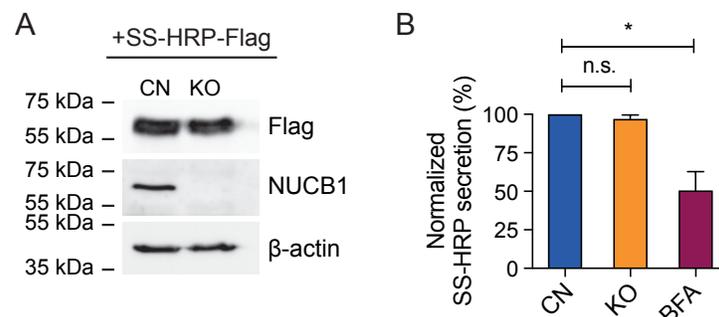
Figure 46. HRP secretion is not affected by the absence of NUCB1. (A) Whole cell lysates of HeLa and NUCB1-KO cells stably expressing SS-HRP-FLAG were analyzed by anti-FLAG, anti-NUCB1 and anti-β-actin Western blotting. SS-HRP-FLAG is expressed in HeLa and NUCB1-KO cells to similar levels. (B) Cell culture supernatants of cells described in (A) were analyzed for HRP activity by chemiluminescence after 4h secretion. Brefeldin A (BFA) serves as a positive control for perturbed secretion and was added for one hour before HRP secretion analysis. No significant differences in HRP secretion were observed between NUCB1-KO and HeLa control cells. *: p-value < 0.05. Experiments performed by Dr. Mehrshad Pakdel.

Given that HeLa cells are not constitutively secretory cells, the secretion of endogenous MMP2 was evaluated in a different cell system, the breast cancer cell line MDA-MB-231. To test MMP2 secretion, MDA-MB-231-MT1-MMP-mCherry cells were double transfected with either a mock siRNA (siControl) or one targeting NUCB1 (siNUCB1) in 24 h intervals. Then cells were carefully washed and incubated with serum-free medium for 20h. After this time, cells were lysed, and supernatants were collected and concentrated 20X using Amicon units. MMP2 secretion was evaluated by Western blot (Figure 47A), observing a strong reduction in its secretion in siNUCB1 cells when compared to siControl (Figure 47B). These results

corroborate our findings in HeLa cells and demonstrate that NUCB1 plays a crucial role in the trafficking of MMP2.
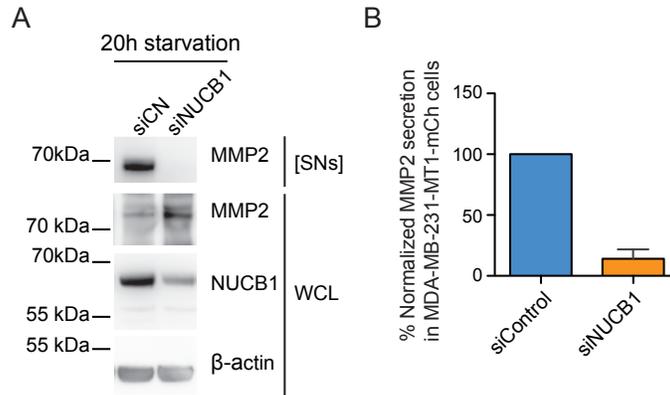
Figure 47. Endogenous MMP2 secretion is also impaired in NUCB1-silenced MDA-MB-231-MT1-MMP-mCherry cells. (A) Cells were incubated with serum-free media for 20h. When NUCB1 was silenced, the secretion of endogenous MMP2 was reduced, confirming the role of NUCB1 in the trafficking of MMP2. (B) Semi-quantitative analysis of this assay. [SN]: 20X concentrated supernatant. WCL: whole cell lysates. Bar graphs illustrate the mean (± range) of three independent experiments.

7.5   NUCB1-KO is also involved in the trafficking of MT1-MMP

To assess if the absence of NUCB1 could affect the trafficking of other MMPs, MT1-MMP trafficking was analyzed. Given that this is a transmembrane protein and could have alternative sorting pathways, an evaluation of its intracellular trafficking was performed using performed using an mCherry-tagged RUSH construct (Figure 48A) and transfected in HeLa control and NUCB1-KO cells.

After biotin incubation, cells were fixed and evaluated using confocal microscopy. HeLa control cells showed different trafficking kinetics than the ones observed of MMP2: MT1-MMP reaches the Golgi only after 30 min of biotin incubation and is sorted into cytoplasmic vesicles after 60 min (Figure 48B). Additionally, an increase in the number of MT1-MMP positive vesicles traveling to the plasma membrane is observed at 90 min, although, unlike MMP2, a strong signal remains at the Golgi at this time point (Figure 48B).
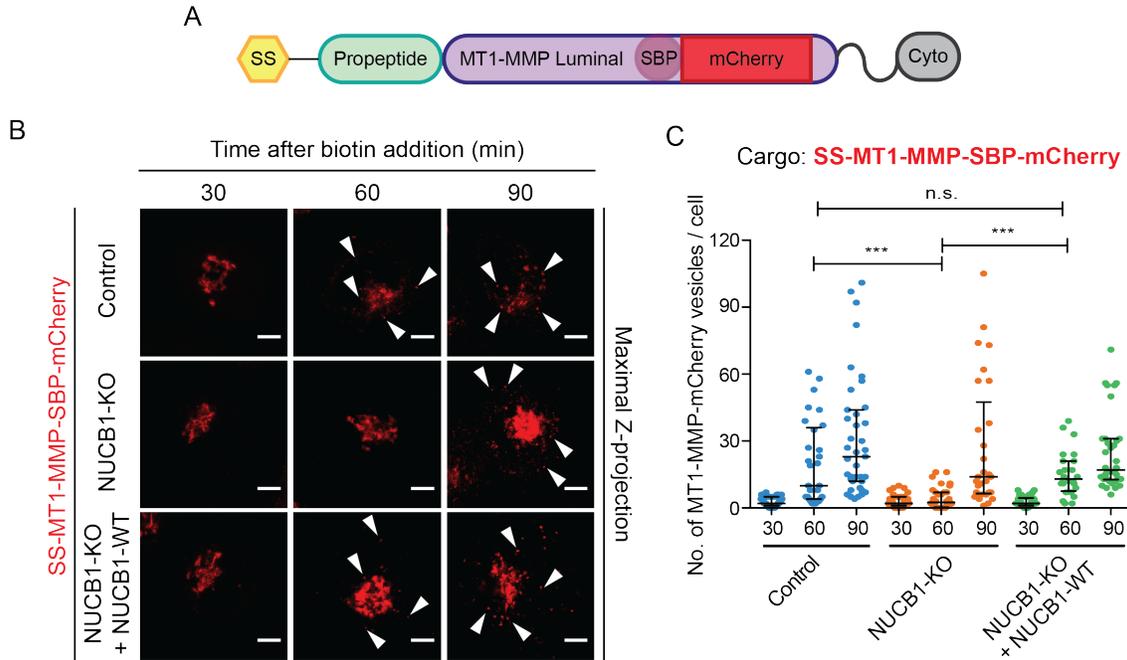
Figure 48. MT1-MMP intracellular trafficking is also delayed in the absence of NUCB1. MT1-MMP trafficking was evaluated using the mCherry (mCh) tagged RUSH construct SS-MT1-MMP-SBP-mCh illustrated in (A). SS: signal sequence. Cyto: cytosolic domain. (B) Confocal fluorescence images of HeLa or NUCB1-KO cells transfected with or without NUCB1-WT and fixed after 30, 60, and 90 min of biotin incubation. Arrowheads depict cytoplasmic vesicles. Scale bars: 5 μm. (C) Quantification of cytoplasmic vesicles observed in (B) from at least 24 cells from two independent experiments. The bars represent median (± interquartile range). X-axis: time in minutes after biotin addition. ***p < 0.001. n.s.: non-significant.

Moreover, the quantification of cytoplasmic vesicles showed a decrease in vesicle number at 60 min after biotin addition in NUCB1-KO cells (median, 2.5; interquartile range, 0.25–7) when compared to HeLa control (median, 10; interquartile range, 4–36), and this phenotype could be restored when NUCB1-WT was re-expressed in NUCB1-KO cells (median, 13; interquartile range, 7.5–21; Figure 48C). These results evidence a role of NUCB1 in MT1-MMP intra-Golgi trafficking and highlight NUBC1 as a key component for MMP trafficking in general.

7.6 NUCB1 alters exclusively the intra-Golgi trafficking of MMP2

To determine where in the secretory pathway the observed delay took place, co-localization experiments using RUSH MMP2 and ER, *cis*- and *trans*-Golgi markers were performed in HeLa

control and NUCB1-KO cells (Figure 49). Co-localization of MMP2 with ERGIC53 (an ER-to-Golgi marker) is not significantly different between NUCB1-KO and HeLa control cells at 2.5, 5 and 7 min after biotin addition, excluding a trafficking delay due to ER retention of MMP2 (Figures 49A and 49B).
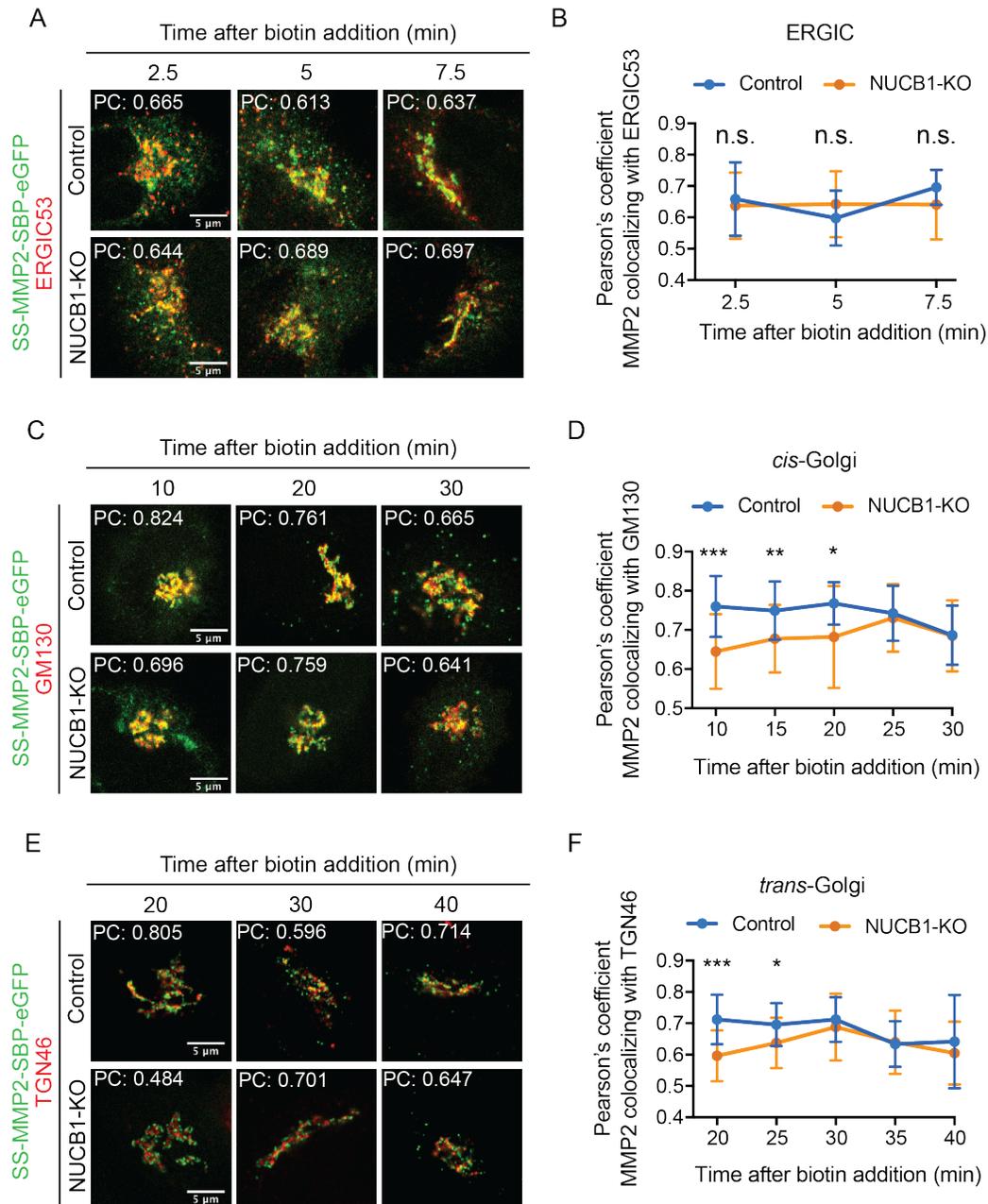
Figure 49. MMP2 trafficking delay occurs exclusively at the *cis*-Golgi. (A) Fluorescence images depicting HeLa or NUCB1-KO cells transiently transfected with SS-MMP2-SBP-eGFP and fixed after 2.5, 5, and 7.5 min after biotin addition. Cells were co-stained with an ER marker (ERGIC53,

red). Scale bars, 5 μm. (B) Average Pearson's coefficient per time point. No significant differences between the correlation coefficients of HeLa or NUCB1-KO cells per time point were found, suggesting that MMP2 trafficking is not impaired at the ER level. (C) Fluorescence images showing the colocalization of MMP2 with the *cis*-Golgi marker GM130. HeLa or NUCB1-KO cells expressing SS-MMP2-SBP-eGFP were fixed at 10, 15, 20, and 25 min after biotin addition. Scale bars, 5 μm. (D) Average Pearson's correlation coefficients illustrate a decreased colocalization of MMP2 with GM130 at 10, 15, and 20 min after biotin addition. This difference disappeared at 25 min after biotin addition, suggesting that after this point, MMP2 traffics with the same kinetics in both NUCB1-KO and HeLa cells. (E) Fluorescence images of HeLa and NUCB1-KO cells expressing SS-MMP2-SBP-eGFP. Cells were fixed at 20, 25, 30, 35, and 40 min after biotin addition and co-stained with TGN46 (red). Scale bars, 5 μm. (F) The average Pearson's coefficient shows that after arrival at the *trans*-Golgi network (TGN), MMP2 is equally colocalizing with TGN46 in HeLa and NUCB1-KO cells. PC, Pearson's correlation coefficient of each picture. $*p < 0.05$; $**p < 0.01$; $***p < 0.001$. At least 17 cells per time point were evaluated for colocalization with each marker. Experiments performed together with Dr. Mehrshad Pakdel.

Further evaluation of the *cis*- and *trans*-Golgi markers (GM130 and TGN46, respectively) showed an exclusive intra-Golgi trafficking defect. Figure 49C illustrates the co-localization of GM130 and MMP2-eGFP, with a significant reduction in the signal overlap after 10, 15 and 20 min of biotin incubation (Figure 49D). Moreover, the co-localization with TGN marker TGN46 was lower in NUCB1-KO cells only at 20 and 25 min after biotin addition, suggesting that the defect in trafficking occurs exclusively from *cis* to *trans*-Golgi (Figure 49E and 49F).

To precisely determine the point at which this delay occurs, wide field live-cell microscopy was used (experiments performed by Dr. Mehrshad Pakdel). Here, HeLa control and NUCB1-KO cells were analyzed using the RUSH construct in 1 min time frames (Figure 50). After data collection, both number of vesicles and ER-to-Golgi signal ratio were analyzed. In the first 30 min of biotin incubation, no differences in vesicle numbers were found, as expected since at this time MMP2 arrives and traffics through the Golgi (Figure 50A). However, in the time frame between 30 and 44 min of biotin incubation, a significantly reduced number of vesicles is observed in NUCB1-KO cells (Figure 50B). This difference, nonetheless, disappeared after 45 min of biotin incubation, supporting our hypothesis of a delay exclusively at the Golgi.
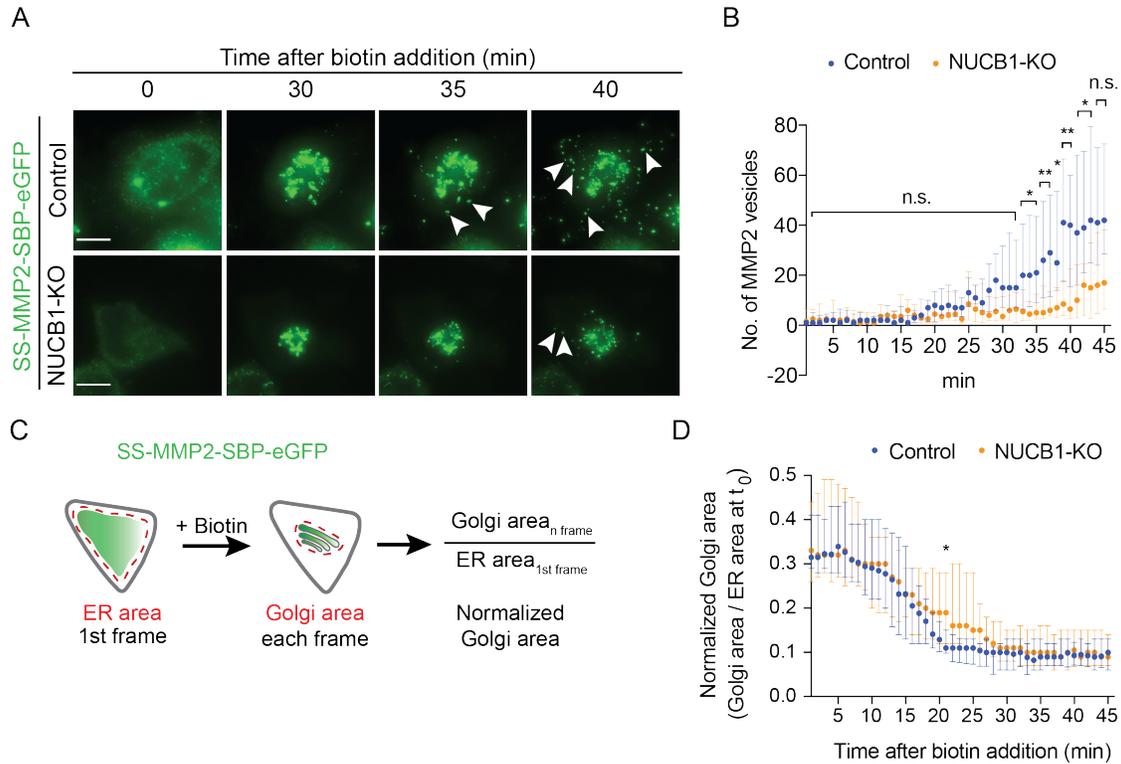
Figure 50. Kinetic evaluation of MMP2 RUSH trafficking using live cell microscopy. (A) HeLa or NUCB1-KO cells expressing SS-SBP-MMP2-eGFP were analyzed by live-cell wide-field microscopy. Representative images show MMP2 trafficking at 0, 30, 35, and 40 min after biotin addition for one control and one NUCB1-KO cell. Images were acquired in 1 min frames for each analyzed cell. Arrowheads point to cytoplasmic MMP2 vesicles. Scale bars: 10 μm. (B) Quantification of cytoplasmic MMP2 vesicles per frame from cells shown in (A). Data from 17 HeLa and 22 NUCB1-KO cells from two independent experiments were plotted as median ± interquartile range. Kruskal–Wallis test with Dunn's multiple comparison evidenced significant differences with p-values < 0.05. n.s.: non-significant. *:p-value < 0.05. (C) Schematic representation of ER–Golgi cargo transport analysis, measured by normalized Golgi area over time in cells shown in (A). (D) Normalized Golgi area for 15 control and 17 NUCB1-KO cells were plotted for each time point as median ± interquartile range. An increased normalized Golgi area in the time range 15 to 18 min observed on NUCB1-KO cells when compared with HeLa control suggests a delay in trafficking occurring exclusively at the cis-Golgi. A significant difference at t = 22 min (*: p-value < 0.05) was documented using the non-parametric Mann–Whitney test.

MMP2 showed a spotty signal in the ER before biotin addition that may lead to an underestimation of the vesicle numbers. To avoid such a bias, an ER-to-Golgi signal ratio was

calculated as depicted in Figure 50C. Here, the Golgi area was defined by measuring the Golgi area at each time frame and normalizing by the ER area at the time 0. At least 15 cells were evaluated per time point during 45 min of biotin incubation, finding a significant difference between NUCB1-KO and HeLa control cells only between 19 and 24 min, i.e. after the protein has already reached the Golgi (Figure 50D). Furthermore, this difference is abolished, after 25 min of biotin incubation, showing once more that the delay occurs only in the trafficking from *cis* to *trans*-Golgi.

Although NUCB1 is considered to play its main role at the *cis*-Golgi, a cytosolic version of the protein has been shown to interact with G-protein and lysosomal receptors, affecting their activation and endosomal trafficking, respectively[113,120,121]. To evaluate if MMP2 trafficking was exclusively influenced by the NUCB1 Golgi resident version, a RUSH experiment using MMP2-eGFP co-transfected with the cytosolic version of NUCB1 (NUCB1-cyto, lacking the first 26 amino acids from the signal sequence) was performed in NUCB1-KO cells (Figure 51A). As expected, the number of vesicles at 30 min after biotin addition is reduced in NUCB1-KO cells (Figure 51B). In comparison, cells re-expressing NUCB1-cyto showed a similar phenotype, indicating that NUCB1-cyto cannot rescue the phenotype and confirming once more that this delay happens exclusively at the Golgi.

Figure 51. Cytosolic NUCB1 does not affect the trafficking of MMP2. HeLa or NUCB1-KO cells expressing SS-SBP-MMP2-eGFP alone or co-expressed with a cytosolic variant of NUCB1 lacking its signal sequence were fixed after 0, 15, 30 and 45 min of biotin incubation and acquired in z-

stacks by confocal microscopy. Representative maximum Z-projection images show MMP2 trafficking from the ER to cytoplasmic vesicles (arrowheads). Scale bars: 10 µm. (F) Quantification of cytoplasmic MMP2 vesicles from cells is shown in (F). Data from at least 18 HeLa and NUCB1-KO cells per time point from 2 independent experiments were plotted as mean ± SD. Significant differences with p-values < 0.05 were obtained after analysis via non-parametric Kruskal-Wallis test with Dunn's multiple comparison. Experiments performed by Dr. Mehrshad Pakdel.

7.7 NUCB1 interacts with MMP2

To further elucidate how NUCB1 is influencing MMP2 trafficking, the interaction between both proteins was evaluated via different approaches. The first approach was performing co-immunoprecipitations overexpressing one of the proteins with a tag and pulling it down. For this purpose, HeLa control, NUCB1-KO and NUCB1-KO cells re-expressing NUCB1-WT-myc were transfected with a pLPCX-Flag-MMP2-HA-eGFP construct. After 24 h incubation, cells were lysed and MMP2 was pulled down via its GFP tag using the GFP-Trap® system. After centrifugation and elution of protein with Laemmli buffer, the interaction with NUCB1 was evaluated by SDS-PAGE and Western blot (Figure 52A). A weak interaction was observed between NUCB1 and MMP2 in control and NUCB1-KO cells re-expressing NUCB1-myc (Figure 52).

Figure 52. Endogenous NUCB1 co-immunoprecipitated with overexpressed MMP2-eGFP. HeLa control (CN) or NUCB1-KO (KO) cells transfected with SS-Flag-MMP2-HA-eGFP (MMP2-eGFP) with or without re-expression of NUCB1-WT-myc were processed for GFP-pull down and Western blot analysis. MMP2 interacts with both endogenous NUCB1 and re-expressed NUCB1-WT in NUCB1-KO cells. Semi-quantitative analysis of the IP signal from two independent

experiments is illustrated in (B). CN: HeLa cells. KO: HeLa NUCB1-KO cells. Molecular weights are indicated on the left side of the blots.

To evaluate if this interaction is specific for MMP2, the same approach was used immunoprecipitating LyzC-eGFP. As expected, no interaction between endogenous NUCB1 and overexpressed LyzC was observed in HeLa cells (Figure 53A). Here is important to note that during the optimization of this method, NUCB1 re-expression in NUCB1-KO cells showed very high expression levels compared to the endogenous protein in HeLa control cells, which might explain the high ratio intensity observed in NUCB1-KO cells overexpressing NUCB1-WT (Figure 53B).
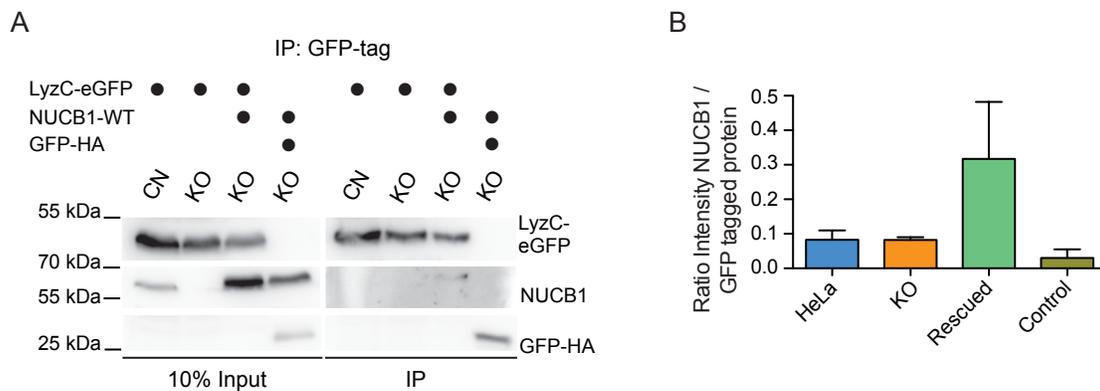
Figure 53. LyzC does not interact with endogenous NUCB1. (A) GFP-co-immunoprecipitation of HeLa or NUCB1-KO cells previously transfected with LyzC-eGFP, with or without NUCB1-WT. GFP-HA was used as a control. Western blotting showed no interaction between endogenous NUCB1 and LyzC or GFP-HA. CN: HeLa control, KO: NUCB1-KO. Semi-quantitative analysis of the IP signal intensity from three independent experiments is shown in (B). Bars depict mean and whiskers represent range of data.

To evaluate which domain of MMP2 would be interacting with NUCB1, co-immunoprecipitation experiments were performed using deletion mutants of the catalytic domain (delCD) and hemopexin domain (delHpex) of MMP2 (Figure 54A). Initially, the evaluation was made with endogenous NUCB1 (data not shown) but given the weakness of the interaction with the MMP2-eGFP full length, new experiments overexpressing NUCB1 together with the corresponding eGFP construct were performed. Nevertheless, the interaction is not lost after deletion of any of these MMP2 domains (Figure 54B).
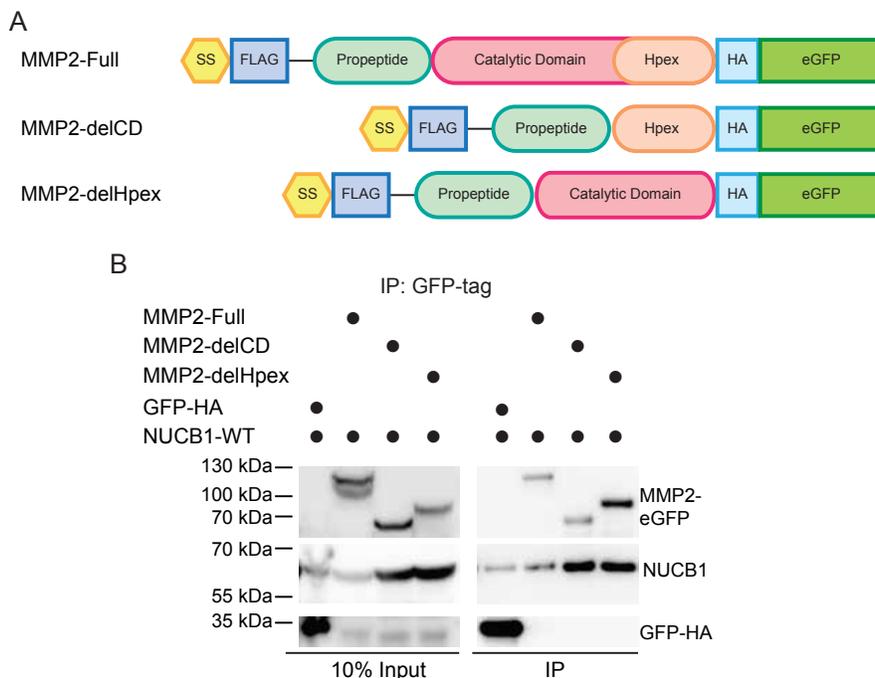
Figure 54. Co-immunoprecipitation of overexpressed MMP2 deletion mutants and overexpressed NUCB1. (A) Illustration of the truncation mutants used for evaluation of specific MMP2 domain interaction with NUCB1. MMP2: full length protein; MMP-delCD: MMP2 with truncated catalytic domain; and MMP2-delHpex: MMP2 with truncated hemopexin domain. (B) GFP immunoprecipitation analysis by Western blot showed no loss of the interaction with overexpressed NUCB1-WT, suggesting that neither the catalytic nor the hemopexin domain are essential for it.

In order to evaluate if, specifically, the propeptide domain of MMP2 was essential for the interaction with NUCB1, experiments using propeptide domain mutants of MMP2 were performed. Given that this domain is critical for the inactivation of the protein, two different constructs were designed to evaluate the interaction: the first one with a complete deletion of the propeptide domain, and the second one with a Cys>Ala substitution at the cysteine switch that controls the activation of the protein (Figure 55A). Once again, the co-immunoprecipitation of NUCB1 with either the propeptide deletion or substitution mutant of MMP2, showed no loss of interaction (Figure 55B).
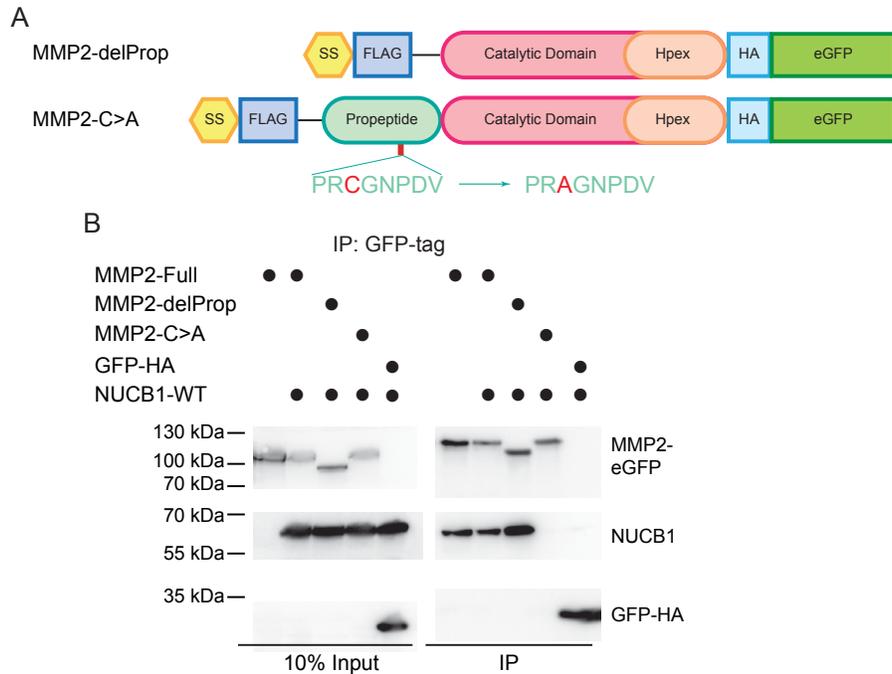
Figure 55. Co-immunoprecipitation of MMP2-eGFP mutants with truncated propeptide domain or substitution at the cysteine switch. (A) Schematic representation of the propeptide domain mutants used to evaluate interaction with NUCB1. MMP2-delProp: MMP2 with truncated propeptide domain; MMP2-C>A: MMP2 full length with a C>A (red) substitution at the cysteine switch (sequence in green), required for activation of MMP2. (B) Evaluation of the co-immunoprecipitation of MMP2 propeptide mutants and overexpressed NUCB1 showed that neither the complete propeptide domain nor the cysteine switch motif are essential for the interaction of MMP2 with NUCB1.

To further strengthen the obtained results, a different approach using recombinant proteins and Golgi membranes was used (see materials and methods). For this purpose, recombinant NUCB1-His (rNUCB1-His) was produced using the piggyBac system. First, a cassette containing NUCB1 6xHis-tagged C-terminally was cloned in a pB-T-PAF vector and transfected, together with pB-RN and pBvase vectors, in HEK293T cells to generate stable cell lines. Then, protein production was induced by incubation of the cells with doxycycline and aprotinin in serum-free media. After at least 20 h starvation, supernatants were collected and rNUCB1-His was purified using immobilized Nickel NTA (NiNTA) beads.

Protein production was analyzed by SDS-PAGE (Figure 56A) and Western blot (Figure 56B). In addition, rNUCB1-His was analyzed by total mass, showing a peak at 53.144 kDa, as

expected (Figure 56C). Other peaks with higher molecular weights reflect reported phosphorylation and glycosylation sites. Notably, analysis of the NUCB1 sequence evidenced that the purified protein lacked the signal sequence, as expected for secreted proteins that traffic through the secretory pathway, and described previously for NUCB1[106].
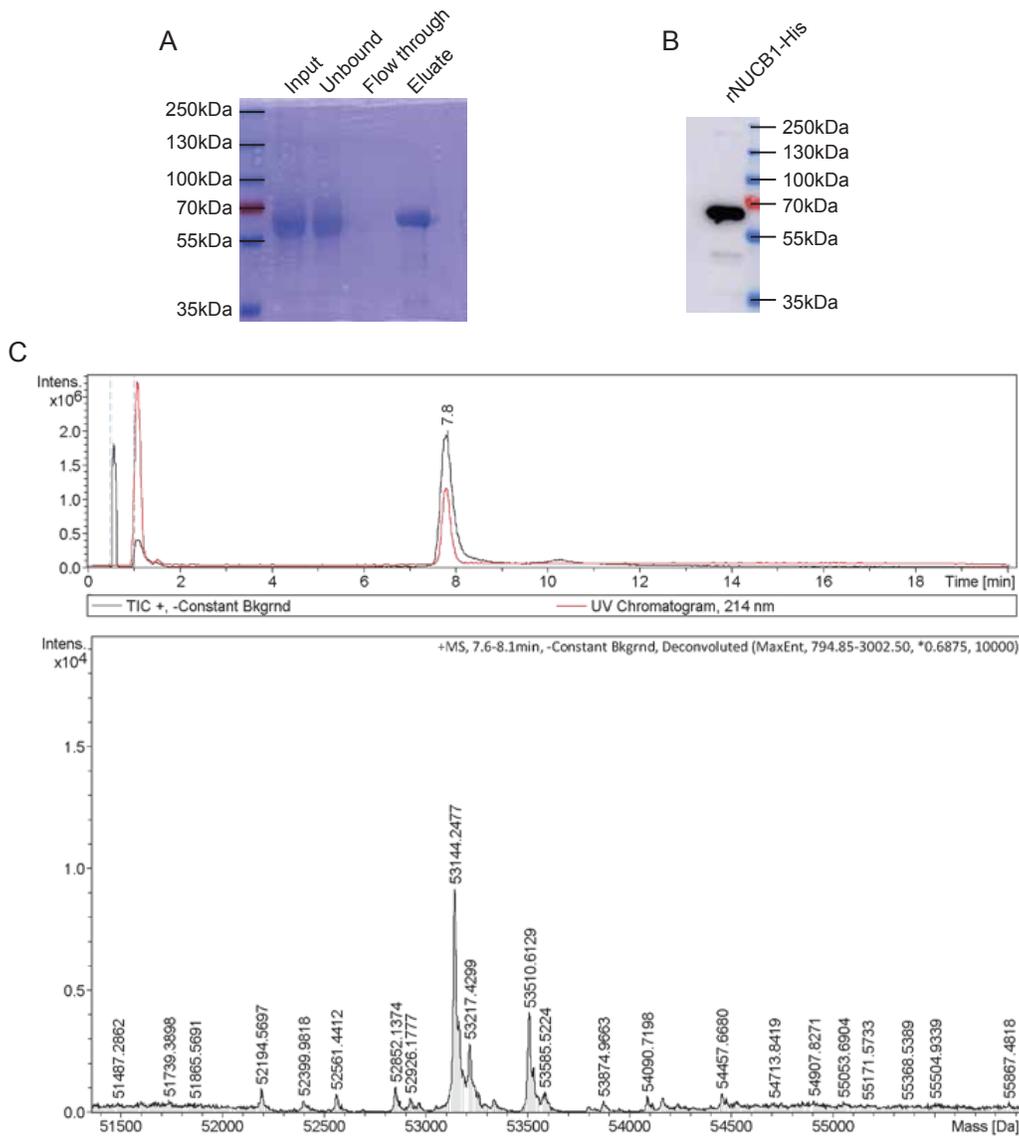
Figure 56. Evaluation of His-tag purification of recombinant NUCB1 produced in HEK293T cells using the piggy-BAC system. (A) Coomassie stained SDS-PAGE and (B) Western blot analysis of the elution fraction (line 4 of Figure 56A). (C) Total mass analysis using microTOF. The above panel displays the chromatogram of rNUCB1-His and illustrates the purity of the eluted

sample. The lower panel shows the mass spectrometry peak of absorbance for rNUCB1-His. Analysis performed by the Core Facility of the Max Planck Institute of Biochemistry.

To evaluate the interaction of rNUCB1-His with endogenous MMP2, co-immunoprecipitation experiments were performed using recombinant GFP-His (rGFP-His) as control. Briefly, the recombinant proteins were bound to Ni-NTA beads, washed and incubated with Golgi membranes, previously isolated from Hela control cells and lysed with IP buffer, as described in the materials and methods section. The interaction was evaluated by Western blot (Figure 57A) and showed a band corresponding to endogenous MMP2 when rNUCB1-His, but not rGFP-His, was pulled down. Three replicates of this experiments confirm the interaction (Figure 57B) and strengthen our hypothesis that both proteins interact specifically at the Golgi.
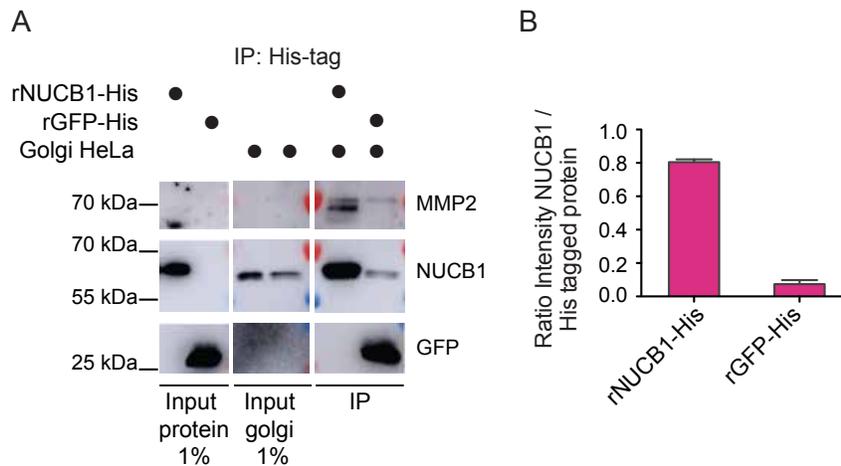
Figure 57. Recombinant NUCB1-His interacts with endogenous MMP2 at the Golgi in HeLa cells. (A) His-tag pull down of recombinant NUCB1 (rNUCB1-His) using recombinant GFP (rGFP-His) as control. Endogenous MMP2 from isolated Golgi membranes of HeLa cells co-immunoprecipitated with rNUCB1-His but not with rGFP-His, confirming the interaction between both molecules. Molecular weights are shown on the left side of the blots. Semi-quantitative analysis of the IP signal of three independent experiments is shown in (B). Columns on semi-quantitative analysis show mean and bars represent the range of data points. IP pictures shown in (A) are the specular image of the photographed blot.

Furthermore, to determine if such interaction is direct, recombinant MMP2 N-terminally tagged with His-SUMO was produced and purified using the same system described for rNUCB1-His. After evaluation by Western Blot (Figure 58A), the purity of the protein was also confirmed via total mass, finding a peak of absorbance around 88 kDa, as expected; the

different peaks around this molecular weight represent glycosylation and phosphorylation sites of the protein (Figure 58C). After peptide sequence confirmation using mass spectrometry, His-SUMO-MMP2 was conjugated with a Cy3 fluorophore via maleimide labelling with a 20% labelling efficiency (Figure 58B).
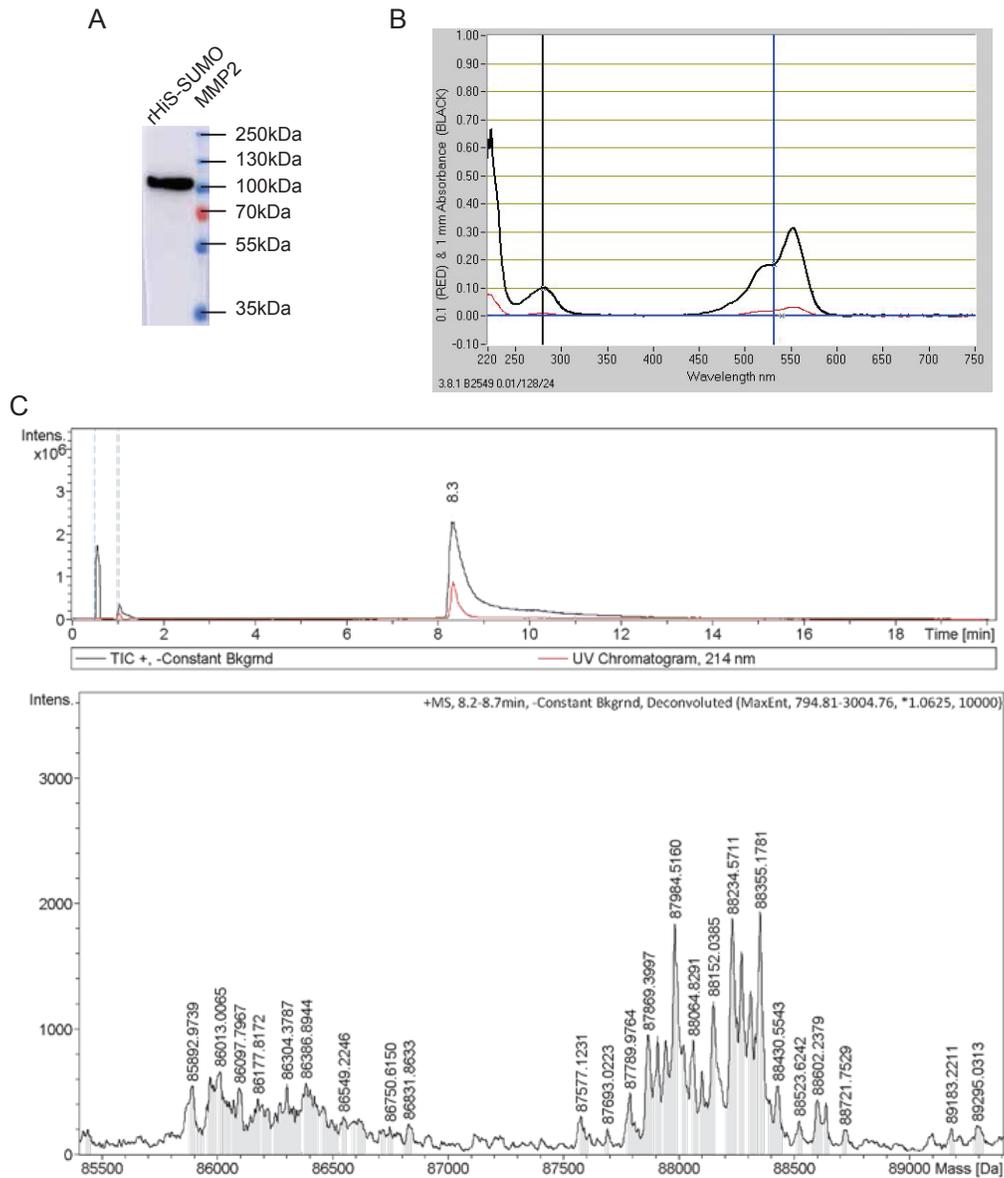
Figure 58. His-SUMO-MMP2 production and labeling. (A) Western blot analysis of purified His-SUMO-MMP2 using MMP2 antibody. (B) UV-Vis spectra of Cy3 labeled His-SUMO-MMP2 via maleimide labelling. The peaks represent the maximum absorbance peak for the protein (at 280 nm) and the maximum peak for the dye (at 532 nm). These values were used to calculate the

labelling efficiency, as previously described[274]. (C) Total mass analysis using microTOF. The above panel displays the chromatogram of unlabeled rHis-SUMO-MMP2 and illustrates the purity of the eluted sample. The lower panel shows the mass spectrometry peak of absorbance for unlabeled r-His-SUMO-MMP2. Analysis performed by the Core Facility of the Max Planck Institute of Biochemistry.

Then, to evidence a direct interaction with NUCB1, Cy3-labelled-His-SUMO-MMP2 was analyzed by analytical ultracentrifugation (AUC) alone (Figure 59B) or in the presence of unlabeled rNUCB1-His (Figure 59A). Although further characterization is required, the obtained results showed a peak of sedimentation at 4.705 S with a measured Stokes Radius (20°C) of 4.41 nm and a calculated molecular weight of 87.1 kDa for His-SUMO-MMP2, which ties with the expected molecular weight. This sedimentation peak shifts towards 3.189 S in the presence of rNUCB1-His, with a concomitant increase in the Stokes Radius (20°C) of 8.41 nm and a predicted molecular weight of 117 kDa, close to the expected theoretical one for the protein complex. This analysis strongly indicates that both proteins interact directly.
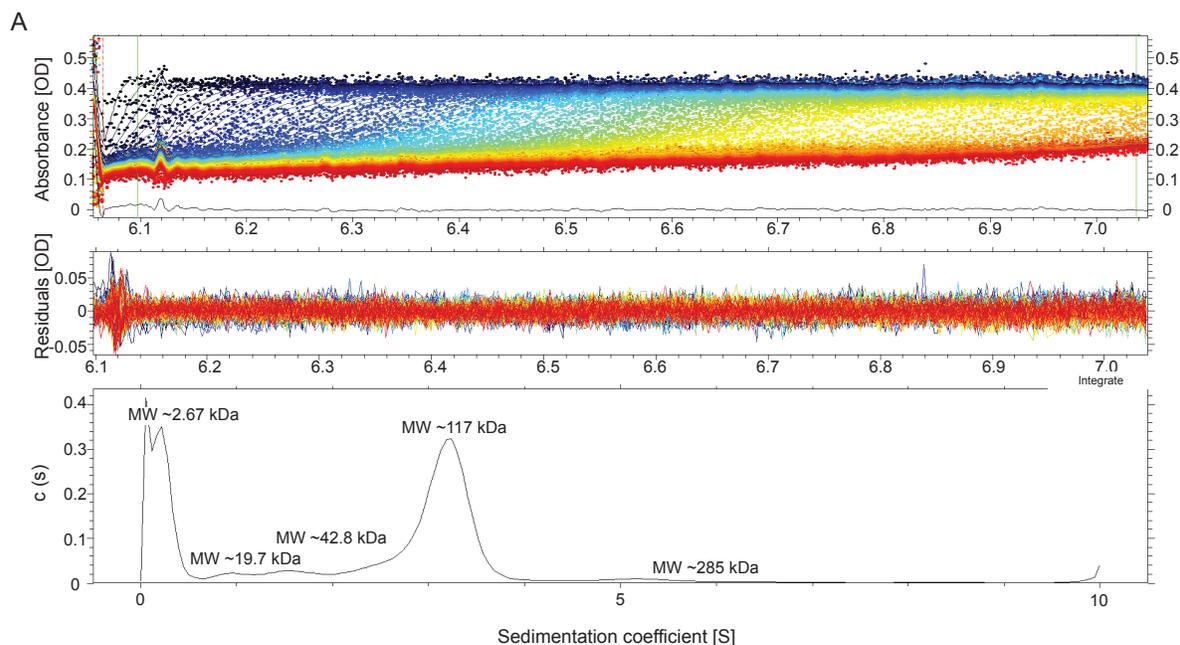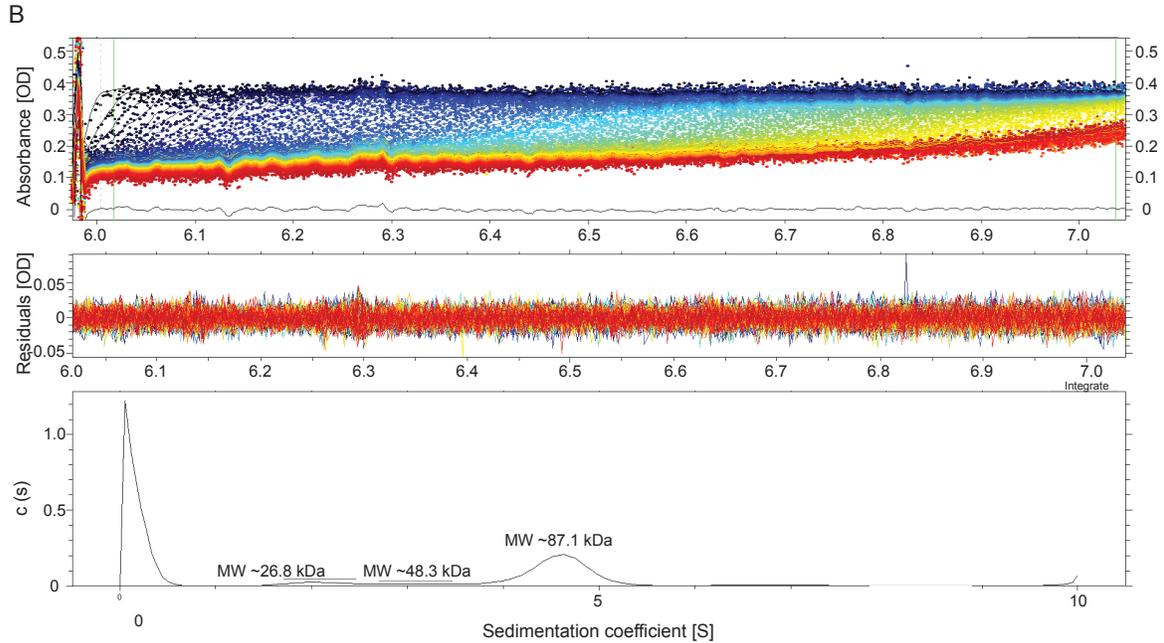
Figure 59. Analytical ultracentrifugation analyses strongly suggest a direct interaction between recombinant NUCB1 and recombinant MMP2. (A) Recombinant His-SUMO-MMP2 was bioconjugated with Cy3 via maleimide labeling and subsequently analyzed by analytical ultracentrifugation (AUC). The lowest panel shows peak of sedimentation of rHis-SUMO-MMP2 at 4.705S. (B) AUC profile of rHis-SUMO-MMP2-Cy3 and NUCB1-His. The lowest panel shows a peak at 3.189S, indicating a change in the sedimentation velocity associated to a direct interaction of NUCB1 and MMP2. These experiments were performed by the Core Facility of the Max Planck Institute of Biochemistry.

Given that NUCB1 influences also MT1-MMP trafficking, I decided to evaluate if an interaction between both proteins is also taking place. For this purpose, HeLa control and NUCB1-KO cells were transiently transfected with a pLPCX-MT1-MMP-pHluorin construct, incubated for 24 h, lysed and MT1-MMP was immunoprecipitated via its pHluorin tag using GFPtrap®. The presence of NUCB1 in the protein complex was evaluated via Western blotting (Figure 60A), evidencing an interaction between MT1-MMP-mCherry and endogenous NUCB1 (Figure 60A, 60B). This result indicates that, as well as with MMP2, both proteins interact at the Golgi.

Figure 60. MT1-MMP interacts with NUCB1. (A) GFP co-immunoprecipitation of MT1-MMP-pHluorin and NUCB1. HeLa or NUCB1-KO cells transiently expressing MT1-MMP-pHluorin with or without the expression of NUCB1-WT were pulled down via GFP and evaluated by Western blotting. NUCB1 interacts with MT1-MMP but not with the GFP control. CN: HeLa control. KO: NUCB1-KO cells. Semi-quantitative analysis of three independent experiments is depicted in (B).

7.8 NUCB1 Ca2+ binding domains are necessary for the trafficking of MMP2

Ca2+ is known to exert a critical function in the trafficking of proteins and one of the main functions of NUCB1 is to maintain the Ca2+ homeostasis at the *cis*-Golgi[9,95,107,108]. In particular, NUCB1 binds Ca2+ via its EF-hand domains and previous reports have documented the importance of the NUCB1 EF-hand motifs in Ca2+ storage and protein-protein interactions[108,275].

To evaluate the role of Ca2+ in the trafficking of MMP2, three NUCB1 EF-hand mutants were generated by substitution of the last amino acid of each EF-hand domain (Figure 61A). A glutamate (E) was substituted by a glutamine (Q) in either the first (mEFh1), the second (mEFh2) or in both EF-hand domains (mEFh1+2).

Figure 61. MMP2-NUCB1 interaction is reduced or lost when EF-hand domains of NUCB1 are mutated. (A) Protein model adapted from PDB: ref. 1SNL; the pictures depict only the EF-hand domains of NUCB1 (cyan). NUCB1-WT depicts the WT EF-hand domains of NUCB1 with the first (D) and last (E) amino acid of the domain in dark blue. NUCB1-mEFh1+2 shows the amino acid substitutions E264Q and E316Q in pink. (B) Co-immunoprecipitation of MMP2-eGFP transiently expressed in NUCB1-KO cells transfected with or without NUCB1-WT, NUCB1-mEFh1, NUCB1-mEFh2, NUCB1-mEFh1+2 and GFP–HA. When either one or both NUCB1-EFh motifs are mutated, the interaction with MMP2 is reduced or lost. The picture is representative of at least three biological replicates, and their semi-quantitative analysis is depicted in (C). Bars on the graph represent mean ± SD.

Then, co-immunoprecipitation experiments were performed using NUCB1-KO stable cell lines re-expressing the mEFh1, mEFh2 or mEFh1+2 mutants. For this purpose, NUCB1-KO cells were transiently transfected with pLPCX-Flag-MMP2-HA-eGFP and either pLPCX-NUCB1-mEFh1, pLPCX-NUCB1-mEFh2, pLPCX-NUCB1-mEFh1+2 or pLPCX-NUCB1-WT. After pulling down MMP2 using GFPtrap® as previously described, Western blot analysis showed that the interaction of MMP2 and NUCB1 is highly reduced when any of the domains is mutated (Figure 61B).

Furthermore, to evaluate the effect of the mutations on the NUCB1 EF-hand mutations on the trafficking dynamics of MMP2, stable cell lines expressing each of the EF-hand mutants (NUCB1-mEFh) were generated. HeLa control, NUCB1-KO, NUCB1-mEFh mutants and NUCB1-KO cells re-expressing NUCB1-WT (NUCB1-KO+NUCB1-WT) were then transiently transfected with RUSH MMP2, incubated with biotin for 0, 15, 30 and 45 min, fixed and co-stained with NUCB1 antibody.
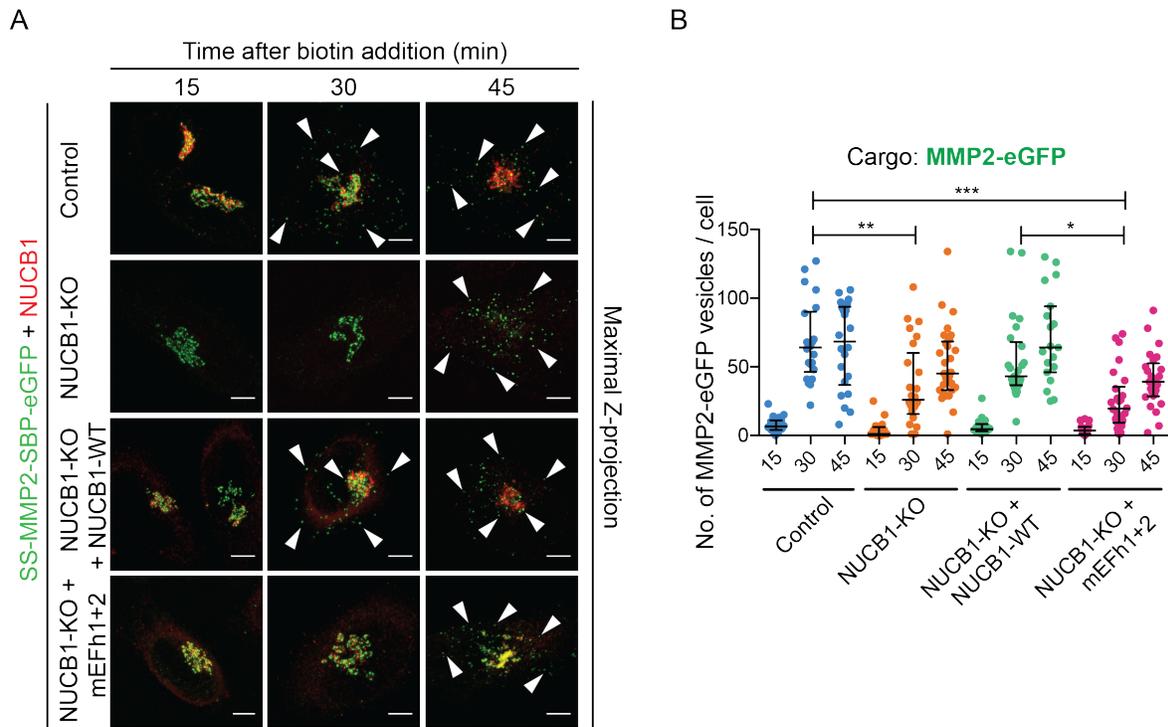
Figure 62. NUCB1 EF-hand motifs are required for the proper intracellular trafficking of MMP2. (A) Confocal fluorescence images depict the expression of SS-MMP2-SBP-eGFP in HeLa or NUCB1-KO cells co-expressing or not NUCB1-WT or NUCB1-mEFh1+2. After 15, 30, and 45 min of biotin incubation, cells were fixed and co-stained with NUCB1 antibody (red). Scale bars: 5 μm. White arrowheads point to cytoplasmic vesicles. (F) Quantification of cytoplasmic vesicles shows the medians (± interquartile range) of at least 19 cells per condition from two independent experiments. Statistical evaluation was performed via the Kruskal–Wallis non-parametric test with Dunn's multiple comparison of groups. X-axis: time in minutes after biotin addition. *p < 0.05, **p < 0.01, ***p < 0.001. These experiments were performed together with Dr. Birgit Blank.

Evaluation by confocal microscopy showed a delay in MMP2 trafficking in NUCB1-mEFh cells (Figure 62A) and further quantitative evaluation evidenced a reduced number of MMP2-

eGFP cytoplasmic vesicles at 30 min after biotin addition, similar to the one observed in NUCB1-KO cells (median mEFh1+2: 20, interquartile range: 8.5 – 42; median KO: 27, interquartile range: 12 – 51) and significantly lower when compared to HeLa control (median: 65, interquartile range: 41 – 93) or NUCB1-KO+NUCB1-WT cells (median: 45, interquartile range: 36 – 74; Figure 62B). These results denote the importance of Ca2+ for the proper trafficking of MMP2.

To further evaluate how Ca2+ impacts the conformation and stability of NUCB1, a His-tagged recombinant NUCB1 with the described mutation in both EF-hand domains was generated as described earlier in this section (rmEFh1+2-His, Figures 63A, 63B) and, together with rNUCB1-His, analyzed by circular dichroism (CD). A comparison of both CD spectra showed a reduced molar ellipticity of the mutant when compared to rNUCB1-His (Figure 63C).
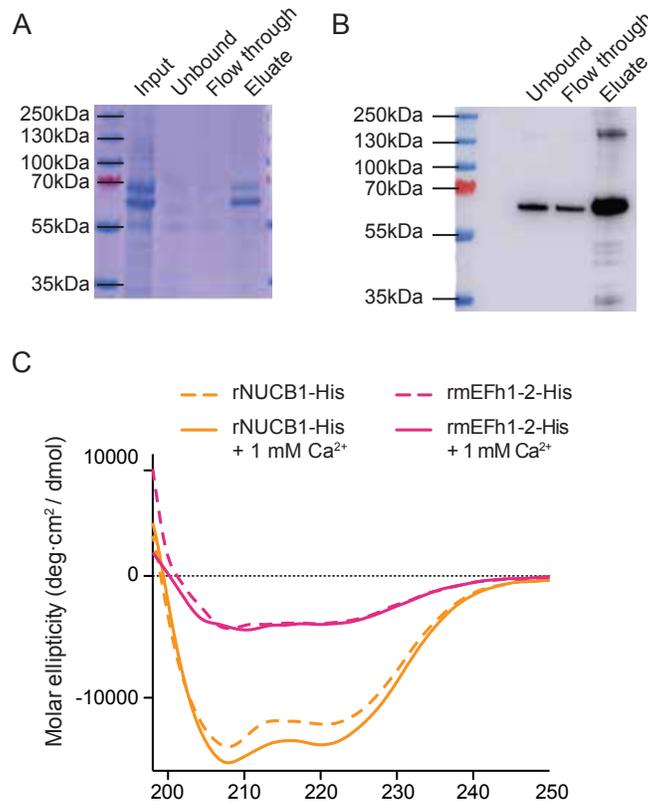
Figure 63. NUCB1 loses its Ca2+ binding ability when EF-hand motifs are mutated. CD measurement of recombinant NUCB1-His and the recombinant mutant mEFh1+2-His under presence or absence of 1 mM Ca2+. rNUCB1-His shows a highly α-helical structure that acquires a more compact conformation in the presence of Ca2+. When EFh1+EF2 domains are mutated,

the protein acquires a structure with higher β-sheet content that is not sensitive anymore to Ca2+ addition.

CD spectra analysis using CONTIN[259] evidenced an increased α-helicity in rNUCB1-His upon Ca2+ addition (from 0.385 to 0.413) that was not observed for the EF-hand binding mutant. Instead, the values obtained from the CONTIN algorithm showed a decrease in α helicity upon Ca2+ addition (from 0.256 to 0.147) together with an increase in β-sheet content, indicating a shift towards a more unstable state with loss of secondary structure, and confirming previous reports that found that the EF-hand motifs of NUCB1 have an open conformation that folds only after Ca2+ addition[108,117,275].
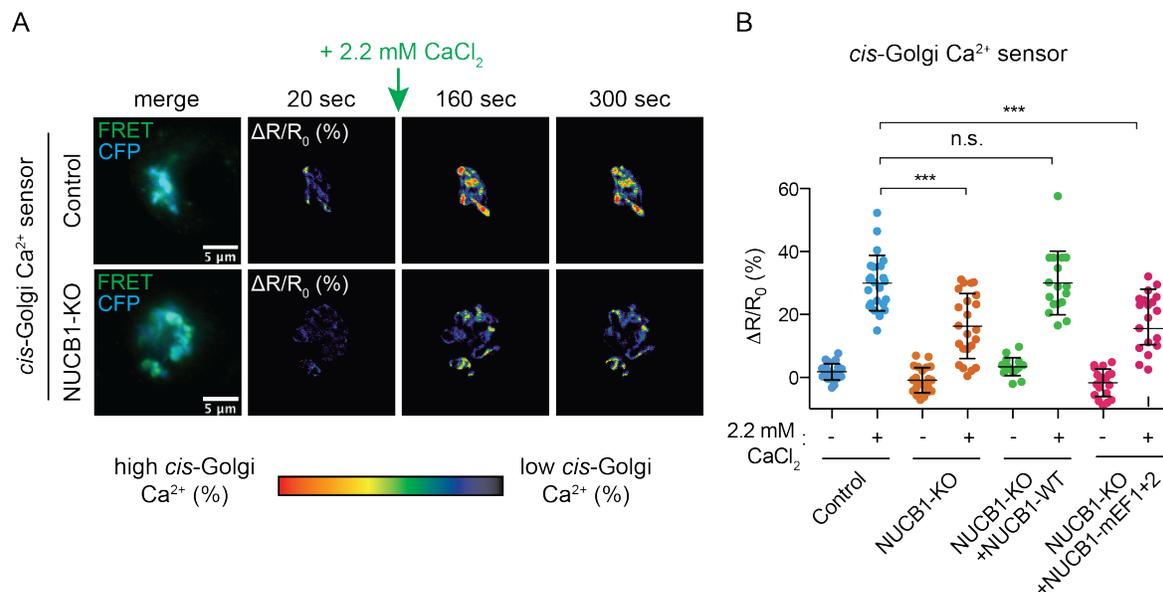
Figure 64. Ca2+ influx is reduced at the *cis*-Golgi in the absence of NUCB1. (A) Fluorescent images depict HeLa or NUCB1-KO cells expressing the GPP130-Twitch5 *cis*-Golgi Ca2+ sensor. The cells were previously treated with ionomycin for 20 seconds to deplete endogenous Ca2+ at the Golgi lumen. Then, 2.2mM Ca2+ were added and the cells were monitored using live-cell ratiometric FRET microscopy. The $\Delta R/R0$ FRET ratio (R0: FRET value before addition of 2.2mM Ca2+) was lower in NUCB1-KO cells compared with HeLa control, indicating the leaking of Ca2+ at the *cis*-Golgi in the absence of NUCB1. (B) Quantification of the *cis*-Golgi $\Delta R/R0$ FRET ratio. Both NUCB1-KO cells with or without expression of NUCB1-mEFh1+2 showed a reduced Ca2+ influx using the GGP13'-Twitch5 *cis*-Golgi Ca2+ sensor. Statistical evaluation was performed using the Mann–Whitney test. ***p < 0.001, n.s.: not significant. The color code in

Figure 64A indicates the $\Delta R/R_o$ in % at the *cis*-Golgi at a specific time point. Experiments performed by Dr. Mehrshad Pakdel.

To deepen into the understanding of the role of NUCB1 in Ca2+ homeostasis, experiments using a Fluorescence Resonance Energy Transfer (FRET) Ca2+ sensor for both the *cis*- and the *trans*-Golgi were performed. For this purpose, both HeLa control, NUCB1-KO cells were transiently transfected with the FRET sensors GPP130-Twitch5, localized at the *cis*-Golgi or GoD1-cpv, at the *trans*-Golgi. After 24 h incubation, Ca2+ was depleted from the intracellular acidic compartments with ionomycin and Ca2+ influx was evaluated using live-cell ratiometric FRET microscopy. Quantification of FRET efficiency was then calculated as the ratio of FRET intensity $\Delta R/R_o$, where ΔR represents the ratio between YFP and CFP intensities at any time point, and R_o is the fluorescence intensity of CFP at time 0.
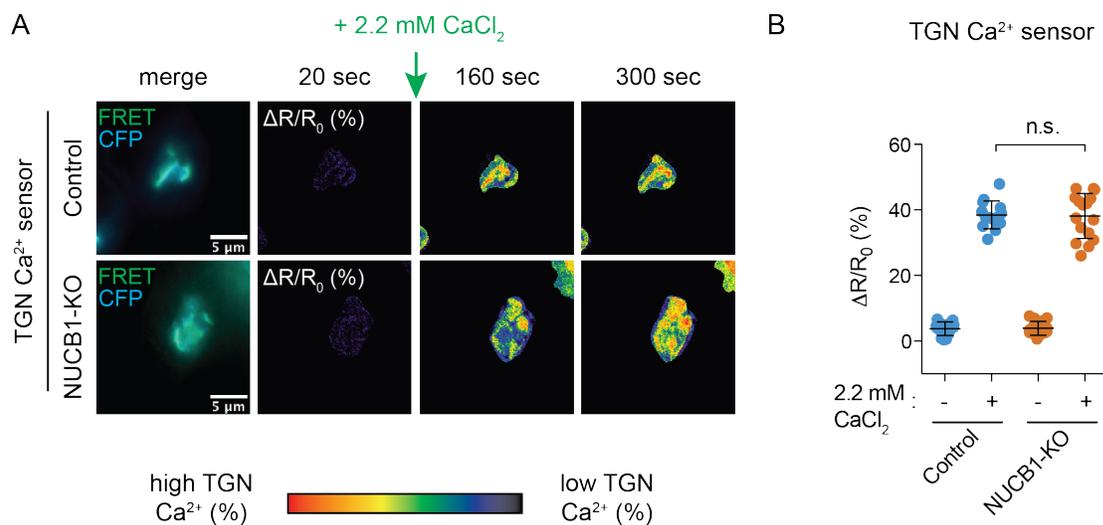
Figure 65. *Trans*-Golgi Ca2+ influx is not altered in NUCB1-KO cells. (A) Fluorescent images illustrate the same experiment described in Figure 64 but using the Go-D1-cpv *trans*-Golgi Ca2+ sensor. (B) Quantification of the *trans*-Golgi $\Delta R/R0$ FRET ratio showed no difference in Ca2+ influx between HeLa control and NUCB1-KO. Quantification was performed with values of at least 20 cells and shows the medians (± interquartile range) from at least two different experiments. Statistical evaluation was performed using the Mann–Whitney test. n.s.: not significant ***p-value<0.001. The color code in (A) indicates the $\Delta R/R_o$ in % at the *trans*-Golgi at a specific time point. Experiments performed by Dr. Mehrshad Pakdel.

Microscopy images showed an increase in Ca2+ concentration at the *cis*-Golgi in HeLa control cells at 160 sec after 2.2 mM Ca2+ addition to the media (Figure 64A). Contrasting, the signal intensity in NUCB1-KO cells was lower than the one registered for control cells, indicating that in the absence of NUCB1 the Ca2+ influx to the *cis*-Golgi is impaired (Figure 64B).

Furthermore, evaluation of Ca2+ influx in NUCB1-KO cells expressing the mEFh1+2 did not restore the phenotype, whereas the ratio of FRET intensity in NUCB1-KO+NUCB1+WT cells was similar to the one observed in HeLa control cells. Altogether, these results demonstrate that not just the absence of NUCB1, but a single point mutation in its EF-hand domains, is enough to impair Ca2+ homeostasis at the *cis*-Golgi.

Instead, observations made at the *trans*-Golgi showed no differences in Ca2+ influx between NUCB1-KO and HeLa control cells, strongly indicating that NUCB1 impairs Ca2+ influx exclusively at the *cis*-Golgi (Figure 65A, 65B). Altogether, these results suggest that MMP2 trafficking is delayed at the *cis* but not the *trans*-Golgi of NUCB1-KO cells due to an impairment of Ca2+ retention and homeostasis alteration caused by the Ca2+ binding incapability of NUCB1.

7.9   NUCB1-KO impairs matrix degradation in human macrophages and cell invasion in MDA-MB-231 cells

To address the physiological role of the impaired traffic of MMP2 in the absence of NUCB1, matrix degradation and invasion experiments were performed in collaboration with the groups of Dr. Angelika Haußer in Stuttgart and Prof. Dr. Stefan Linder in Hamburg.
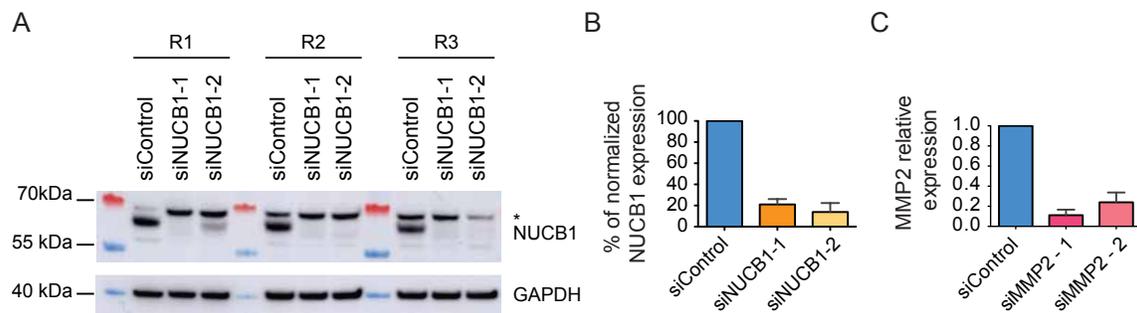
Figure 66.   Silencing of MDA-MB-231 cells. (A) Western blot depicts the reduction in expression levels of NUCB1 in silenced cells from three independent experiments (R1, R2, and R3). *:

unspecific band. GAPDH was used as loading control. Semi-quantitative analysis of silencing is depicted in (B). (C) qPCR analysis to evaluate MMP2 reduced relative expression upon silencing in MDa-MB-231-MT1-MMP-mCherry cells.

For this purpose, two different models were studied: the Haußer group evaluated the behavior of MDA-MB-231-MT1-MMP-mCherry cells using Matrigel cell invasion and gelatin degradation analyses, while the Linder group studied gelatin degradation of primary human macrophages. NUCB1 (siNUCB1, Figure 66A, 66B) or MMP2 (siMMP2, Figure 66C) were silenced in MDA-MB-231-MT1-MMP-mCherry cells using 2 different siRNAs.

After 72 h transfection, cells were seeded in transwell inserts on top of Matrigel® (to evaluate cell invasion) or on top of fluorescently labeled gelatin (to evaluate matrix degradation). After 24 h incubation, invading cells were evaluated by microscopy, showing that siNUCB1 cells migrated to a less extent compared with siControl (Figure 67A, 67B). Moreover, such behavior resembled the one observed when siMMP2 is silenced, indicating that the reduced expression of NUCB1 in this cell model impaired the matrix invasion of cancer cells (Figure 67B).
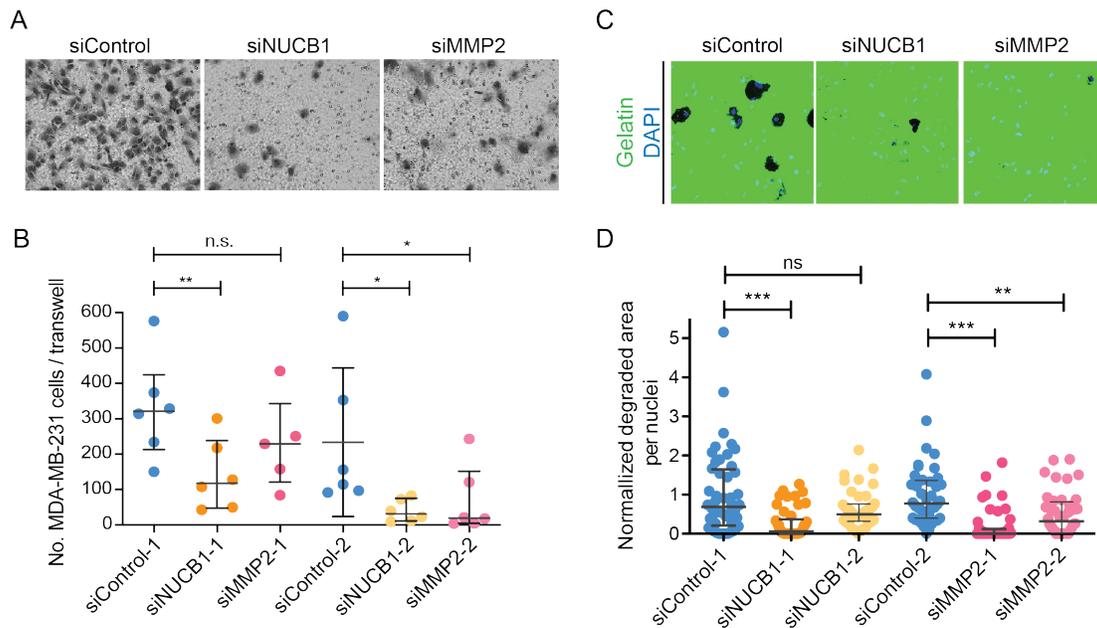
Figure 67. Matrix invasion and degradation are impaired in MDA-MB-231 cells when NUCB1 is silenced. Three days post-transfection cells were seeded on (A) Matrigel-coated transwell inserts and allowed to invade for 24 h or (C) on Oregon488-conjugated gelatin and allowed to degrade for 5 h. Cells were fixed and either stained with crystal blue (for the invasion assays) or nuclei

counterstained with DAPI (for the gelatin degradation assays). (B) Quantification of the number of cells migrating through the Transwell or (D) degraded gelatin showed a marked reduction in NUCB1 siRNA-treated cells in both Matrigel invasion and gelatin degradation. Two different siRNAs were used to confirm the reduction. Data are presented as median ± interquartile range from 3 independent experiments. n.s.: not significant *p <0.05, **p < 0.01, ***p < 0.001. Statistical significance was evaluated via the Kruskal–Wallis test with Dunn's multiple comparison of groups. Experiments performed by the Haußer group.

Matrix degradation was evaluated by gelatinolytic assays using both MDA-MB-231-MT1-MMP-mCherry cells (Figures 67C, 67D) and primary human macrophages (Figure 68). The results showed an impaired capacity to degrade gelatin in both cell models when NUCB1 expression is reduced. Such degradation levels are comparable to the ones observed on MMP2 silenced cells, strongly suggesting that NUCB1 plays a fundamental role in the overall trafficking of MMPs and that its presence is crucial for MMP2 mediated cell migration and matrix invasion.
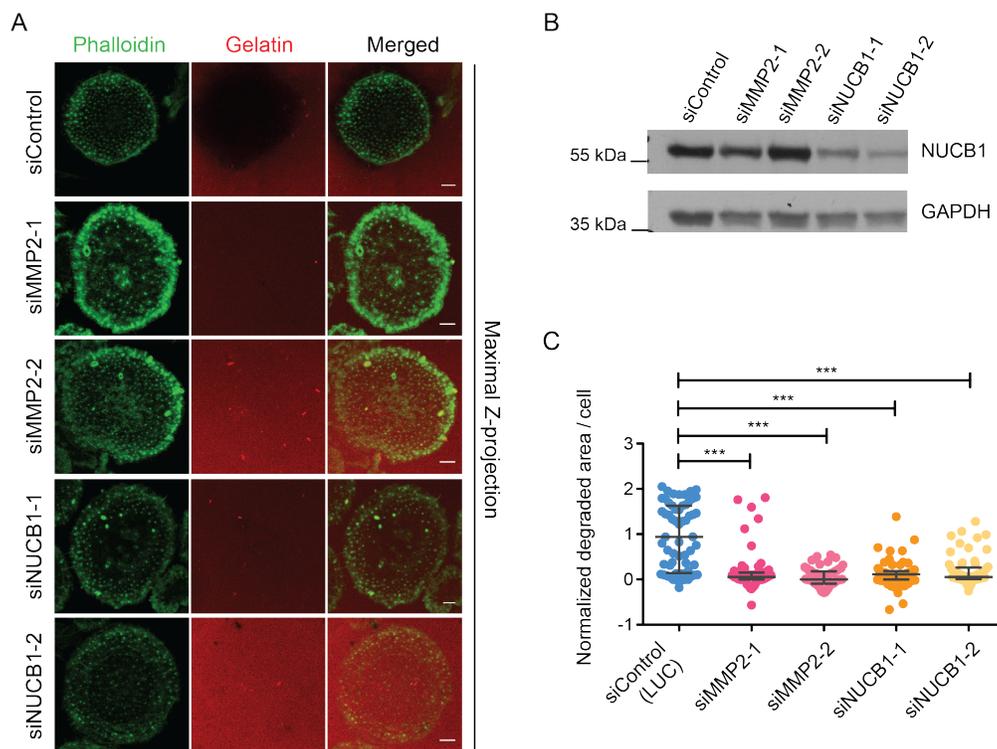
Figure 68. Gelatin degradation is impaired in NUCB1 silenced human primary macrophages. Primary macrophages differentiated from human plasma donors were seeded on a gelatin-Rhodamine substrate and incubated for 6 h. Representative confocal fluorescent images are

depicted in (A). Scale bars: 5 μm. (B) Validation of NUCB1 knock down of siRNA1 and siRNA2 in primary macrophages by western blotting. GAPDH was used as loading control. (C) Quantification of gelatin degraded area per cell. Silencing either NUCB1 or MMP2 impairs gelatin degradation in human primary macrophages. Two different siRNAs were used to corroborate the phenotype. At least eight fields of view per condition were analyzed. Data are represented as median (± interquartile range). Kruskal–Wallis and Dunn's group comparison tests were used to estimate statistical significance. ***p < 0.001. Experiments performed by the Linder group.

Finally, given that MT1-MMP activates MMP2, it could be argued that the reduced availability of MMP2 at the plasma membrane is due to an activation defect (caused by the delay on trafficking of MT1-MMP) rather than to a trafficking delay. To rule out this possibility, *in* gel zymography experiments were performed using lysates and supernatants of HeLa control or NUCB1 cells expressing RUSH MMP2 (Figure 69)). The results obtained showed no difference in the activity of MMP2, indicating that the observed phenotype in the matrix degradation and invasion experiments is not due to a defect in activation but rather a delay in the sorting of MMP2 when NUCB1 is not present.
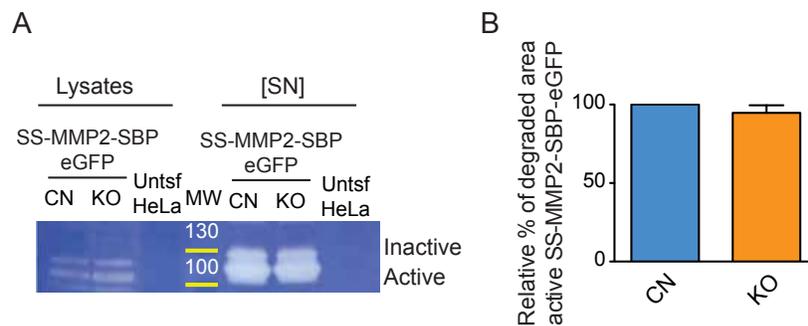
Figure 69. MMP2 activity is not affected in NUCB1-KO cells. Zymography assay of HeLa cells expressing SS-MMP2-SBP-eGFP. After overnight transfection, cells were incubated with OptiMEM media + biotin for 45 min and lysates and supernatant samples were prepared for zymography evaluation. No differences in gelatin degradation were observed in NUCB1-KO cells when compared to the HeLa control. The two bands observed correspond to MMP2-SBP-eGFP inactive (~110kDa) and active (~101kDa) versions of the protein. CN: HeLa control cells, KO: NUCB1-KO cells, Untsf HeLa: Hela cells without transfection. [SN]: 10X concentrated supernatants. The semi-quantitative analysis of this experiment is depicted in (B).

In conclusion, the results here shown identify NUCB1 as a novel component of MMP2 trafficking. They show that NUCB1 interacts with MMP2 at the Golgi, exclusively delaying its

intra-Golgi trafficking at the *cis* compartment and, as a consequence, decreasing MMP2 mediated cell migration and matrix invasion. Moreover, they show that not only MMP2, but also MT1-MMP intra-Golgi trafficking is impaired, implying that this mechanism could also influence the trafficking of other MMPs. Further studies are required to establish the extent to which NUCB1 influences trafficking dynamics of extracellular matrix degrading proteins in the cell.

8. Discussion

MMPs are one of the most important components in ECM remodeling[186,250,276–278]. Profuse literature has studied their roles in cell migration and tissue invasion during cancer metastasis, as well as in inflammatory processes, where macrophages secrete MMPs in antagonist manners and only under certain stimuli[184,190,211,215,250]. MMPs degrade mainly extracellular substrates, though their role in intracellular cleavage has also been demonstrated[182,198,279]. Although the literature describing MMPs multiple functions and their potential role as biomarkers is abundant[186,188,195,202,204,214,215,279], little is known about their intracellular trafficking mechanisms.

Some studies have shown that MMPs are transported in kinesin-driven vesicles across microtubules from the TGN to the plasma membrane[225,241,246,249,280]. Also, recent reports haven shown that Rab GTPases, such as Rab8, Rab2A and Rab40b are required for MMP transport and MT-MMPs recycling[212,242,243,245]. However, the machinery behind these routes remains unknown. The work presented here aimed to elucidate components of MMP intracellular trafficking. Hence, this chapter will discuss the findings that revealed NUCB1 as a novel component of MMPs intracellular trafficking and outline how Ca2+ is essential for MMP2 intra-Golgi trafficking.

8.1   NUCB1 as regulator of anterograde MMP trafficking

A mass spectrometry approach combined with the synchronized secretion of GFP tagged MMP2 allowed to identify NUCB1 as a novel component of MMP2 trafficking. NUCB1 literature describes its role in G-protein activation[113,114,116,117], the inhibition of β-amyloid precursor protein (APP) formation[118,119,265] and a role in endosomal trafficking[120,121], but no report so far links NUCB1 with anterograde cargo trafficking. Notably, NUCB1 resides in the *cis*-Golgi, where it is retained for a period of time that varies between 12 and 24 h –depending on the cell type– and is then secreted to the extracellular milieu[106,112]. Another form of the protein localizes in the cytoplasm (sNUCB1) and has been described to activate Giα3 protein and exert a chaperone-like function on amyloid-β precursor protein (APP), avoiding its aggregation[112–114,117–119,265,281].

In order to determine the effect of NUCB1 on MMP2 trafficking, NUCB1-KO cells were generated via CRISPR/Cas9 technology and MMP2 intracellular transport was evaluated using

the RUSH system. Results from these experiments (Figures 42A, 42B) showed that MMP2 trafficking is not altered at the ER and arrives to the *cis*-Golgi in NUCB1-KO cells with the same kinetics compared to HeLa control cells. However, once MMP2 reaches the *cis*- and traffics towards the *trans*-Golgi a trafficking delay is observed. Particularly, such delay disappears once the protein reaches the TGN and can be transported to the plasma membrane with no kinetic differences between NUCB1-KO and HeLa control cells. Furthermore, evaluation of MT1-MMP trafficking evidenced a similar delay in NUCB1-KO cells without a complete block in trafficking. Then the question arises, why is there a delay instead of a whole arrest of protein trafficking in the absence of NUCB1?

One possibility is that another protein interacting with MMP2 at the Golgi could compensate for the loss of NUCB1. Calumenin could be a good candidate for such a role since it is also an EF-hand protein associated with the ER that localizes to the Golgi before being secreted[21]. In this regard, calumenin could, under impaired Ca2+ homeostasis at the *cis*-Golgi, compensate for the lack of NUCB1 activity. Remarkably, calumenin has been shown to interact with thrombospondin-1, an extracellular matrix protein important for coagulation, and is suggested to be involved in its trafficking[282]. Not just calumenin, but also proteins continuously cycling between ER and Golgi, such as the complex formed by MCDF2 and LMAN1[26–28], known to participate in the early trafficking of coagulation factors in a Ca2+-regulated manner, could also compensate for the lack of NUCB1. Nevertheless, further investigation is required to confirm their potential compensation.

Given that Ca2+ gradients along the Golgi are important for cargo trafficking, another possibility is that the absence of NUCB1 causes a local change of Ca2+ concentration exclusively at the *cis*-Golgi. Among the EF-hand proteins present along the secretory pathway, NUCB1 and Cab45 have been shown to be essential for keeping Golgi Ca2+ homeostasis[103,106]. Interestingly, both proteins share several similarities: they possess homologous Ca2+ binding EF-hand domains, they regulate Ca2+ homeostasis by association with Ca2+ ATPases (NUCB1 with SERCA in the *cis*- and Cab45 with SPCA1 in the *trans*-Golgi) and in their absence cargo trafficking is delayed or blocked[9,95,96,104,112].

Importantly, Cab45 has been shown to be crucial to sort cargo at the TGN in a Ca2+-dependent manner and previous studies have already evidenced the importance of Ca2+ for the proper sorting of soluble cargo at the TGN[83,93–96,107,273], therefore, NUCB1 could act as the

Cab45 counterpart at the *cis*-Golgi regulating cargo trafficking in a Ca2+-dependent manner (see below). Moreover, results from secretion assays showed that the observed delay at the *cis*-Golgi generated a reduced availability of MMP2 in the extracellular milieu, whereas HRP, and even LyzC, a protein known to be sorted by Cab45, showed no reduction (Figures 43, 46). These results point towards a specific impairment of *cis*-Golgi Ca2+ homeostasis, rather than an overall Ca2+ deficiency and support the hypothesis of NUCB1 as an essential component of MMP2 intra-Golgi trafficking.

8.2   NUCB1 influences MMP2 trafficking exclusively at the *cis*-Golgi

Live-cell microscopy experiments using RUSH MMP2 evidenced that MMP2 trafficking delay in NUCB1-KO cells occurs exclusively at the *cis*-Golgi, since kinetics at both ER and *trans*-Golgi showed no differences when compared to HeLa control cells. Moreover, Ca2+ influx experiments with both NUCB1-KO and NUCB1-mEFh1+2 mutants evidenced an impairment in Ca2+ homeostasis at the *cis* but not the *trans*-Golgi.

It is well known that *cis* and *trans*-Golgi compartments store Ca2+ at different concentrations in a gradient manner, with the higher Ca2+ concentration at the *cis* (~300 μM)[51,52,89,99]. SERCA pumps provide most of the Ca2+ at the ER and *cis*-Golgi, whereas at the *trans*-Golgi is SPCA1 the main Ca2+ provider[49,83,85]. In addition, the Ca2+ channel distribution also varies, with the IP3 receptors (IP3R) predominantly localizing at the *cis* and Ryanodine receptors (RyR) at the *trans*[85]; this differential distribution of Ca2+ effectors pinpoints how the maintenance of Ca2+ gradients is essential for Golgi compartmentalization.

Nowadays the mechanism by which this compartmentalization is maintained, is still under debate, however, two main models have been generally accepted: the cisternal maturation/progression model and the fixed compartment model (Figure 8)[46,48,56]. One could argue that the observed kinetics of MMP2 transport would support a trafficking model where Golgi compartments are fixed given that no differences between NUCB1-KO and HeLa control cells were observed before 30 min and after 44 min of biotin incubation. However, given the restricted time frame evaluated is not possible to come to this conclusion. Actually, one could also argue that after the 45 min evaluated, or even, once the ER is newly refilled with MMP2-eGFP, a new Golgi cisterna is generated and, upon recycling of medial-Golgi

resident proteins, Ca2+ levels equilibrate and MMP2 can mature and be efficiently sorted into secretory vesicles.

8.3   NUCB1 interacts with MMP2 at the Golgi

Most of the literature describing NUCB1 function is based on experiments performed with sNUCB1, the cytosolic version of the protein[113,114,117,119,120]. However, results from RUSH MMP2 experiments showed that sNUCB1 does not rescue MMP2 trafficking when expressed in NUCB1-KO cells. Moreover, my results demonstrate that NUCB1 interacts in a weak manner with MMP2 specifically at the Golgi, as shown by IP experiments using Golgi membranes, and that such interaction is direct, as evidenced by the analytical ultracentrifugation experiments. However, validating this interaction was one of the biggest challenges of this work, mainly because it turned out to be very difficult to confirm the direct interaction between endogenous proteins using coIP experiments.

To determine the specific domain of interaction between MMP2 and NUCB1, I generated MMP2-domain truncated mutants (Figures 54, 55). Although I could evidence that both proteins interact, the specific domain for such an interaction remains unidentified. It is possible that the approach I used, with whole cell lysates, did not provide the right environment for MMP2 truncated mutants and NUCB1 to interact. In addition, the use of overexpressed NUCB1 in whole cell lysates –even though the amount of transfected NUCB1 was adjusted according to previous titration experiments (data not shown)– may also explain why the interaction was always present in the Western blots. Moreover, experiments performed with overexpressed MMP2 truncated mutants only, showed inconclusive results about the interaction with endogenous NUCB1 (data not shown).

Nonetheless, I cannot rule out the possibility that a third component is required for the stabilization of the interaction between NUCB1 and MMP2. Given that different TIMPs interact with MMP2, it is possible to hypothesize that such an interaction could work as a scaffold for NUCB1 binding. Also, it is possible that both proteins interact very transiently in a switch way, where Ca2+ waves allow transient binding of MMP2 to NUCB1 and reduction of Ca2+ concentration towards a medial Golgi, causes MMP2 release.

In this regard, my CD measurements showed conformational changes in rNUCB1 that favored a more compact form in the presence of Ca2+, a behavior that has been observed in other EF-hand proteins such as p54/NEFA[123] and Cab45[95,96]. Such changes could expose hydrophobic residues that enable further protein-protein interactions. Moreover, similarities between the conformational changes of NUCB1 and Cab45 upon Ca2+ addition suggest that Ca2+ is a regulator switch that promotes NUCB1-dependent protein trafficking. In this regard, the requirement of Cab45 EF-hand domains for its oligomerization and sorting of soluble cargo in sphingomyelin-rich vesicles, supports this premise. Furthermore, the impaired interaction between NUCB1 and MMP2 when NUCB1 EF-hand motifs 1 and 2 are mutated, strengthen the hypothesis of a Ca2+-dependent interaction and posterior delivery of MMP2 to the next compartment.

8.4 Physiological relevance of impaired MMP2 intra-Golgi trafficking

MMP2 is characterized for its upregulation in metastatic cells and its role in promotion of cell invasion[212–214,216,248]. Also, under physiological conditions, MMP2 has been described as a key player in neurological development, tissue repair and control of inflammation processes by promotion of leukocyte transmigration and active ECM degradation[215,218,247,283]. Already Yu et al. (2014) demonstrated that a general knock out of Rab11a caused a defect in MMP2 secretion and a deficient embryo implantation in Rab11^{null} mice[284]. Also, Wiesner at al. (2013) showed that the ablation of Rab5a, Rab8a and Rab14 impaired MT1-MMP delivery to the plasma membrane, decreasing the contact between MT1-MMP containing vesicles and podosomes, and therefore, reducing proteolytic invasion of human macrophages[242].

Our collaborative work evidenced a reduced invasion of MDA-MB-231 cancer cells and an impairment in gelatin degradation, both in MDA-MB-231 cells and human macrophages when NUCB1 was silenced. Moreover, the observed impairments highly resembled the phenotype observed when MMP2 was silenced, illustrating the role of NUCB1 in proper MMP2 trafficking and highlighting its relevance for proper ECM remodeling. Here is important to highlight that NUCB1 also modulates MT1-MMP intra-Golgi trafficking, which explains why its effect in MDA-MB-231 cell invasion is slightly stronger than the one observed in MMP2 silenced cells (Figure 67). Furthermore, given that MMP2 is mainly activated by MT1-MMP at

the plasma membrane, it would be possible that the observed phenotype is due to an MMP2 activation defect, rather than a delay in trafficking. However, the zymography confirm that it is the delay, but not an activation defect, which impairs matrix degradation.

8.5   A model for NUCB1-dependent MMP intra-Golgi trafficking

Defining a common model for intra-Golgi trafficking remains a matter of debate in the field[29,46,61,285]. So far, 4 models have been described: vesicular model (VM), diffusion model (DM), cisternal maturation-progression model (CMPM)[46] and kiss-and-run model (KARM)[285]. In addition, a model in which intra-Golgi trafficking occurs via tunnels generated between the Golgi stacks has been used to explain the trafficking of large cargo in mammalian cells[29]. Although there is evidence favoring each model[25,48,56,62], no consensus has been reached so far. Instead, it has been suggested that, depending on the cargo, the distance and the time regulation of membrane fusion and fission, proteins could be transported following different models in parallel[29].

A diffusion model where the arrival of cargo from the ER to the *cis*-Golgi promotes Ca2+ efflux and the subsequent formation of Golgi tubules could explain why in the absence of NUCB1 there is a delay in trafficking[285]. Trucco et al. (2004) demonstrated that Golgi tubules are destabilized when no Ca2+ is liberated to the cytosol, therefore, an impairment in Ca2+ homeostasis at the *cis*-Golgi would destabilize the tubules around this compartment and delay, although not completely block, the transport to the next compartment[286]

The results of this work show that NUCB1 impairs MMP2 trafficking exclusively at the Golgi in a Ca2+-dependent manner, probably by interacting in a Ca2+-regulated switch-manner at specific exit sites in the rims of the *cis*-Golgi. The accumulation of cargo at the highly curved rims of the *cis*-Golgi is a well-known mechanism for vesicle transport to the medial compartment[55,56,58–60,64,287,288].

Although Lin et al. (1998) identified NUCB1 as a luminal protein, it was also present in the membrane fraction of Golgi isolations, suggesting its association with Golgi membranes in an unknown manner[104]. Furthermore, Lavoie et al. (2002) found that NUCB1 is associated with Golgi membranes in AtT20 cells and Leclerc et al. (2008) identified NUCB1, COX-2 and

cytosolic phospholipase A2α (cPLA2α) in Golgi membrane fractions of human neutrophils, strengthening the hypothesis of an association with the membrane[102,106].

Lavoie et al. (2002) proposed that NUCB1 could be retained at the *cis*-Golgi by binding to an unknown transmembrane protein. Although no studies have evaluated membrane association of *cis*-resident NUCB1, FRET experiments from Weiss et al. (2002) showed that sNUCB1 interacts with the heteromeric Gαi3 protein at the cytoplasmic face of the Golgi only when Gαi3 is anchored to the membrane via palmitoylation and myristoylation[114]. Based on these findings, it is possible to hypothesize that Golgi-resident NUCB1 uses a similar mechanism to associate with and unknown transmembrane candidate that act as an anchor on the luminal side of the Golgi.

Lipid modifications, and particularly myristoylation and palmitoylation, are known to be important for the association of proteins to membranes[68,70,289]. Moreover, N-glycine-myristoylation is necessary for the correct association of proteins to membranes of an intracellular compartment, though, it requires additional lipid modification or the presence of positively charged amino acid clusters in the targeting protein[68]. These additional requirements allow that protein myristoylation acts as an activation switch modulated by changes in GTP or Ca2+[68].

In this context, it has been shown that myristoylated proteins involved in Golgi structure maintenance, such as cPLA2α and GRASP65, localize to the Golgi in a Ca2+-dependent manner[59,67,70,85]. Furthermore, Micaroni et al. (2010) showed that intra-Golgi trafficking induces changes in Ca2+ concentration at the cytosol surrounding the Golgi, triggering the recruitment of Ca2+-dependent proteins or inducing cytosolic signaling cascades[83,85].

In particular, both cPLA2α C2 domain as well as its catalytic activity are required for the maintenance of Golgi curvatures and tubulation[59,124]. cPLA2α generates wedge-like lysolipids by hydrolysis of fatty acids in cylindrical phospholipids[85], whereas cPLA2α C2 domain has been identified as a Ca2+ sensor important for the translocation of cPLA2α from the plasma membrane to Golgi membranes[124].

Moreover, Ward et al (2012) demonstrated that, after membrane binding, the C2 domain of CPLA2α is sufficient to induce positive membrane curvature in giant unilamellar vesicles (GUVs), whereas only the full-length protein is able to initiate tubulation[124]. In this regard, the

accumulation of wedge-like lysolipids in cPLA2α-induced curved Golgi regions would stimulate the formation of vesicles or tubules that interconnect Golgi cisternae[59,85]. Altogether, cPLA2α could be considered a potential candidate for the Ca2+-dependent indirect regulation of NUCB1-driven anterograde trafficking (Figure 70).
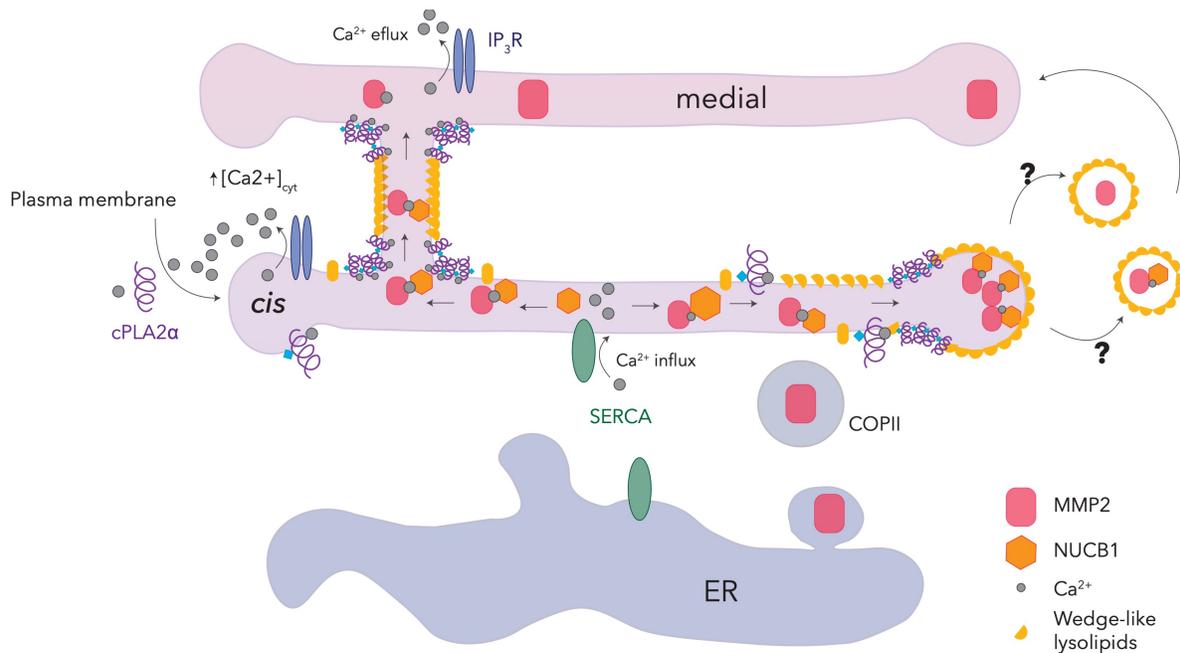
Figure 70. Model for Ca2+-dependent NUCB1-mediated MMP2 trafficking. In this model, MMP2 is transported from the ER to the *cis*-Golgi in COPII vesicles. The vesicle fusion with the *cis*-Golgi generates a transient increase in local Ca2+ that subsequently promotes Ca2+ efflux, which in turn increases Ca2+ concentration in the surrounding cytosol. Such a change induces cPLA2α translocation from the plasma membrane to the Golgi and Ca2+ mediated association with the Golgi membrane. The translocation of several units of cPLA2α induces positive membrane curvature that, after accumulation of wedge-like lysolipids, promotes membrane tubulation or vesiculation. In parallel, Ca2+ concentration increase at the luminal Golgi induces a conformational change in NUCB1 that enables its interaction with MMP2. Such conformational change uncovers negatively charged residues that could induce NUCB1 association to Golgi membranes and by an unknown intermediary, transport the NUCB1-MMP2 complex towards the rims or, by proximity, towards tubulations that will drive cargo to the next compartment.

Likewise, Ernst et al. (2018) showed that S-palmitoylation could also work as a biophysical switch to accumulate cargo at the rims of the *cis*-Golgi and promote its trafficking to the next compartment[60]. Interestingly, MT1-MMP is palmitoylated in its cytoplasmic tail and such

modification has been shown to be important for its recycling to endosomal compartments via clathrin-coated vesicles[290]. Therefore, we cannot rule out the possibility that its anterograde trafficking is mediated by a similar mechanism. Furthermore, given that MT1-MMP and MMP2 interact via TIMP2[220] it is also possible that MT1-MMP aids in the anterograde trafficking of MMP2 by promoting its accumulation at the Golgi rims and posterior transport to the medial compartment.
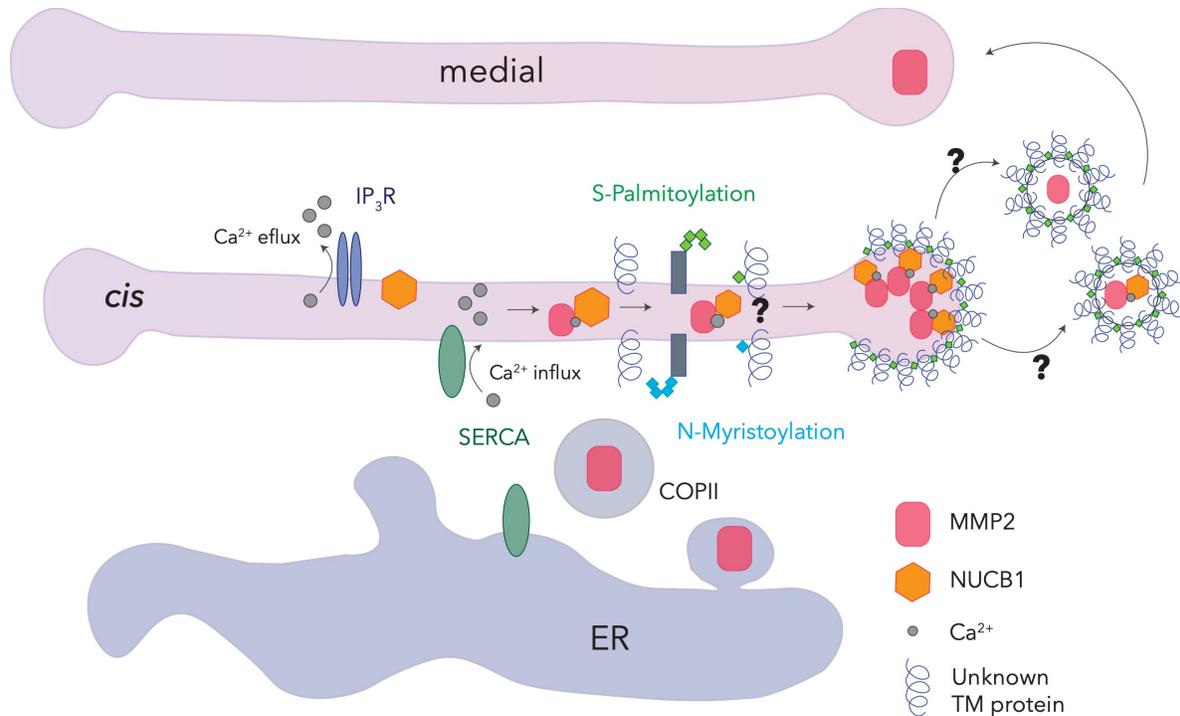
Figure 71. Model for N-myristoylation or S-palmitoylation-dependent MMP2 trafficking. MMP2 is transported from the ER to the *cis*-Golgi in COPII vesicles. Once it reaches the Golgi, Ca2+ concentration increases in the lumen and induces a conformational change in NUCB1 that enables its interaction with MMP2. Such conformational change promotes membrane association via interaction with either an unknown palmitoylated protein or an unknown myristoylated partner. The accumulation of S-palmitoylated proteins towards the Golgi rims induces accumulation NUCB1-MMP2 complexes and further vesicle-mediated transport to the medial-Golgi.

In conclusion, this work allowed to gain a better understanding on intracellular MMP trafficking by uncovering NUCB1 as a novel component of the intra-Golgi trafficking machinery for MMP2. Based on these results, we propose 2 models:

1. *Model for Ca2+-dependent NUCB1-mediated MMP2 trafficking:* MMP2 arrival from the ER to the *cis*-Golgi generates a transient increase in local Ca2+ that subsequently promotes Ca2+ efflux and a raise of Ca2+ concentration in the surrounding cytosol. This change induces cPLA2α translocation from the plasma membrane to the Golgi, where Ca2+ mediated membrane association occurs. The translocation of cPLA2α units to the Golgi induces positive membrane curvature and accumulation of wedge-like lysolipids that promote membrane tubulation or vesicle formation. In parallel, luminal Ca2+ concentration increase at the Golgi induces a conformational change in NUCB1 that enables its interaction with MMP2. Such conformational change uncovers negatively charged residues that could induce NUCB1 association to Golgi membranes and by an unknown intermediary, transport the NUCB1-MMP2 complex towards the rims or, by proximity, towards tubulations that will drive cargo to the next compartment (Figure 70).

2. *Model for S-palmitoylation-dependent MMP2-trafficking.* Increase in luminal Ca2+ due to cargo arrival at the *cis*-Golgi induces Ca2+-dependent NUCB1 binding with MMP2. The interaction generates a conformational change that uncovers potential protein interacting regions, promoting NUCB1-MMP2 binding to an unknown S-palmitoylated transmembrane protein and anchoring the complex to the Golgi membrane. This association accumulates NUCB1-MMP2 complex and other cargo to the Golgi rims. The accumulation of S-palmitoylated proteins at the rims acts as a biophysical switch that induces an increase in membrane curvature and leads eventually to vesicle budding and cargo export to the next compartment (Figure 71).

9. Outlook and future perspectives

The results of this thesis contributed to enlighten the mechanism of MMP2 intracellular trafficking by identifying NUCB1 as a critical player in MMP transport. Importantly, this work highlights the requirement of Ca2+ for proper trafficking, not just at the TGN, as has been documented, but also at the *cis*-Golgi. Although this is a big step towards the understanding of MMP intracellular trafficking, several questions remain unanswered.

Further investigation should address the specific interacting domains between NUCB1 and MMP2. Although I could prove the NUCB1-MMP2 interaction, additional exploration is required to identify the interacting regions between both proteins. Also, an evaluation of alternative Ca2+ regulators at the Golgi is required to determine if a compensation affect is taking place in the absence of NUCB1. A proper characterization of the Ca2+ dynamics would give a better insight in how is actually NUCB1 regulating Ca2+ concentrations at the Golgi lumen.

Importantly, further analysis should evaluate changes in tubulation or vesicle formation in NUCB1-KO cells. This would give some light into the participation of structural components of the Golgi in trafficking. Specifically, an evaluation of cPLA2α activity and localization in NUCB1-KO cells will allow to better understand the observed changes in trafficking dynamics.

Finally, NUCB1 interaction with palmitoylated proteins should be evaluated, in particular with MT1-MMP, in order to gain a better understanding of the retention mechanism of NUCB1 at the *cis*-Golgi lumen and a deeper insight into the regulation of intra-Golgi protein trafficking.

10.   References

1.   Alberts, B. *et al.* General Principles of Cell Communication. in *Molecular biology of the cell* (Garland Science, 2002).

2.   Wu, M., Massaeli, H., Durston, M. & Mesaeli, N. Differential expression and activity of matrix metalloproteinase-2 and -9 in the calreticulin deficient cells. *Matrix Biol.* **26**, 463–72 (2007).

3.   Nyathi, Y., Wilkinson, B. M. & Pool, M. R. Co-translational targeting and translocation of proteins to the endoplasmic reticulum. *Biochim. Biophys. Acta* **1833**, 2392–2402 (2013).

4.   Barlowe, C. K. & Miller, E. A. Secretory protein biogenesis and traffic in the early secretory pathway. *Genetics* **193**, 383–410 (2013).

5.   Walter, P., Ibrahimi, I. & Blobel, G. Translocation of proteins across the endoplasmic reticulum. I. Signal recognition protein (SRP) binds to in-vitro-assembled polysomes synthesizing secretory protein. *J. Cell Biol.* **91**, 545–550 (1981).

6.   Alberts, B., Johnson, A. & Lewis, J. The Compartmentalization of Cells. in *Molecular biology of the cell* (Garland Science, 2002).

7.   Lippincott-Schwartz, J., Roberts, T. H. & Hirschberg, K. Secretory Protein Trafficking and Organelle Dynamics in Living Cells. *Annu. Rev. Cell Dev. Biol.* **16**, 557–589 (2000).

8.   Guo, Y., Sirkis, D. W. & Schekman, R. Protein sorting at the trans-Golgi network. *Annu. Rev. Cell Dev. Biol.* **30**, 169–206 (2014).

9.   Kienzle, C. & von Blume, J. Secretory cargo sorting at the trans-Golgi network. *Trends Cell Biol.* **24**, 584–593 (2014).

10.   Barlowe, C. & Helenius, A. Cargo Capture and Bulk Flow in the Early Secretory Pathway. *Annu. Rev. Cell Dev. Biol.* **32**, 197–222 (2016).

11.   Hegde, R. S. & Bernstein, H. D. The surprising complexity of signal sequences. *Trends Biochem. Sci.* **31**, 563–571 (2006).

12.   Halic, M. *et al.* Structure of the signal recognition particle interacting with the elongation-arrested ribosome. *Nature* **427**, 808–814 (2004).

13. McCaughey, J. & Stephens, D. J. COPII-dependent ER export in animal cells: adaptation and control for diverse cargo. *Histochem. Cell Biol.* **150**, 119–131 (2018).

14. Walter, P. & Blobel, G. Purification of a membrane-associated protein complex required for protein translocation across the endoplasmic reticulum. *Proc. Natl. Acad. Sci. U. S. A.* **77**, 7112–7116 (1980).

15. Wild, K. *et al.* Reconstitution of the human SRP system and quantitative and systematic analysis of its ribosome interactions. *Nucleic Acids Res.* **47**, 3184–3196 (2019).

16. Aviram, N. & Schuldiner, M. Targeting and translocation of proteins to the endoplasmic reticulum at a glance. *J. Cell Sci.* **130**, 4079–4085 (2017).

17. Schwarz, D. S. & Blower, M. D. The endoplasmic reticulum: structure, function and response to cellular signaling. *Cell. Mol. Life Sci.* **73**, 79–94 (2016).

18. Wu, H., Carvalho, P. & Voeltz, G. K. Here, there, and everywhere: The importance of ER membrane contact sites. *Science (80-.).* **361**, (2018).

19. Phillips, M. J. & Voeltz, G. K. Structure and function of ER membrane contact sites with other organelles. *Nat. Rev. Mol. Cell Biol.* **17**, 69–82 (2016).

20. Johnson, S., Michalak, M., Opas, M. & Eggleton, P. The ins and outs of calreticulin: From the ER lumen to the extracellular space. *Trends Cell Biol.* **11**, 122–129 (2001).

21. Vorum, H., Hager, H., Christensen, B. M., Nielsen, S. & Honoré, B. Human calumenin localizes to the secretory pathway and is secreted to the medium. *Exp. Cell Res.* **248**, 473–81 (1999).

22. Honoré, B. The rapidly expanding CREC protein family: members, localization, function, and role in disease. *BioEssays* **31**, 262–277 (2009).

23. Chen, Y., Gershlick, D. C., Park, S. Y. & Bonifacino, J. S. Segregation in the Golgi complex precedes export of endolysosomal proteins in distinct transport carriers. *J. Cell Biol.* **216**, 4141–4151 (2017).

24. Hanna, M. G., Peotter, J. L., Frankel, E. B. & Audhya, A. Membrane Transport at an Organelle Interface in the Early Secretory Pathway: Take Your Coat Off and Stay a While: Evolution of the metazoan early secretory pathway. *BioEssays* **40**, 1–6 (2018).

25. Kurokawa, K., Okamoto, M. & Nakano, A. Contact of cis-Golgi with ER exit sites executes cargo capture and delivery from the ER. *Nat. Commun.* **5**, 1–7 (2014).

26. Nyfeler, B., Michnick, S. W. & Hauri, H.-P. Capturing protein interactions in the secretory pathway of living cells. *Proc. Natl. Acad. Sci. U. S. A.* **102**, 6350–6355 (2005).

27. Zheng, C., Liu, H.-H., Yuan, S., Zhou, J. & Zhang, B. Molecular basis of LMAN1 in coordinating LMAN1-MCFD2 cargo receptor formation and ER-to-Golgi transport of FV/FVIII. *Blood* **116**, 5698–5706 (2010).

28. Zheng, C., Liu, H., Zhou, J. & Zhang, B. EF-hand domains of MCFD2 mediate interactions with both LMAN1 and coagulation factor V or VIII. *Blood* **115**, 1081–1087 (2010).

29. Raote, I. & Malhotra, V. Protein transport by vesicles and tunnels. *J. Cell Biol.* **218**, 737–739 (2019).

30. Kuehn, M. J., Herrmann, J. M. & Schekman, R. COPII-cargo interactions direct protein sorting into ER-derived transport vesicles. *Nature* **391**, 187–90 (1998).

31. Campelo, F. & Malhotra, V. Membrane fission: the biogenesis of transport carriers. *Annu. Rev. Biochem.* **81**, 407–27 (2012).

32. Gomez-Navarro, N. & Miller, E. Protein sorting at the ER-Golgi interface. *J. Cell Biol.* **215**, 769–778 (2016).

33. Krijnse-Locker, J., Ericsson, M., Rottier, P. J. & Griffiths, G. Characterization of the budding compartment of mouse hepatitis virus: evidence that transport from the RER to the Golgi complex requires only one vesicular transport step. *J. Cell Biol.* **124**, 55–70 (1994).

34. Mellman, I. & Simons, K. The Golgi complex: in vitro veritas? *Cell* **68**, 829–840 (1992).

35. Saraste, J. & Marie, M. Intermediate compartment (IC): from pre-Golgi vacuoles to a semi-autonomous membrane system. *Histochem. Cell Biol.* **150**, 407–430 (2018).

36. Ward, T. H., Polishchuk, R. S., Caplan, S., Hirschberg, K. & Lippincott-Schwartz, J. Maintenance of Golgi structure and function depends on the integrity of ER export. *J. Cell Biol.* **155**, 557–570 (2001).

37.	Farhan, H. *et al.* Signal-dependent export of GABA transporter 1 from the ER-Golgi intermediate compartment is specified by a C-terminal motif. *J. Cell Sci.* **121**, 753–761 (2008).

38.	Ben-Tekaya, H., Kahn, R. A. & Hauri, H.-P. ADP ribosylation factors 1 and 4 and group VIA phospholipase A_2 regulate morphology and intraorganellar traffic in the endoplasmic reticulum-Golgi intermediate compartment. *Mol. Biol. Cell* **21**, 4130–40 (2010).

39.	Park, S. Y., Yang, J. S., Schmider, A. B., Soberman, R. J. & Hsu, V. W. Coordinated regulation of bidirectional COPI transport at the Golgi by CDC42. *Nature* **521**, 529–532 (2015).

40.	Heffernan, L. F. & Simpson, J. C. The trials and tubule-ations of Rab6 involvement in Golgi-to-ER retrograde transport. *Biochem. Soc. Trans.* **42**, 1453–1459 (2014).

41.	Golgi, C. On the structure of nerve cells. *J. Microsc.* **155**, 3–7 (1898).

42.	Farquhar, M. G. & Palade, G. E. The Golgi apparatus (complex)-(1954-1981)-from artifact to center stage. *J. Cell Biol.* **91**, 77s-103s (1981).

43.	Ladinsky, M. S., Mastronarde, D. N., McIntosh, J. R., Howell, K. E. & Staehelin, L. A. Golgi Structure in Three Dimensions: Functional Insights from the Normal Rat Kidney Cell . *J. Cell Biol.* **144**, 1135–1149 (1999).

44.	Klumperman, J. Architecture of the mammalian Golgi. *Cold Spring Harb. Perspect. Biol.* **3**, 1–19 (2011).

45.	Marsh, B. J. & Howell, K. E. The mammalian Golgi--complex debates. *Nat. Rev. Mol. Cell Biol.* **3**, 789–95 (2002).

46.	Pantazopoulou, A. & Glick, B. S. A kinetic view of membrane traffic pathways can transcend the classical view of Golgi compartments. *Front. Cell Dev. Biol.* **7**, 1–12 (2019).

47.	Glick, B. S. & Nakano, A. Membrane traffic within the Golgi apparatus. *Annu. Rev. Cell Dev. Biol.* **25**, 113–32 (2009).

48.	Beznoussenko, G. V *et al.* Transport of soluble proteins through the Golgi occurs by diffusion via continuities across cisternae. *Elife* **3**, e02009 (2014).

49. Lissandron, V., Podini, P., Pizzo, P. & Pozzan, T. Unique characteristics of Ca2+ homeostasis of the trans-Golgi compartment. *Proc. Natl. Acad. Sci. U. S. A.* **107**, 9198–203 (2010).

50. Mironov, A. A. & Beznoussenko, G. V. The kiss-and-run model of intra-Golgi transport. *Int. J. Mol. Sci.* **13**, 6800–6819 (2012).

51. Wong, A. K. C. *et al.* Heterogeneity of Ca2+ handling among and within Golgi compartments. *J. Mol. Cell Biol.* **5**, 266–276 (2013).

52. Aulestia, F. J., Alonso, M. T. & García-Sancho, J. Differential calcium handling by the cis and trans regions of the Golgi apparatus. *Biochem. J.* **466**, 455–65 (2015).

53. Glick, B. S. & Luini, A. Models for Golgi traffic: a critical assessment. *Cold Spring Harb. Perspect. Biol.* **3**, a005215 (2011).

54. Rizzo, R. *et al.* The dynamics of engineered resident proteins in the mammalian Golgi complex relies on cisternal maturation. *J. Cell Biol.* **201**, 1027–36 (2013).

55. Dancourt, J. *et al.* Small cargoes pass through synthetically glued Golgi stacks. *FEBS Lett.* **590**, 1675–86 (2016).

56. Dunlop, M. H. *et al.* Land-locked mammalian Golgi reveals cargo transport between stable cisternae. *Nat. Commun.* **8**, 432 (2017).

57. Pfeffer, S. R. How the Golgi works: a cisternal progenitor model. *Proc. Natl. Acad. Sci. U. S. A.* **107**, 19614–8 (2010).

58. Lavieu, G., Zheng, H. & Rothman, J. E. Stapled Golgi cisternae remain in place as cargo passes through the stack. *Elife* **2**, e00558 (2013).

59. San Pietro, E. *et al.* Group IV phospholipase A2α controls the formation of inter-cisternal continuities involved in intra-golgi transport. *PLoS Biol.* **7**, (2009).

60. Ernst, A. M. *et al.* S-Palmitoylation Sorts Membrane Cargo for Anterograde Transport in the Golgi. *Dev. Cell* **47**, 479-493.e7 (2018).

61. Kurokawa, K. *et al.* Visualization of secretory cargo transport within the Golgi apparatus. *J. Cell Biol.* **218**, 1602–1618 (2019).

62. Casler, J. C., Papanikou, E., Barrero, J. J. & Glick, B. S. Maturation-driven transport and

AP-1-dependent recycling of a secretory cargo in the Golgi. *J. Cell Biol.* **218**, 1582–1601 (2019).

63. Wei, J.-H. & Seemann, J. Unraveling the Golgi Ribbon. *Traffic* **11**, 1391–1400 (2010).

64. Ernst, A. M., Toomre, D. & Bogan, J. S. Acylation - A New Means to Control Traffic Through the Golgi. *Front. cell Dev. Biol.* **7**, 109 (2019).

65. Barinaga-Rementeria Ramirez, I. & Lowe, M. Golgins and GRASPs: Holding the Golgi together. *Semin. Cell Dev. Biol.* **20**, 770–779 (2009).

66. Rabouille, C. & Linstedt, A. D. GRASP: A Multitasking Tether . *Frontiers in Cell and Developmental Biology* **4**, 1 (2016).

67. Zhang, X. & Wang, Y. GRASPs in Golgi Structure and Function . *Frontiers in Cell and Developmental Biology* **3**, 84 (2016).

68. Jiang, H. *et al.* Protein Lipidation: Occurrence, Mechanisms, Biological Functions, and Enabling Technologies. *Chem. Rev.* **118**, 919–988 (2018).

69. Marra, P. *et al.* The GM130 and GRASP65 golgi proteins cycle through and define a subdomain of the intermediate compartment. *Nat. Cell Biol.* **3**, 1101–1113 (2001).

70. Heinrich, F. *et al.* Myristoylation restricts orientation of the GRASP domain on membranes and promotes membrane tethering. *J. Biol. Chem.* **289**, 9683–9691 (2014).

71. Moyer, B. D., Allan, B. B. & Balch, W. E. Rab1 interaction with a GM130 effector complex regulates COPII vesicle cis--Golgi tethering. *Traffic* **2**, 268–276 (2001).

72. Sinka, R., Gillingham, A. K., Kondylis, V. & Munro, S. Golgi coiled-coil proteins contain multiple binding sites for Rab family G proteins. *J. Cell Biol.* **183**, 607–615 (2008).

73. Ungermann, C. & Kümmel, D. Structure of membrane tethers and their role in fusion. *Traffic* **20**, 479–490 (2019).

74. Liu, S. & Storrie, B. How Rab proteins determine Golgi structure. *Int. Rev. Cell Mol. Biol.* **315**, 1–22 (2015).

75. Pfeffer, S. R. Rab GTPases: master regulators that establish the secretory and endocytic pathways. *Mol. Biol. Cell* **28**, 712–715 (2017).

76. Zerial, M. & McBride, H. Rab proteins as membrane organizers. *Nat. Rev. Mol. Cell Biol.* **2**, 107–117 (2001).

77. Gillingham, A. K. & Munro, S. Finding the Golgi: Golgin Coiled-Coil Proteins Show the Way. *Trends Cell Biol.* **26**, 399–408 (2016).

78. Cheung, P. P. & Pfeffer, S. R. Transport Vesicle Tethering at the Trans Golgi Network: Coiled Coil Proteins in Action . *Frontiers in Cell and Developmental Biology* **4**, 18 (2016).

79. Muschalik, N. & Munro, S. Golgins. *Curr. Biol.* **28**, R374–R376 (2018).

80. Rathore, S. S., Ghosh, N., Ouyang, Y. & Shen, J. Topological arrangement of the intracellular membrane fusion machinery. *Mol. Biol. Cell* **22**, 2612–2619 (2011).

81. Lou, X. & Shin, Y. K. SNARE zippering. *Biosci. Rep.* **36**, 1–7 (2016).

82. Park, Y. & Ryu, J. K. Models of synaptotagmin-1 to trigger Ca2+-dependent vesicle fusion. *FEBS Lett.* **592**, 3480–3492 (2018).

83. Micaroni, M. *et al.* Synchronous intra-Golgi transport induces the release of Ca2+ from the Golgi apparatus. *Exp. Cell Res.* **316**, 2071–86 (2010).

84. Hu, K. *et al.* Vesicular restriction of synaptobrevin suggests a role for calcium in membrane fusion. *Nature* **415**, 646–650 (2002).

85. Micaroni, M. *Calcium Signaling. Advances in experimental medicine and biology* **740**, (Springer Netherlands, 2012).

86. Carafoli, E. & Krebs, J. Why calcium? How calcium became the best communicator. *J. Biol. Chem.* **291**, 20849–20857 (2016).

87. Morel-Huaux, V. M. *et al.* The calcium-binding protein p54/NEFA is a novel luminal resident of medial Golgi cisternae that traffics independently of mannosidase II. *Eur. J. Cell Biol.* **81**, 87–100 (2002).

88. Aradhyam, G. K., Balivada, L. M., Kanuru, M., Vadivel, P. & Vidhya, B. S. Calnuc: Emerging roles in calcium signaling and human diseases. *IUBMB Life* **62**, 436–446 (2010).

89. Pizzo, P., Lissandron, V. & Pozzan, T. The trans-golgi compartment: A new distinct intracellular Ca store. *Commun. Integr. Biol.* **3**, 462–4 (2010).

90.   Micaroni, M., Perinetti, G., Berrie, C. P. & Mironov, A. A. The SPCA1 Ca2+ Pump and Intracellular Membrane Trafficking. *Traffic* **11**, 1315–1333 (2010).

91.   Jarvis, S. E. & Zamponi, G. W. Interactions between presynaptic Ca2+ channels, cytoplasmic messengers and proteins of the synaptic vesicle release complex. *Trends Pharmacol. Sci.* **22**, 519–25 (2001).

92.   Yang, J., Zhao, Z., Gu, M., Feng, X. & Xu, H. Release and uptake mechanisms of vesicular Ca 2+ stores. *Protein Cell* **10**, 8–19 (2019).

93.   von Blume, J. *et al.* ADF/cofilin regulates secretory cargo sorting at the TGN via the Ca2+ ATPase SPCA1. *Dev. Cell* **20**, 652–62 (2011).

94.   Kienzle, C. *et al.* Cofilin recruits F-actin to SPCA1 and promotes Ca2+-mediated secretory cargo sorting. *J. Cell Biol.* **206**, 635–54 (2014).

95.   Crevenna, A. H. *et al.* Secretory cargo sorting by Ca2+-dependent Cab45 oligomerization at the trans-Golgi network. *J. Cell Biol.* **213**, 305–14 (2016).

96.   Deng, Y. *et al.* Activity of the SPCA1 Calcium Pump Couples Sphingomyelin Synthesis to Sorting of Secretory Proteins in the Trans-Golgi Network. *Dev. Cell* **47**, 464-478.e8 (2018).

97.   Micaroni, M. Calcium around the Golgi apparatus: implications for intracellular membrane trafficking. *Adv. Exp. Med. Biol.* **740**, 439–460 (2012).

98.   Van Baelen, K. *et al.* The Ca2+/Mn2+ pumps in the Golgi apparatus. *Biochim. Biophys. Acta - Mol. Cell Res.* **1742**, 103–112 (2004).

99.   Porat, A. & Elazar, Z. Regulation of intra-Golgi membrane transport by calcium. *J. Biol. Chem.* **275**, 29233–7 (2000).

100. Vanoevelen, J. *et al.* Inositol trisphosphate producing agonists do not mobilize the thapsigargin-insensitive part of the endoplasmic-reticulum and Golgi Ca2+ store. *Cell Calcium* **35**, 115–21 (2004).

101. Vanoevelen, J. *et al.* Cytosolic Ca2+ signals depending on the functional state of the Golgi in HeLa cells. *Cell Calcium* **38**, 489–95 (2005).

102. Leclerc, P. *et al.* Nucleobindin co-localizes and associates with cyclooxygenase (COX)-2

in human neutrophils. *PLoS One* **3**, (2008).

103. Scherer, P. E. *et al.* Cab45, a novel (Ca2+)-binding protein localized to the Golgi lumen. *J. Cell Biol.* **133**, 257–68 (1996).

104. Lin, P. *et al.* The mammalian calcium-binding protein, nucleobindin (CALNUC), is a Golgi resident protein. *J. Cell Biol.* **141**, 1515–27 (1998).

105. Nesselhut, J. *et al.* Golgi retention of human protein NEFA is mediated by its N-terminal Leu/Ile-rich region. *FEBS Lett.* **509**, 469–475 (2001).

106. Lavoie, C., Meerloo, T., Lin, P. & Farquhar, M. G. Calnuc, an EF-hand Ca(2+)-binding protein, is stored and processed in the Golgi and secreted by the constitutive-like pathway in AtT20 cells. *Mol. Endocrinol.* **16**, 2462–74 (2002).

107. von Blume, J. *et al.* Cab45 is required for Ca(2+)-dependent secretory cargo sorting at the trans-Golgi network. *J. Cell Biol.* **199**, 1057–66 (2012).

108. De Alba, E. & Tjandra, N. Structural studies on the Ca2+-binding domain of human nucleobindin (calnuc). *Biochemistry* **43**, 10039–10049 (2004).

109. Busch, E., Hohenester, E., Timpl, R., Paulsson, M. & Maurer, P. Calcium affinity, cooperativity, and domain interactions of extracellular EF-hands present in BM-40. *J. Biol. Chem.* **275**, 25508–15 (2000).

110. Kawasaki, H. & Kretsinger, R. H. Structural and functional diversity of EF-hand proteins: Evolutionary perspectives. *Protein Sci.* **26**, 1898–1920 (2017).

111. Honoré, B. & Vorum, H. The CREC family, a novel family of multiple EF-hand, low-affinity Ca(2+)-binding proteins localised to the secretory pathway of mammalian cells. *FEBS Lett.* **466**, 11–8 (2000).

112. Lin, P., Yao, Y., Hofmeister, R., Tsien, R. Y. & Farquhar, M. G. Overexpression of CALNUC (nucleobindin) increases agonist and thapsigargin releasable Ca2+ storage in the Golgi. *J. Cell Biol.* **145**, 279–89 (1999).

113. Kapoor, N. *et al.* Nucleobindin 1 is a calcium-regulated guanine nucleotide dissociation inhibitor of G{alpha}i1. *J. Biol. Chem.* **285**, 31647–60 (2010).

114. Weiss, T. S. *et al.* G i3 binding to calnuc on Golgi membranes in living cells monitored

by fluorescence resonance energy transfer of green fluorescent protein fusion proteins. *Proc. Natl. Acad. Sci.* **98**, 14961–14966 (2002).

115. Lin, P., Fischer, T., Lavoie, C., Huang, H. & Farquhar, M. G. Calnuc plays a role in dynamic distribution of Gαi but not Gβ subunits and modulates ACTH secretion in AtT-20 neuroendocrine secretory cells. *Mol. Neurodegener.* **4**, 1–16 (2009).

116. Kanuru, M., Samuel, J. J., Balivada, L. M. & Aradhyam, G. K. Ion-binding properties of Calnuc, Ca2+ versus Mg2+--Calnuc adopts additional and unusual Ca2+-binding sites upon interaction with G-protein. *FEBS J.* **276**, 2529–46 (2009).

117. Garcia-Marcos, M., Kietrsunthorn, P. S., Wang, H., Ghosh, P. & Farquhar, M. G. G Protein binding sites on Calnuc (nucleobindin 1) and NUCB2 (nucleobindin 2) define a new class of G(alpha)i-regulatory motifs. *J. Biol. Chem.* **286**, 28138–49 (2011).

118. Lin, P. *et al.* Calnuc binds to Alzheimer's β-amyloid precursor protein and affects its biogenesis. *J. Neurochem.* **100**, 1505–1514 (2007).

119. Bonito-Oliva, A., Barbash, S., Sakmar, T. P. & Graham, W. V. Nucleobindin 1 binds to multiple types of pre-fibrillar amyloid and inhibits fibrillization. *Sci. Rep.* **7**, 42880 (2017).

120. Brodeur, J. *et al.* Calnuc binds to LRP9 and affects its endosomal sorting. *Traffic* **10**, 1098–114 (2009).

121. Larkin, H., Costantino, S., Seaman, M. N. J. & Lavoie, C. Calnuc Function in Endosomal Sorting of Lysosomal Receptors. *Traffic* **17**, 416–32 (2016).

122. Barnikol-Watanabe, S. *et al.* Human Protein NEFA, a Novel DNA Binding / EF-Hand / Leucine Zipper Protein. Molecular Cloning and Sequence Analysis of the cDNA, Isolation and Characterization of the Protein. *Biol. Chem. Hoppe. Seyler.* **375**, 497–512 (1994).

123. Kroll, K. A. *et al.* Heterologous overexpression of human NEFA and studies on the two EF-hand calcium-binding sites. *Biochem. Biophys. Res. Commun.* **260**, 1–8 (1999).

124. Ward, K. E., Ropa, J. P., Adu-Gyamfi, E. & Stahelin, R. V. C2 domain membrane penetration by group IVA cytosolic phospholipase A 2 induces membrane curvature changes. *J. Lipid Res.* **53**, 2656–2666 (2012).

125. de Figueiredo, P., Drecktrah, D., Katzenellenbogen, J. A., Strang, M. & Brown, W. J.

Evidence that phospholipase A2 activity is required for Golgi complex and trans Golgi network membrane tubulation. *Proc. Natl. Acad. Sci. U. S. A.* **95**, 8642–7 (1998).

126.   Park, S. Y. *et al.* The late stage of COPI vesicle fission requires shorter forms of phosphatidic acid and diacylglycerol. *Nat. Commun.* **10**, 1–14 (2019).

127.   Bonnans, C., Chou, J. & Werb, Z. Remodelling the extracellular matrix in development and disease. *Nat. Rev. Mol. Cell Biol.* **15**, 786–801 (2014).

128.   Theocharis, A. D., Manou, D. & Karamanos, N. K. The extracellular matrix as a multitasking player in disease. *FEBS J.* **286**, 2830–2869 (2019).

129.   Ford, A. J. & Rajagopalan, P. Extracellular matrix remodeling in 3D: implications in tissue homeostasis and disease progression. *Wiley Interdiscip. Rev. Nanomedicine Nanobiotechnology* **10**, (2018).

130.   Sorokin, L. The impact of the extracellular matrix on inflammation. *Nat. Rev. Immunol.* **10**, 712–23 (2010).

131.   Bhattacharjee, O., Ayyangar, U., Kurbet, A. S., Ashok, D. & Raghavan, S. Unraveling the ECM-immune cell crosstalk in skin diseases. *Front. Cell Dev. Biol.* **7**, 1–24 (2019).

132.   Mouw, J. K., Ou, G. & Weaver, V. M. Extracellular matrix assembly: A multiscale deconstruction. *Nat. Rev. Mol. Cell Biol.* **15**, 771–785 (2014).

133.   Clementz, A. G. & Harris, A. Collagen XV: Exploring Its Structure and Role within the Tumor Microenvironment. *Mol. Cancer Res.* **11**, 1481 LP – 1486 (2013).

134.   Muiznieks, L. D., Sharpe, S., Pomès, R. & Keeley, F. W. Role of Liquid–Liquid Phase Separation in Assembly of Elastin and Other Extracellular Matrix Proteins. *Journal of Molecular Biology* (2018). doi:10.1016/j.jmb.2018.06.010

135.   Pozzi, A., Yurchenco, P. D. & Iozzo, R. V. The nature and biology of basement membranes. *Matrix Biol.* **57–58**, 1–11 (2017).

136.   Sivaraman, K. & Shanthi, C. Matrikines for therapeutic and biomedical applications. *Life Sciences* (2018). doi:10.1016/j.lfs.2018.10.056

137.   Eble, J. A. & Niland, S. The extracellular matrix in tumor progression and metastasis. *Clin. Exp. Metastasis* **36**, 171–198 (2019).

138. Lindahl, U., Couchman, J., Kimata, K. & Esko, J. D. Proteoglycans and Sulfated Glycosaminoglycans. in *Essentials of Glycobiology* (eds. Varki, A., Cummings, R., Esko, J. & et. al) (Cold Spring Harbor (NY): Cold Spring Harbor Laboratory Press, 2017).

139. Multhaupt, H. A. B., Leitinger, B., Gullberg, D. & Couchman, J. R. Extracellular matrix component signaling in cancer. *Adv. Drug Deliv. Rev.* **97**, 28–40 (2016).

140. Theocharis, A. D., Skandalis, S. S., Gialeli, C. & Karamanos, N. K. Extracellular matrix structure. *Adv. Drug Deliv. Rev.* **97**, 4–27 (2016).

141. McEver, R. P. & Luscinskas, F. W. Cell Adhesion. in *Hematology* 127–134 (Elsevier, 2018). doi:10.1016/B978-0-323-35762-3.00012-3

142. Alberts, B., Johnson, A., Lewis, J. & Al., E. The Extracellular Matrix of Animals. in *Molecular Biology of the Cell* (Garland Science, 2002).

143. Kechagia, J. Z., Ivaska, J. & Roca-Cusachs, P. Integrins as biomechanical sensors of the microenvironment. *Nat. Rev. Mol. Cell Biol.* (2019). doi:10.1038/s41580-019-0134-2

144. Alberts, B., Johnson, A., Lewis, J. & Al., E. Integrins. in *Molecular Biology of the Cell* (Garland Science, 2002).

145. Moreno-Layseca, P., Icha, J., Hamidi, H. & Ivaska, J. Integrin trafficking in cells and tissues. *Nat. Cell Biol.* **21**, 122–132 (2019).

146. McEver, R. P. & Luscinskas, F. W. Chapter 12 – Cell Adhesion. in *Hematology* 127–134 (2018). doi:10.1016/B978-0-323-35762-3.00012-3

147. Deryugina, E. I. *et al.* Prointegrin maturation follows rapid trafficking and processing of MT1-MMP in Furin-Negative Colon Carcinoma LoVo Cells. *Traffic* **5**, 627–41 (2004).

148. Wickström, S. A. & Fässler, R. Regulation of membrane traffic by integrin signaling. *Trends Cell Biol.* **21**, 266–73 (2011).

149. Itoh, Y. Discoidin domain receptors: Microenvironment sensors that promote cellular migration and invasion. *Cell Adh. Migr.* **12**, 378–385 (2018).

150. Saby, C. *et al.* DDR1 and MT1-MMP Expression Levels Are Determinant for Triggering BIK-Mediated Apoptosis by 3D Type I Collagen Matrix in Invasive Basal-Like Breast Carcinoma Cells . *Frontiers in Pharmacology* **10**, 462 (2019).

151. Hou, G., Vogel, W. F. & Bendeck, M. P. Tyrosine Kinase Activity of Discoidin Domain Receptor 1 Is Necessary for Smooth Muscle Cell Migration and Matrix Metalloproteinase Expression. *Circ. Res.* **90**, 1147–1149 (2002).

152. Reger de Moura, C. *et al.* Discoidin domain receptors: A promising target in melanoma. *Pigment Cell Melanoma Res.* pcmr.12809 (2019). doi:10.1111/pcmr.12809

153. Hascall, V. & Esko, J. Hyaluronan. in *Essentials of Glycobiology [Internet]* (ed. Varki A, Cummings RD, Esko JD, et al.) (Cold Spring Harbor (NY): Cold Spring Harbor Laboratory Press, 2017). doi:10.1101/glycobiology.3e.016

154. Fallacara, A., Baldini, E., Manfredini, S. & Vertuani, S. Hyaluronic Acid in the Third Millennium. *Polymers (Basel).* **10**, 701 (2018).

155. Bono, P., Rubin, K., Higgins, J. M. G. & Hynes, R. O. Layilin, a Novel Integral Membrane Protein, Is a Hyaluronan Receptor. *Mol. Biol. Cell* **12**, 891–900 (2001).

156. Pan, J.-H. *et al.* LAYN Is a Prognostic Biomarker and Correlated With Immune Infiltrates in Gastric and Colon Cancers. *Front. Immunol.* **10**, 6 (2019).

157. Kim, Y. *et al.* Layilin is critical for mediating hyaluronan 35kDa-induced intestinal epithelial tight junction protein ZO-1 in vitro and in vivo. *Matrix Biol.* **66**, 93–109 (2018).

158. Linder, S. & Wiesner, C. Feel the force: Podosomes in mechanosensing. *Exp. Cell Res.* **343**, 67–72 (2016).

159. Mahankali, M., Peng, H.-J., Cox, D. & Gomez-Cambronero, J. The mechanism of cell membrane ruffling relies on a phospholipase D2 (PLD2), Grb2 and Rac2 association. *Cell. Signal.* **23**, 1291–1298 (2011).

160. Apte, S. S. & Parks, W. C. Metalloproteinases: A parade of functions in matrix biology and an outlook for the future. *Matrix Biol.* **44–46**, 1–6 (2015).

161. Parsons, J. T., Horwitz, A. R. & Schwartz, M. A. Cell adhesion: Integrating cytoskeletal dynamics and cellular tension. *Nat. Rev. Mol. Cell Biol.* **11**, 633–643 (2010).

162. Block, M. R. *et al. Podosome-type adhesions and focal adhesions, so alike yet so different. European Journal of Cell Biology* **87**, 491–506 (Urban & Fischer, 2008).

163. Peláez, R., Pariente, A., Pérez-Sala, Á. & Larrayoz, I. M. Integrins: Moonlighting proteins in invadosome formation. *Cancers (Basel).* **11**, (2019).

164. Sun, Z., Guo, S. S. & Fässler, R. Integrin-mediated mechanotransduction. *J. Cell Biol.* **215**, 445–456 (2016).

165. Linder, S. & Wiesner, C. Tools of the trade: podosomes as multipurpose organelles of monocytic cells. *Cell. Mol. Life Sci.* **72**, 121–35 (2015).

166. Aguilar-Cuenca, R., Juanes-García, A. & Vicente-Manzanares, M. Myosin II in mechanotransduction: master and commander of cell migration, morphogenesis, and cancer. *Cell. Mol. Life Sci.* **71**, 479–492 (2014).

167. Khokha, R., Murthy, A. & Weiss, A. Metalloproteinases and their natural inhibitors in inflammation and immunity. *Nat. Rev. Immunol.* **13**, 649–65 (2013).

168. Bond, J. S. Proteases: History, discovery, and roles in health and disease. *J. Biol. Chem.* **294**, 1643–1651 (2019).

169. Russell, D. L., Brown, H. M. & Dunning, K. R. ADAMTS proteases in fertility. *Matrix Biol.* **44–46**, 54–63 (2015).

170. Gomis-Rüth, F. X., Trillo-Muyo, S. & Stöcker, W. Functional and structural insights into astacin metallopeptidases. *Biol. Chem.* **393**, 1027–41 (2012).

171. Sterchi, E. E., Stöcker, W. & Bond, J. S. Meprins, membrane-bound and secreted astacin metalloproteinases. *Mol. Aspects Med.* **29**, 309–328 (2008).

172. Becker-Pauly, C. & Rose-John, S. Meprin and ADAM Metalloproteases: Two Sides of the Same Coin? in *Matrix Metalloproteinase Biology* (eds. Sagi, I. & Gaffney, J. P.) 115–130 (John Wiley & Sons, Inc., 2015).

173. Vadon-Le Goff, S., Hulmes, D. J. S. & Moali, C. BMP-1/tolloid-like proteinases synchronize matrix assembly with growth factor activation to promote morphogenesis and tissue remodeling. *Matrix Biol.* **44–46**, 14–23 (2015).

174. Troilo, H. *et al.* Mammalian tolloid proteinases: role in growth factor signalling. *FEBS Lett.* **590**, 2398–2407 (2016).

175. Murphy, G. The ADAMs: signalling scissors in the tumour microenvironment. *Nat. Rev.*

Cancer **8**, 932 (2008).

176. Dubail, J. & Apte, S. S. Insights on ADAMTS proteases and ADAMTS-like proteins from mammalian genetics. *Matrix Biology* (2015). doi:10.1016/j.matbio.2015.03.001

177. Takeda, S. ADAM and ADAMTS Family Proteins and Snake Venom Metalloproteinases: A Structural Overview. *Toxins* **8**, (2016).

178. Stanton, H., Melrose, J., Little, C. B. & Fosang, A. J. Proteoglycan degradation by the ADAMTS family of proteinases. *Biochimica et Biophysica Acta - Molecular Basis of Disease* (2011). doi:10.1016/j.bbadis.2011.08.009

179. Yang, C. Y., Chanalaris, A. & Troeberg, L. ADAMTS and ADAM metalloproteinases in osteoarthritis – looking beyond the 'usual suspects'. *Osteoarthr. Cartil.* **25**, 1000–1009 (2017).

180. Mead, T. J. & Apte, S. S. ADAMTS proteins in human disorders. *Matrix Biol.* **71–72**, 225–239 (2018).

181. McCulloch, D. R. *et al.* ADAMTS metalloproteases generate active versican fragments that regulate interdigital web regression. *Dev. Cell* **17**, 687–98 (2009).

182. Alaseem, A. *et al.* Matrix Metalloproteinases: A challenging paradigm of cancer management. *Semin. Cancer Biol.* **56**, 100–115 (2017).

183. Gross, J. & Lapiere, C. M. Collagenolytic activity in amphibian tissues: a tissue culture assay. *Proc. Natl. Acad. Sci. U. S. A.* **48**, 1014–1022 (1962).

184. Dufour, A. & Overall, C. M. Missing the target: matrix metalloproteinase antitargets in inflammation and cancer. *Trends Pharmacol. Sci.* **34**, 233–42 (2013).

185. Kessenbrock, K., Plaks, V. & Werb, Z. Matrix metalloproteinases: regulators of the tumor microenvironment. *Cell* **141**, 52–67 (2010).

186. Cui, N., Hu, M. & Khalil, R. A. Biochemical and Biological Attributes of Matrix Metalloproteinases. *Prog. Mol. Biol. Transl. Sci.* **147**, 1–73 (2017).

187. Stawikowski, M. J. & Fields, G. B. Matrix Metalloproteinases: From Structure to Function. in *Matrix Metalloproteinase Biology* (eds. Sagi, I. & Gaffney, J. P.) 1–16 (John Wiley & Sons, Inc., 2015).

188. Tallant, C., Marrero, A. & Gomis-Rüth, F. X. Matrix metalloproteinases: fold and function of their catalytic domains. *Biochim. Biophys. Acta* **1803**, 20–8 (2010).

189. Murphy, G. & Nagase, H. Progress in matrix metalloproteinase research. *Mol. Aspects Med.* **29**, 290–308 (2008).

190. Parks, W. C., Wilson, C. L. & López-Boado, Y. S. Matrix metalloproteinases as modulators of inflammation and innate immunity. *Nat. Rev. Immunol.* **4**, 617–29 (2004).

191. Brew, K., Dinakarpandian, D. & Nagase, H. Tissue inhibitors of metalloproteinases: evolution, structure and function. *Biochim. Acta* **1477**, 267–283 (2000).

192. Morgunova, E., Tuuttila, A., Bergmann, U. & Tryggvason, K. Structural insight into the complex formation of latent matrix metalloproteinase 2 with tissue inhibitor of metalloproteinase 2. *Proc. Natl. Acad. Sci. U. S. A.* **99**, 7414–9 (2002).

193. Berg, G., Barchuk, M. & Miksztowicz, V. Behavior of Metalloproteinases in Adipose Tissue, Liver and Arterial Wall: An Update of Extracellular Matrix Remodeling. *Cells* **8**, 158 (2019).

194. Vandooren, J., Van den Steen, P. E. & Opdenakker, G. Biochemistry and molecular biology of gelatinase B or matrix metalloproteinase-9 (MMP-9): the next decade. *Crit. Rev. Biochem. Mol. Biol.* **48**, 222–72 (2013).

195. Itoh, Y. Membrane-type matrix metalloproteinases: Their functions and regulations. *Matrix Biol.* **44–46**, 207–23 (2015).

196. Weaver, S. a *et al.* Basal localization of MT1-MMP is essential for epithelial cell morphogenesis in 3D collagen matrix. *J. Cell Sci.* **44**, 1203–1213 (2014).

197. Woskowicz, A. M., Weaver, S. A., Shitomi, Y., Ito, N. & Itoh, Y. MT-LOOP-dependent Localization of Membrane Type I Matrix Metalloproteinase (MT1-MMP) to the Cell Adhesion Complexes Promotes Cancer Cell Invasion. *J. Biol. Chem.* **288**, 35126–35137 (2013).

198. Jobin, P. G., Butler, G. S. & Overall, C. M. New intracellular activities of matrix metalloproteinases shine in the moonlight. *Biochim. Biophys. acta. Mol. cell Res.* **1864**, 2043–2055 (2017).

199. Fanjul-Fernández, M., Folgueras, A. R., Cabrera, S. & López-Otín, C. Matrix

metalloproteinases: Evolution, gene regulation and functional analysis in mouse models. *Biochim. Biophys. Acta - Mol. Cell Res.* **1803**, 3–19 (2010).

200. Fields, G. B. Interstitial collagen catabolism. *J. Biol. Chem.* **288**, 8785–93 (2013).

201. Rodríguez, D., Morrison, C. J. & Overall, C. M. Matrix metalloproteinases: What do they not do? New substrates and biological roles identified by murine models and proteomics. *Biochim. Biophys. Acta - Mol. Cell Res.* **1803**, 39–54 (2010).

202. Tomlinson, M. L., Garcia-Morales, C., Abu-Elmagd, M. & Wheeler, G. N. Three matrix metalloproteinases are required in vivo for macrophage migration during embryonic development. *Mech. Dev.* **125**, 1059–1070 (2008).

203. Ogata, Y., Enghild, J. J. & Nagase, H. Matrix metalloproteinase 3 (stromelysin) activates the precursor for the human matrix metalloproteinase 9. *J. Biol. Chem.* **267**, 3581–4 (1992).

204. Zhang, X. *et al.* Insights into the distinct roles of MMP-11 in tumor biology and future therapeutics (Review). *Int. J. Oncol.* **48**, 1783–93 (2016).

205. von Bredow, D. C., Cress, A. E., Howard, E. W., Bowden, G. T. & Nagle, R. B. Activation of gelatinase-tissue-inhibitors-of-metalloproteinase complexes by matrilysin. *Biochem. J.* **331**, 965–972 (1998).

206. Winer, A., Adams, S. & Mignatti, P. Matrix Metalloproteinase Inhibitors in Cancer Therapy: Turning Past Failures Into Future Successes. *Mol. Cancer Ther.* **17**, 1147–1155 (2018).

207. Marchant, D. J. *et al.* A new transcriptional role for matrix metalloproteinase-12 in antiviral immunity. *Nat. Med.* **20**, 493–502 (2014).

208. Min, D., Moore, A. G., Bain, M. a, Breit, S. N. & Lyons, J. G. Activation of macrophage promatrix metalloproteinase-9 by lipopolysaccharide-associated proteinases. *J. Immunol.* **168**, 2449–55 (2002).

209. Gong, Y., Hart, E., Shchurin, A. & Hoover-Plow, J. Inflammatory macrophage migration requires MMP-9 activation by plasminogen in mice. *J. Clin. Invest.* **118**, 3012–24 (2008).

210. Song, J. *et al.* Focal MMP-2 and MMP-9 activity at the blood-brain barrier promotes

chemokine-induced leukocyte migration. *Cell Rep.* **10**, 1040–1054 (2015).

211. Fingleton, B. Matrix metalloproteinases as regulators of inflammatory processes. *Biochim. Biophys. Acta - Mol. Cell Res.* **1864**, 2036–2042 (2017).

212. Jacob, A. *et al.* Rab40b regulates trafficking of MMP2 and MMP9 during invadopodia formation and invasion of breast cancer cells. *J. Cell Sci.* **126**, 4647–58 (2013).

213. Shaverdashvili, K. *et al.* MT1-MMP modulates melanoma cell dissemination and metastasis through activation of MMP2 and RAC1. *Pigment Cell Melanoma Res.* **27**, 287–96 (2014).

214. Henriet, P. & Emonard, H. Matrix metalloproteinase-2: Not (just) a 'hero' of the past. *Biochimie* **166**, 223–232 (2019).

215. Hannocks, M.-J. *et al.* The gelatinases, MMP-2 and MMP-9, as fine tuners of neuroinflammatory processes. *Matrix Biol.* **75–76**, 102–113 (2019).

216. Jacob, A., Linklater, E., Bayless, B. A., Lyons, T. & Prekeris, R. The role and regulation of Rab40b-Tks5 complex during invadopodia formation and cancer cell invasion. *J. Cell Sci.* **129**, 4341–4353 (2016).

217. Packard, B. Z., Artym, V. V, Komoriya, A. & Yamada, K. M. Direct visualization of protease activity on cells migrating in three-dimensions. *Matrix Biol.* **28**, 3–10 (2009).

218. Matsumura, S. *et al.* Targeted deletion or pharmacological inhibition of MMP-2 prevents cardiac rupture after myocardial infarction in mice. *J. Clin. Invest.* **115**, 599–609 (2005).

219. Reel, B., Sala-Newby, G. B., Huang, W.-C. & Newby, A. C. Diverse patterns of cyclooxygenase-independent metalloproteinase gene regulation in human monocytes. *Br. J. Pharmacol.* **163**, 1679–90 (2011).

220. Fernandez-Catalan, C. *et al.* Crystal structure of the complex formed by the membrane type 1-matrix metalloproteinase with the tissue inhibitor of metalloproteinases-2, the soluble progelatinase A receptor. *EMBO J.* **17**, 5238–48 (1998).

221. Hernandez-Barrantes, S. *et al.* Binding of active (57 kDa) membrane type 1-matrix metalloproteinase (MT1-MMP) to tissue inhibitor of metalloproteinase (TIMP)-2 regulates MT1-MMP processing and pro-MMP-2 activation. *J. Biol. Chem.* **275**, 12080–12089 (2000).

222. Pendas, A. M. *et al.* Identification and characterization of a novel human matrix metalloproteinase with unique structural characteristics, chromosomal location, and tissue distribution. *J. Biol. Chem.* **272**, 4281–4286 (1997).

223. Stracke, J. O. *et al.* Biochemical characterization of the catalytic domain of human matrix metalloproteinase 19. Evidence for a role as a potent basement membrane degrading enzyme. *J. Biol. Chem.* **275**, 14809–14816 (2000).

224. Takino, T., Tsuge, H., Ozawa, T. & Sato, H. MT1-MMP promotes cell growth and ERK activation through c-Src and paxillin in three-dimensional collagen matrix. *Biochem. Biophys. Res. Commun.* **396**, 1042–7 (2010).

225. Poincloux, R., Lizárraga, F. & Chavrier, P. Matrix invasion by tumour cells: a focus on MT1-MMP trafficking to invadopodia. *J. Cell Sci.* **122**, 3015–24 (2009).

226. Linder, S. & Scita, G. RABGTPases in MT1-MMP trafficking and cell invasion: Physiology versus pathology. *Small GTPases* **6**, 145–52 (2015).

227. Endo, K. *et al.* Cleavage of syndecan-1 by membrane type matrix metalloproteinase-1 stimulates cell migration. *J. Biol. Chem.* **278**, 40764–70 (2003).

228. Frittoli, E., Palamidessi, A., Disanza, A. & Scita, G. Secretory and endo/exocytic trafficking in invadopodia formation: the MT1-MMP paradigm. *Eur. J. Cell Biol.* **90**, 108–14 (2011).

229. Monteiro, P. *et al.* Endosomal WASH and exocyst complexes control exocytosis of MT1-MMP at invadopodia. *J. Cell Biol.* **203**, 1063–79 (2013).

230. Vandooren, J., Geurts, N., Martens, E., Van den Steen, P. E. & Opdenakker, G. Zymography methods for visualizing hydrolytic enzymes. *Nat. Methods* **10**, 211–20 (2013).

231. Morrison, C. J., Butler, G. S., Rodríguez, D. & Overall, C. M. Matrix metalloproteinase proteomics: substrates, targets, and therapy. *Curr. Opin. Cell Biol.* **21**, 645–653 (2009).

232. Ridley, A. J. *et al.* Cell Migration: Integrating Signals from Front to Back. *Science (80-.).* **302**, 1704–1709 (2003).

233. Linder, S. The matrix corroded: podosomes and invadopodia in extracellular matrix degradation. *Trends Cell Biol.* **17**, 107–117 (2007).

234. Wiesner, C., Le-Cabec, V., El Azzouzi, K., Maridonneau-Parini, I. & Linder, S. Podosomes in space: macrophage migration and matrix degradation in 2D and 3D settings. *Cell Adh. Migr.* **8**, 179–91 (2014).

235. Van Goethem, E., Poincloux, R., Gauffre, F., Maridonneau-Parini, I. & Le Cabec, V. Matrix architecture dictates three-dimensional migration modes of human macrophages: differential involvement of proteases and podosome-like structures. *J. Immunol.* **184**, 1049–61 (2010).

236. Nourshargh, S. & Alon, R. Leukocyte migration into inflamed tissues. *Immunity* **41**, 694–707 (2014).

237. Murphy, D. A. & Courtneidge, S. A. The 'ins' and 'outs' of podosomes and invadopodia: characteristics, formation and function. *Nat. Rev. Mol. Cell Biol.* **12**, 413–26 (2011).

238. Nusblat, L. M., Dovas, A. & Cox, D. The non-redundant role of N-WASP in podosome-mediated matrix degradation in macrophages. *Eur. J. Cell Biol.* **90**, 205–12 (2011).

239. van den Dries, K., Linder, S., Maridonneau-Parini, I. & Poincloux, R. Probing the mechanical landscape - new insights into podosome architecture and mechanics. *J. Cell Sci.* **132**, (2019).

240. Linder, M. E. & Deschenes, R. J. Palmitoylation: policing protein stability and traffic. *Nat. Rev. Mol. Cell Biol.* **8**, 74–84 (2007).

241. Wiesner, C., Faix, J., Himmel, M., Bentzien, F. & Linder, S. KIF5B and KIF3A/KIF3B kinesins drive MT1-MMP surface exposure, CD44 shedding, and extracellular matrix degradation in primary macrophages. *Blood* **116**, 1559–69 (2010).

242. Wiesner, C., El Azzouzi, K. & Linder, S. A specific subset of RabGTPases controls cell surface exposure of MT1-MMP, extracellular matrix degradation and three-dimensional invasion of macrophages. *J. Cell Sci.* **126**, 2820–33 (2013).

243. Bravo-Cordero, J. J. *et al.* MT1-MMP proinvasive activity is regulated by a novel Rab8-dependent exocytic pathway. *EMBO J.* **26**, 1499–510 (2007).

244. Frittoli, E. *et al.* A RAB5/RAB4 recycling circuitry induces a proteolytic invasive

program and promotes tumor dissemination. *J. Cell Biol.* **206**, 307–28 (2014).

245. Kajiho, H. *et al.* RAB2A controls MT1-MMP endocytic and E-cadherin polarized Golgi trafficking to promote invasive breast cancer programs. *EMBO Rep.* **17**, 1061–80 (2016).

246. Sbai, O. *et al.* Vesicular trafficking and secretion of matrix metalloproteinases-2, -9 and tissue inhibitor of metalloproteinases-1 in neuronal cells. *Mol. Cell. Neurosci.* **39**, 549–68 (2008).

247. Sbai, O. *et al.* Differential vesicular distribution and trafficking of MMP-2, MMP-9, and their inhibitors in astrocytes. *Glia* **58**, 344–66 (2010).

248. Kean, M. J. *et al.* VAMP3, syntaxin-13 and SNAP23 are involved in secretion of matrix metalloproteinases, degradation of the extracellular matrix and cell invasion. *J. Cell Sci.* **122**, 4089–98 (2009).

249. Gueye, Y. *et al.* Trafficking and secretion of matrix metalloproteinase-2 in olfactory ensheathing glial cells: A role in cell migration? *Glia* **59**, 750–70 (2011).

250. Young, D., Das, N., Anowai, A. & Dufour, A. Matrix Metalloproteases as Influencers of the Cells' Social Media. *Int. J. Mol. Sci.* **20**, 3847 (2019).

251. Nguyen, A. T. *et al.* Organelle Specific O-Glycosylation Drives MMP14 Activation, Tumor Growth, and Metastasis. *Cancer Cell* **32**, 639-653.e6 (2017).

252. Gibson, D. G. Enzymatic assembly of overlapping DNA fragments. *Methods Enzymol.* **498**, 349–361 (2011).

253. Blank, B. Cab45 – analysis of key features of a multifunctional secretory pathway component. (Ludwig-Maximiliäns-Universität, 2017).

254. Pfeiffer, J. K., Georgiadis, M. M. & Telesnitsky, A. Structure-based moloney murine leukemia virus reverse transcriptase mutants with altered intracellular direct-repeat deletion frequencies. *J. Virol.* **74**, 9629–9636 (2000).

255. Pettersen, E. F. *et al.* UCSF Chimera--a visualization system for exploratory research and analysis. *J. Comput. Chem.* **25**, 1605–12 (2004).

256. Shapovalov, M. V & Dunbrack, R. L. A smoothed backbone-dependent rotamer library for proteins derived from adaptive kernel density estimates and regressions. *Structure* **19**,

844–58 (2011).

257. Toth, M., Sohail, A. & Fridman, R. Assessment of Gelatinases (MMP-2 and MMP-9) by Gelatin Zymography. in *Metastasis Research Protocols* (eds. Dwek, M., Brooks, S. A. & Schumacher, U.) 121–135 (Humana Press, 2012). doi:10.1007/978-1-61779-854-2_8

258. Tyanova, S. *et al.* The Perseus computational platform for comprehensive analysis of (prote)omics data. *Nat. Methods* **13**, 731–40 (2016).

259. Wiech, H. *et al.* Characterization of Green Alga, Yeast, and Human Centrins: specific subdomain features determine functional diversity. *J. Biol. Chem.* **271**, 22453–22461 (1996).

260. Thestrup, T. *et al.* Optimized ratiometric calcium sensors for functional in vivo imaging of neurons and T lymphocytes. *Nat. Methods* **11**, 175–82 (2014).

261. Kardash, E., Bandemer, J. & Raz, E. Imaging protein activity in live embryos using fluorescence resonance energy transfer biosensors. *Nat. Protoc.* **6**, 1835–46 (2011).

262. Boncompain, G. *et al.* Synchronization of secretory protein traffic in populations of cells. *Nat. Methods* **9**, 493–8 (2012).

263. Petersson, U. *et al.* Nucleobindin is produced by bone cells and secreted into the osteoid, with a potential role as a modulator of matrix maturation. *Bone* **34**, 949–960 (2004).

264. Kriventseva, E. V *et al.* OrthoDB v10: sampling the diversity of animal, plant, fungal, protist, bacterial and viral genomes for evolutionary and functional annotations of orthologs. *Nucleic Acids Res.* **47**, D807–D811 (2019).

265. Kanuru, M. & Aradhyam, G. K. Chaperone-like Activity of Calnuc Prevents Amyloid Aggregation. *Biochemistry* **56**, 149–159 (2017).

266. Tsukumo, Y. *et al.* Nucleobindin 1 controls the unfolded protein response by inhibiting ATF6 activation. *J. Biol. Chem.* **282**, 29264–72 (2007).

267. Prigent, M. *et al.* ARF6 controls post-endocytic recycling through its downstream exocyst complex effector. *J. Cell Biol.* **163**, 1111–1121 (2003).

268. Haass, N. K., Kartenbeck, J. & Leube, R. E. Pantophysin is a ubiquitously expressed

synaptophysin homologue and defines constitutive transport vesicles. *J. Cell Biol.* **134**, 731–746 (1996).

269. Brooks, C. C. *et al.* Pantophysin is a phosphoprotein component of adipocyte transport vesicles and associates with GLUT4-containing vesicles. *J. Biol. Chem.* **275**, 2029–2036 (2000).

270. Adams, D. J., Arthur, C. P. & Stowell, M. H. B. Architecture of the Synaptophysin/Synaptobrevin Complex: Structural Evidence for an Entropic Clustering Function at the Synapse. *Sci. Rep.* **5**, 13659 (2015).

271. Canver, M. C. *et al.* Integrated design, execution, and analysis of arrayed and pooled CRISPR genome-editing experiments. *Nat. Protoc.* **13**, 946–986 (2018).

272. Bard, F. & Malhotra, V. The Formation of TGN-to-Plasma-Membrane Transport Carriers. *Annu. Rev. Cell Dev. Biol.* **22**, 439–455 (2006).

273. Von Blume, J. *et al.* Actin remodeling by ADF/cofilin is required for cargo sorting at the trans-Golgi network. *J. Cell Biol.* **187**, 1055–1069 (2009).

274. Kim, Y. *et al.* Efficient site-specific labeling of proteins via cysteines. *Bioconjug. Chem.* **19**, 786–91 (2008).

275. Miura, K., Kurosawa, Y. & Kanai, Y. Calcium-Binding Activity of Nucleobindin Mediated by an EF Hand Moiety. *Biochem. Biophys. Res. Commun.* **199**, 1388–1393 (1994).

276. Revach, O. & Geiger, B. The interplay between the proteolytic, invasive, and adhesive domains of invadopodia and their roles in cancer invasion. *Cell Adh. Migr.* **8**, 215–25 (2014).

277. Shimoda, M. & Khokha, R. Metalloproteinases in extracellular vesicles. *Biochim. Biophys. acta. Mol. cell Res.* **1864**, 1989–2000 (2017).

278. Krishnaswamy, V. R., Benbenishty, A., Blinder, P. & Sagi, I. Demystifying the extracellular matrix and its proteolytic remodeling in the brain: structural and functional insights. *Cell. Mol. Life Sci.* (2019). doi:10.1007/s00018-019-03182-6

279. Cauwe, B. & Opdenakker, G. Intracellular substrate cleavage: a novel dimension in the biochemistry, biology and pathology of matrix metalloproteinases. *Crit. Rev. Biochem. Mol. Biol.* **45**, 351–423 (2010).

280. Cornfine, S. *et al.* The kinesin KIF9 and reggie/flotillin proteins regulate matrix degradation by macrophage podosomes. *Mol. Biol. Cell* **22**, 202–15 (2011).

281. Gupta, R., Kapoor, N., Raleigh, D. P. & Sakmar, T. P. Nucleobindin 1 Caps Human Islet Amyloid Polypeptide Protofibrils to Prevent Amyloid Fibril Formation. *J. Mol. Biol.* **421**, 378–389 (2012).

282. Hansen, G. A. W., Vorum, H., Jacobsen, C. & Honoré, B. Calumenin but not reticulocalbin forms a Ca2+-dependent complex with thrombospondin-1. A potential role in haemostasis and thrombosis. *Mol. Cell. Biochem.* **320**, 25–33 (2009).

283. Viappiani, S. *et al.* Activation and modulation of 72kDa matrix metalloproteinase-2 by peroxynitrite and glutathione. *Biochem. Pharmacol.* **77**, 826–34 (2009).

284. Yu, S. *et al.* Global ablation of the mouse Rab11a gene impairs early embryogenesis and matrix metalloproteinase secretion. *J. Biol. Chem.* **289**, 32030–43 (2014).

285. Mironov, A. A. & Beznoussenko, G. V. Models of Intracellular Transport: Pros and Cons. *Front. cell Dev. Biol.* **7**, 146 (2019).

286. Trucco, A. *et al.* Secretory traffic triggers the formation of tubular continuities across Golgi sub-compartments. *Nat. Cell Biol.* **6**, 1071–1081 (2004).

287. Farquhar, M. G. Progress in unraveling pathways of Golgi traffic. *Annu. Rev. Cell Biol.* **1**, 447–88 (1985).

288. Orci, L., Glick, B. S. & Rothman, J. E. A new type of coated vesicular carrier that appears not to contain clathrin: its possible role in protein transport within the Golgi stack. *Cell* **46**, 171–84 (1986).

289. Tortosa, E. & Hoogenraad, C. C. Polarized trafficking: the palmitoylation cycle distributes cytoplasmic proteins to distinct neuronal compartments. *Curr. Opin. Cell Biol.* **50**, 64–71 (2018).

290. Anilkumar, N. *et al.* Palmitoylation at Cys574 is essential for MT1-MMP to promote cell migration. *FASEB J.* **19**, 1326–8 (2005).

Acknowledgements

At the end of this work I would like to thank to all the people that made part of this journey. Their support made all the way (way) much better.

First, I would like to thank Dr. Julia von Blume, for making me part of such an incredible group as is the von Blume lab. Thank you for the trust and for believing we would accomplish great things. In particular, thank you very much for all your support in spite of the distance, it was extremely helpful both professionally and personally.

My deep gratitude to Prof. Dr. Reinhard Fässler, whose support and opportune advice were essential to excel in the realization of this project.

I have not enough words to thank my colleagues from the von Blume lab. To Dr. Birgit Blank for her infinite patience, her wisdom and for always having an answer for me. To Dr. Mehrshad Pakdel for his enormous support, permanent good mood and nurtured discussions. To Gisela Beck, for her full support, especially during the last year of my PhD. To Tobias Hecht, for always making my ugly days better in the lab, but specially for the funniest German-Spanish lessons I ever had. To MaiLy Tran, for the late-lab conversations and a shared passion for food. And last but not least, to Renate Gautsch for her support with the cell culture work in days we were growing HeLas like crazy.

I would also like to thank Prof. Dr. Stefan Linder for his always useful comments during my Thesis Advisory Committee meetings, fruitful discussions and the great collaboration we created. In this regard, also my gratitude goes to Dr. Angelika Haußer and her group in Stuttgart for the collaboration in our paper. Thank you too to Dr. Christoph Reichel for his time and participation in TAC meetings.

My thanks go also to the people from the core facility at the Max Planck Institute of Biochemistry –Dr. Uebel, Naga, Sabine, Lizzy– who were extremely diligent and helpful. To the people on the Molecular medicine department for their kindness, advice and good conversations around a coffee. In particular thanks to Raquel for her nice words and support.

To the Grasshoff group for always helpful Monday seminars and, in particular to Anna-Lena and Verena for their encouragement during the last months.

My special thanks to DAAD. Their support, not just through the scholarship, but also with practical matters made my arrival and integration in Germany much more smoothly. To Verena Kochan and all the people from the SFB914 for the great research atmosphere and very fruitful discussions on student symposiums.

To my spanish-speaking colony at the MPI (Daniela, Favio, Diego, Jose, Adrian) for great lunches, salsa dances and long debates. To Sebastian and Delia for sharing the joy and the pain at moments when we felt a bit lost. To Ma. Antonia for the extended lunches and summer beers. To Camilita, for sharing the passion for traveling together. And to Lina, for her unconditional support above time and distance.

And finally, my infinite thanks to Markus, for his patience, thoughtfulness and care. For his love and for the fortune to find him and share our lives together.

Todo este esfuerzo no hubiera sido posible sin el apoyo de mi familia. A Libardito, que siempre me acompaña. A mi tío y Eliza por siempre estar pendientes de mí, como si fuera su hija. A Juan por traerme la mejor de las sorpresas de mi vida. A Aurita, por ser el hombro que me ha cargado siempre cuando me siento muy cansada para seguir. A mi papá, por su amor infinito y por creer ciegamente en mí. Y a mi mamá, por creer que nada es imposible y por compartirme su certeza de que al final, todo va a estar bien. Gracias por sus vidas en mi vida.

Todo pasa y todo queda

Pero lo nuestro es pasar

Pasar haciendo caminos

Caminos sobre la mar

Cantares (A. Machado, 1917)